



**UNIVERSIDADE DE LISBOA**  
**INSTITUTO SUPERIOR TÉCNICO**

**Definition of mitigation strategies for the seismic risk reduction of  
old RC residential buildings**

**Claudia Caruso**

**Supervisor:** Doctor Rita Maria do Pranto Nogueira Leite Pereira Bento

**Co-Supervisor:** Doctor José Miguel de Freitas Castro

**Thesis approved in public session to obtain the PhD Degree in Civil  
Engineering**

**Jury final classification: Pass with distinction**

**2019**





**UNIVERSIDADE DE LISBOA  
INSTITUTO SUPERIOR TÉCNICO**

**Definition of mitigation strategies for the seismic risk reduction of  
old RC residential buildings**

**Claudia Caruso**

**Supervisor:** Doctor Rita Maria do Pranto Nogueira Leite Pereira Bento

**Co-Supervisor:** Doctor José Miguel da Freitas Castro

**Thesis approved in public session to obtain the PhD Degree in Civil  
Engineering**

**Jury final classification: Pass with distinction**

**Jury**

**Chairperson:** Doctor Eduardo Nuno Brito Santos Júlio, Instituto Superior Técnico, Universidade de Lisboa

**Members of the Committee:**

Doctor Rita Maria do Pranto Nogueira Leite Pereira Bento, Instituto Superior Técnico, Universidade de Lisboa

Doctor António José Coelho Dias Arêde, Faculdade de Engenharia, Universidade do Porto.

Doctor Antonio José da Silva Costa, Instituto Superior Técnico, Universidade de Lisboa

Doctor Carlos Paulo Novais Oliveira da Silva Cruz, Instituto Superior Técnico, Universidade de Lisboa

Doctor Hugo Filipe Pinheiro Rodrigues, Escola Superior de Tecnologia e Gestão, Instituto Politécnico de Leiria

Funding Institution: FCT

**2019**



## **ABSTRACT**

Seismic vulnerability evaluation of existing buildings and the application of adequate retrofitting solutions is key to reduce the levels of physical damage, loss of life and economic impact of future seismic events. Reinforced concrete framed and dual wall-frame structures represent an important fraction of the building stock in some European cities, such as Lisbon, in Portugal. Many of these structures were constructed without seismic provisions or based on early seismic codes (pre-1980) and present deficiencies which determine a high seismic vulnerability. Furthermore, many important cities in Europe are characterised by high seismic hazard, which, combined with a large exposure of vulnerable buildings, results in high seismic risk.

In this work, a specific loss estimation methodology is proposed to estimate economic losses of old reinforced concrete buildings. Focusing on the wall-frame building typology, the different steps of the procedure are described in detail and illustrated with a case study. A detailed three dimensional numerical model is developed and the main modelling issues are addressed. A particular focus is devoted to the numerical simulation of reinforced concrete walls with smooth bars, making use of fibre-based nonlinear beam elements. Practical recommendations and simplified solution are given for modelling strain penetration effects, which can be particularly relevant in older reinforced concrete members.

The procedure adopted for the loss analysis makes use of component based-fragility and loss functions to assess damage in structural and non-structural elements. The expected level of damage for a given ground motion intensity is estimated through the employment of numerical modelling and nonlinear response-history analysis. An analytical procedure is proposed to estimate the fragility functions of non-ductile reinforced concrete walls with smooth reinforcing bars and light transversal reinforcement, taking into account the strength penetration effects. Different repair techniques are considered, for which repair costs associated to the Portuguese reality are adopted. The results provide the economic losses of the building typology as a function of the ground motion intensity level. Ultimately, the feasibility of partial strengthening of such buildings is examined, with the ultimate aim to develop an efficient retrofitting plan for this typology.

**Key-words:** Seismic vulnerability, fragility functions, performance-based assessment, non-linear analyses, retrofitting.



## RESUMO

A avaliação da vulnerabilidade sísmica de edifícios existentes e a aplicação de soluções adequadas de reforço são essenciais para a redução dos níveis de danos físicos, da perda de vidas e do impacto económico de futuros eventos sísmicos. As estruturas em pórtico de betão armado e as estruturas mistas pórtico-parede representam uma fração importante do parque imobiliário em algumas cidades europeias, como Lisboa, em Portugal. Muitas destas estruturas foram construídas sem disposições sísmicas ou baseadas nos primeiros regulamentos sísmicos (pré-1980) e apresentam deficiências que determinam uma significativa vulnerabilidade sísmica. Além disso, muitas das cidades importantes na Europa são caracterizadas por uma elevada sismicidade, que, combinada com uma vasta exposição de edifícios vulneráveis, conduz a um alto risco sísmico.

Neste trabalho, é proposta uma metodologia específica de estimativa de perdas, de modo a estimar perdas económicas de edifícios antigos em betão armado. Com foco na tipologia de edifícios mistos – pórtico-parede, os diferentes passos do procedimento são descritos em detalhe e ilustrados com um caso de estudo. É desenvolvido um modelo numérico tridimensional pormenorizado e são abordados os principais problemas da modelação, dando uma atenção particular à simulação numérica de paredes em betão armado com varões lisos, com recurso a modelos não lineares de elementos finitos de barra de plasticidade distribuída (modelo de fibras). Recomendações práticas e soluções simplificadas são dadas para a modelação dos efeitos dos varões lisos e do comprimento de amarração, que podem ser particularmente relevantes nos elementos estruturais de betão armado existentes em edifícios antigos.

O procedimento adotado para a análise de perdas recorre a funções de fragilidade, com base em componentes, e a funções de perdas para avaliar os danos em elementos estruturais e não estruturais. O nível esperado de danos para uma dada intensidade de movimento do solo é estimado através da utilização da modelação numérica e do recurso a análises dinâmicas não lineares. Um procedimento analítico é proposto para estimar as funções de fragilidade de paredes de betão armado não-dúctil com varões lisos e reduzida quantidade de armadura transversal. São consideradas diferentes técnicas de reparação, para as quais são adotados custos de reparação associados à realidade portuguesa. Os resultados fornecem as perdas económicas da tipologia do edifício em função do nível de intensidade do movimento do solo. Numa última análise, a viabilidade do reforço parcial destes edifícios é examinada, com o objetivo final de desenvolver um plano de reforço eficiente para esta tipologia.

**Palavras-chave:** vulnerabilidade sísmica, funções de fragilidade, avaliação de desempenho, análises não lineares, reforço.



## ACKNOWLEDGEMENTS

Firstly, I would like to express my sincere gratitude to my supervisor, Doctor Rita Bento, for the continuous support of my Ph.D study, for her unconditional dedication, motivation and close supervision. Her guidance helped me in all the time of the research and writing of this thesis.

I would also like to thank my co-supervisor, Doctor José Miguel Castro, for his support, guidance and valuable scientific contribution to the enrichment of the work herein presented

My sincere thanks also goes to Doctor Edoardo Marino and Doctor João Pacheco de Almeida for their insightful comments and encouragement during my work.

I would like to thank my colleagues and friends Jelena Milosevic, Madalena Ponte and Rita Peres for all the good moments we spent together, inside and outside university. I would also like to express my appreciation to my colleagues from Instituto Superior Técnico and from the InfraRisk project that contributed, in some way, to reach this achievement, Vitor Camacho, Vieri Cardinali, Rui Maio, Ana Simões, Sanam Moghimi, Gideon Goitom, Giorgos Karanikoloudis and Bruno Oliveira.

I would like to thank all the friends I meet in Portugal for making this stay so special, especially Cristina Gemmino, Sergio Sabino, Ciro Pappalardo, Rui Martinho, Kariné Gharibyan, Michele Pisani, Marija Cosović, Domenico Nicosia. Special thanks to my dear friends in Italy, even though we have been long time far away we are always close, Irene Lioni, Valentina Carlisi, Ilaria Brachitta, Vincenzo Castro, Stefania Avellino, Simona Bascetta, Erica Bascetta, Alberto Puleo, Giona Messina, Agatino Pellegriti, Irene Russo, Salvo Reina, Emanuela La Mela, Rose Montalto, Valeria Battiato.

Most importantly, I would like to thank my family, my parents and my sister Alessandra, for their unconditional love and support throughout these years.

Finally, I would like to thank Fundação para a Ciência e a Tecnologia for the four years of financial support under the PhD grant PD / BD / 127923 / 2016.



## LIST OF CONTENTS

Abstract.....	v
Resumo .....	vii
Acknowledgements.....	ix
List of Contents.....	xi
List of Figures .....	xv
List of Tables .....	xxi
List of Symbols.....	<b>Errore. Il segnalibro non è definito.</b>
List of Acronyms .....	xxv
1. INTRODUCTION .....	27
1.1. Motivation.....	27
1.2. Research focus and background.....	30
1.3. Objectives and main contributions.....	35
1.4. Thesis layout .....	35
2. MODELLING STRAIN PENETRATION EFFECTS IN RC WALLS WITH SMOOTH BARS ..	39
2.1. Introduction.....	39
2.2. Modelling Issues Associated with the Numerical Simulation of RC Walls .....	40
2.2.1. Element Formulation.....	40
2.2.2. Strain Penetration Effects.....	41
2.3. Case studies.....	44
2.3.1. Description of the experimental tests.....	44
2.3.2. Numerical Modelling Options .....	46
2.4. Numerical Results.....	47
2.4.1. Effects for Different Anchorage Conditions .....	47
2.4.2. Calibration of Reinforcement Properties to Account for SP Effects.....	52
2.5. Conclusions.....	53
3. SEISMIC ASSESSMENT OF AN EXISTING OLD FRAME-WALL RC BUILDING IN LISBON	
.....	57
3.1. Introduction.....	57

3.2. Characteristics of Old RC buildings .....	59
3.2.1. Mechanical properties of materials .....	60
3.3. Case study .....	63
3.3.1. Case study RC wall-frame building .....	63
3.3.2. Structural Design Options .....	65
3.3.3. Structural modelling.....	68
3.3.4. Dynamic properties .....	71
3.4. Sensitivity analysis and seismic performance assessment .....	72
3.4.1. Parameters of sensitivity analysis .....	73
3.4.2. Ageing effects .....	74
3.4.3. Results and discussion .....	75
3.5. Conclusions.....	78
4. RELEVANCE OF TORSIONAL EFFECTS ON THE SEISMIC ASSESSMENT OF OLD RC FRAME-WALL BUILDINGS .....	81
4.1. Introduction.....	81
4.2. Seismic response assessment procedures.....	82
4.2.1. Application of the Extended N2 method.....	82
4.2.2. A proposal for shear demand prediction .....	83
4.2.3. Analysis procedures .....	84
4.2.4. Ground motion record selection.....	85
4.3. Discussion of the results .....	86
4.3.1. Dynamic properties .....	86
4.3.2. Determination of the target displacement .....	87
4.3.3. Assessment of the torsional response.....	88
4.3.4. Application of Extended N2 method for the evaluation of storey drifts .....	90
4.3.5. Application of Extended N2 method for the evaluation of shear demand .....	91
4.4. Seismic safety - Deformation capacity and shear strength .....	93
4.5. Conclusion .....	96
5. A CONTRIBUTION TO THE SEISMIC PERFORMANCE AND LOSS ASSESSMENT OF OLD RC WALL-FRAME BUILDINGS .....	99

5.1. Introduction.....	99
5.2. Methodology for loss assessment .....	101
5.2.1. Hazard Analysis .....	101
5.2.2. Structural Analysis and Engineering Demand Parameters .....	101
5.2.3. Damage Analysis .....	102
5.2.4. Loss Analysis.....	104
5.3. Analytical evaluation of fragility parameters for RC walls .....	105
5.3.1. Modelling considerations.....	106
5.3.2. Parametric investigation.....	107
5.3.3. Identification of damage states .....	108
5.3.4. Analysis and discussion of the results.....	109
5.4. Estimation of repair and replacement costs .....	111
5.4.1. Costs for repairing structural damage .....	111
5.4.2. Damage to non-structural components.....	113
5.5. Application to the case study building.....	115
5.5.1. Hazard Analysis and Engineering Demand Parameters.....	115
5.5.2. Damage analysis .....	118
5.5.3. Cost of structural and non-structural components .....	120
5.5.4. Estimation of economic losses.....	121
5.6. Comparison with other studies – capacity and fragility curves .....	126
5.6.1. Capacity curves .....	126
5.6.2. Fragility curves .....	127
5.7. Conclusions.....	129
<b>6. FEASIBILITY OF RETROFITTING SOLUTIONS FOR OLD RC WALL-FRAME BUILDINGS</b> .....	<b>131</b>
6.1. Introduction.....	131
6.2. Retrofitting strategies.....	133
6.2.1. Criteria for strengthening.....	133
6.2.2. Definition of retrofitting strategies.....	134

6.2.3. Retrofitting using FRP .....	134
6.2.4. Retrofitting with steel braces .....	135
6.2.5. Preliminary Results .....	137
6.3. Performance-based cost-benefit assessment .....	139
6.3.1. Hazard analysis .....	140
6.3.2. Structural analysis .....	140
6.3.3. Damage analysis .....	141
6.3.4. Loss analysis .....	142
6.3.5. Cost-benefit analysis .....	143
6.4. Conclusions .....	146
7. FINAL REMARKS AND FUTURE WORK .....	149
7.1. Final remarks .....	149
7.2. Future developments .....	151
REFERENCES .....	153
Annex A .....	165
Annex B .....	170
Annex C .....	173

## LIST OF FIGURES

Figure 1.1 – Earthquake related economic and insurance losses (adapted from (Goda et al., 2014)) ..	28
Figure 1.2 – Risk assessment model (on the left) and measures for mitigation of seismic risk (on the right) through reduction of exposure at risk (risk avoidance), transfer of risk and vulnerability reduction (adapted from (Wei et al., 2015)).....	29
Figure 1.3 – Evolution of the construction of reinforced concrete buildings in the last century with the introduction of the seismic design code in Portugal (adapted from (Sousa et al., 2019)).....	31
Figure 1.4 – Methodology to estimate losses in a probabilistic framework. ....	33
Figure 2.1 –Detailing of foundation system of an RC wall (Montepio Geral, 1690) .....	40
Figure 2.2 – Behaviour of anchorage region with adequate (left) and limited (right) embedment length (adapted from Zhao and Sritharan 2007) .....	42
Figure 2.3 – Correction of the steel reinforcing law (adapted from (Varum, 2003)).....	43
Figure 2.4 –Reinforcement layout in the plastic zone of the wall WSH4 [dimensions in mm].....	45
Figure 2.5 – Shear force-top displacement for the RC wall specimen WSH4, considering both FB and DB formulation .....	47
Figure 2.6 – Schematic representation of the different components of the bond-slip model by Sousa (2015) (adapted from Sousa (2015)).....	48
Figure 2.7 – Moment-rotation (M-R) relation for ribbed and smooth rebars with different embedment length for the RC wall specimens WSH4 (a), R1 (b) and R2 (c).....	50
Figure 2.8 – Shear force-top displacement relations for ribbed and smooth rebars with different embedment length for the RC wall specimens WSH4 (a), R1 (b) and R2 (c) .....	51
Figure 2.9 – Comparison of the shear force-top displacement relations wall WSH4 (a), R1 (b) and R2 (c), considering the cases of ribbed and smooth rebars with different embedment length, considering the model with calibrated reinforcement parameters (SP model) and the one considering a rotational spring with a tri-linear relation.....	54
Figure 3.1 – GIS data-base and thematic maps with identification of the Alvalade district.....	60
Figure 3.2 – Elongation stages (a) and stress-strain relationship (b) for specimen 1. ....	62

Figure 3.3 – Location of the building within Avenida do Brasil and Rua Aprígio Mafra .....	63
Figure 3.4 – Views of the building in Av. do Brasil and front view of the building .....	64
Figure 3.5 – Plan of the building floors 1-7 (adapted from Montepio-Geral, 1960) (dimensions in [m]) .....	64
Figure 3.6 – Plan of the ground floor (adapted from Montepio-Geral, 1960) (dimensions in [m]).....	65
Figure 3.7 – Case study building, dimensions in [m]: (a) structural plan layout, (b) elevation in Y- direction. ....	66
Figure 3.8 – Detail of the reinforced concrete core and RC walls .....	67
Figure 3.9 – Detail of the lightened slab.....	67
Figure 3.10 – (a) Plan of the foundation; (b) detailing of foundation system of a RC column (Montepio Geral, 1960). Dimensions in [m].....	67
Figure 3.11 – Schematic quadrilinear force-displacement relationship of the compressed diagonal struts (adapted from (Celarec et al., 2012)). ....	71
Figure 3.12 –Pushover curves for X direction (base model and models with parameters set at 16 <sup>th</sup> or 84 <sup>th</sup> fractiles) and top displacements-base shear for flexural failure (FF) and shear failure (SF).....	76
Figure 3.13 – Variation of peak ground acceleration for parameters uncertainties corresponding to flexural failure (FF) and shear failure (SF) in columns and walls and for all directions of loading.....	77
Figure 3.14 – Pushover curves for Y direction (base model and models with parameters set at 16 <sup>th</sup> or 84 <sup>th</sup> fractiles) and top displacements-base shear for flexural failure (FF) and shear failure (SF).....	78
Figure 4.1 –Amplification of the shear demand of the member (column or wall): (a) shear demand of the member of the balanced model and (b) increased shear demand of the member due to torsion.....	84
Figure 4.2 – Individual acceleration response spectrum of each of the 60 signals and corresponding average. ....	85
Figure 4.3 – Schematic plan of the building with the location of CM considering the accidental eccentricity.....	86
Figure 4.4 – Pushover curves in X (a) and Y directions (b). ....	88
Figure 4.5 – Normalized roof displacements ( $u/u_{CM}$ ) in the horizontal plane for X and Y direction at 0.0765g .....	89

Figure 4.6 – Normalized roof displacements ( $u/u_{CM}$ ) in the horizontal plane for X and Y direction at 0.115g .....	89
Figure 4.7 –Normalized roof displacements ( $u/u_{CM}$ ) in the horizontal plane for X and Y direction at 0.153g .....	90
Figure 4.8 – Storey-drifts at the SE, at the CM and at the FE for the X direction.....	91
Figure 4.9 – Storey-drifts at the SE, at the CM and at the FE for the Y direction.....	91
Figure 4.10 – Shear demand for the shear walls W1 and W4 in the X direction.....	92
Figure 4.11 – Shear demand for walls W1, W2, W3 and W4 in the Y direction.....	92
Figure 4.12 –Locations of the plastic hinges and demand/capacity ratios in the X direction for the frame in the FE and the RC walls in the same direction.....	94
Figure 4.13 – Locations of the plastic hinges and demand/capacity ratios in the positive Y direction for the frames in the SE and FE and the RC walls in the same direction. ....	94
Figure 4.14 –Pushover curves for X direction. Target displacement and flexural and shear failure are indicated considering (a) and not considering (b) the torsional response.....	95
Figure 4.15 –Pushover curves for positive Y direction. Target displacement and flexural and shear failure are indicated (a) considering and (b) not considering the torsional response.....	95
Figure 5.1 – Logic tree adopted in the parametric study.....	108
Figure 5.2 – Pushover curves with different embedment length of the rebars, for two values of shear span ratio and for specific values of horizontal reinforcement ratio and axial load ratio. ....	110
Figure 5.3 – Variation of IDR with respect to (a) the axial load ratio and (b) horizontal reinforcement for DS4.....	110
Figure 5.4 – Seismic hazard curves for Lisbon, for a return period $T1 = 0.89$ seconds. ....	116
Figure 5.5 – Engineering demand Parameter (EDP) data as a function of the building levels for (a) the X and (b) Y direction. IDR, inter-storey drift ratio (left); PFA, peak floor acceleration (right).....	117
Figure 5.6 – Fragility functions corresponding to four damage states for RC columns 2 and 9 at three storey levels (1st, 5th and 8th storeys) of the case study building.....	119
Figure 5.7 – Fragility functions of the RC wall: (a) probability of exceeding a damage state and (b) probability of being in each damage state.....	120

Figure 5.8 – Variation of the expected loss in an exterior and an interior column of the case study building as a function of the IDR, at levels 1 <sup>st</sup> , 5 <sup>th</sup> and 8 <sup>th</sup> . .....	121
Figure 5.9 –Variation of the expected loss in RC walls of the case study building. ....	121
Figure 5.10 –Normalized losses due to repair in structural components and drift sensitive and acceleration non-structural components, for increasing levels of ground motion intensity. ....	122
Figure 5.11 – Probability of collapse for the case study building. ....	124
Figure 5.12 –Variations of the expected loss in the case study building as a function of the ground motion intensity, IM and (b) MAF of exceeding a specific ground motion intensity level, $\lambda_{Sa}$ , as a function of the total expected losses, for each IM. ....	125
Figure 5.13 – Capacity curves for the case study buildings for the X and Y directions (identified as “Frame-wall”) and the results from (a) Carvalho et al. (2002) and (b) Silva et al. (2015) .....	127
Figure 5.14 – Shear demand ratio in columns (dashed lines) and walls (continuous lines) at different IM levels in (a) the X direction and (b) Y direction .....	128
Figure 5.15 – Comparison of fragility functions between the RC wall-frame building typology in this study and the RC frame typology for Mid-Code soil type A analysed in (Silva et al., 2015a).....	129
Figure 6.1 – Comparison of shear demand ( $V_d$ ) and shear strength as per different seismic codes, i.e. EC2-1, EC8-3 and ATC 40, for the RC walls in the X direction (a) and Y direction (b). ....	133
Figure 6.2 – Retrofitting scheme.....	136
Figure 6.3 – Pushover curves in the X direction for the retrofitted building with (a) steel braces and (b) FRP. Target displacement and shear failure of the RC walls is indicated for the strengthened structure. ....	138
Figure 6.4 - Inter-storey drifts (IDR) (a) and lateral displacements profile (b) in the X direction. ....	139
Figure 6.5 - Shear D/C ratio in (a) RC Wall1 and (b) RC Wall4 in the X direction.....	139
Figure 6.6 – IDR as a function of the building height for the (a) X and (b) Y direction for the building strengthened with FRPs. ....	141
Figure 6.7 – IDR as a function of the building height for the (a) X and (b) Y direction for the building strengthened with steel braces.....	141

Figure 6.8 – Collapse fragility functions for the original structure and the structure retrofitted with steel braces, FRPs and a combination of the two..... 142

Figure 6.9 – Variations of the expected loss in the case study building retrofitted with FRP (a), steel braces (b) and the combination of FRP along all the height and steel braces (c). ..... 143

Figure A.1 – Case study building: structural plan layout..... 168

Figure B.1 – Response spectra for all the records in the set along with the target conditional spectrum (left), comparison between the standard deviation of the set and the target standard (right), for probabilities of occurrence of 1%, 2%, 5%, 10% and 30% in 50 years..... 172



## LIST OF TABLES

Table 2.1 –Mechanical ratios of reinforced concrete wall specimens .....	45
Table 2.2 – Mechanical properties of concrete material .....	45
Table 2.3 – Mechanical properties of reinforcing steel.....	45
Table 2.4 – Anchorage conditions considered .....	48
Table 2.5 –Summary of the percentage reduction for the Young's modulus ( $E$ ) and the maximum strength ( $F_{y,max}$ ) of the reinforcing steel .....	53
Table 3.1 – Evolution of material properties associate to building codes.....	61
Table 3.2 – Summary of T-shaped walls' properties .....	68
Table 3.3 – Summary of material properties.....	69
Table 3.4 – Periods of vibration and frequencies of the first 3 modes of vibration .....	72
Table 3.5 – Parameters of sensitivity analysis .....	74
Table 4.1 – Results of the modal analysis of the torsionally balanced model. ....	87
Table 4.2 –Shear demand and resistance for walls W1 and W4. ....	93
Table 5.1 – Parameters and corresponding values considered in the study. ....	108
Table 5.2 – Unit cost for repair action required for each damage state in reinforced concrete columns. ....	112
Table 5.3 – Unit cost for repair action required for concrete jacketing of walls required at DS3. ....	112
Table 5.4 – Classification of drift-sensitive and acceleration-sensitive non-structural components. .	113
Table 5.5 – Fragility and loss function parameters for masonry infills walls (Cardone and Perrone, 2015).....	115
Table 5.6 – Cost estimates for the evaluation of replacement cost of the case study building. ....	120
Table 5.7 – Logarithmic mean ( $\lambda$ ) and logarithmic standard deviation ( $\sigma$ ) for the case study building and for the mid-code fragility functions for soil type A from (Silva et al., 2015a) .....	129
Table 6.1 – Shear contribution of FRPs. ....	135
Table 6.2 –Section profile of steel braces. ....	137

Table 6.3 – Median collapse capacity and mean annual frequency of collapse of the original and retrofitted structure.....	143
Table 6.4 – Cost of retrofitting with FRP. ....	144
Table 6.5 – Cost of retrofitting with steel braces. ....	144
Table 6.6 – Benefit-cost ratios for the original building and for each one of the strengthening strategies. ....	146
Table A.1 – Geometric characteristics and reinforcement of the RC walls. ....	165
Table A.2 – Geometric characteristics and reinforcement of the columns. ....	166
Table A.3 – Geometric characteristics and reinforcement of the beams. ....	168
Table C.1 – Estimated cost of repairing light damage (DS1) for a column (0.3x0.7m). ....	174
Table C.2 – Estimated cost of repairing moderate damage (DS2) for a column (0.3x0.7m).....	174
Table C.3 – Estimated cost of repairing severe damage (DS3) for a column (0.3x0.7m). ....	175
Table C.4 – Linear cost of concrete jacketing (DS3) of RC walls.....	175

## LIST OF SYMBOLS

$L_e$	embedment length
$\lambda$	slippage factor
$\rho_{bound}$	boundary reinforcement ratio
$\rho_{web}$	web reinforcement ratio
$\rho_{long}$	Longitudinal reinforcement ratio
$\rho_h$	Horizontal reinforcement ratio
$f_c$	Concrete peak strength
$\varepsilon_c$	Concrete strain at peak strength
$E_c$	Concrete modulus of elasticity
$f_y$	Reinforcement yield strength
$f_u$	Reinforcement ultimate strength
$\varepsilon_{sy}$	Reinforcement yield strain
$\varepsilon_{su}$	Reinforcement ultimate strain
$\sigma_{sy}$	Steel yield stress
$E_s$	Reinforcement modulus of elasticity
$\tau_{max}$	Maximum constant averaged bond stress
$d_b$	Bar diameters
$F_a$	Anchorage force
$F_{y,max}$	Force in the rebar
$A_s$	Area of the rebar
$P$	Perimeter of the rebar
$f_{cm}$	Mean value of the concrete compressive strength
$d_t$	Target displacement
$V_i$	Shear demand
$r_x$	Effective modal mass in X direction
$r_y$	Effective modal mass in Y direction
$\Omega$	Ratio of the translational period to the rotational period
$d_{max}$	Maximum top floor displacement independently of time at which it occurs

$V_{max}$	Maximum base shear independently of time at which it occurs
$V(d_{max})$	Base shear attained at the same instant of $d_{max}$
<i>ATC-40</i>	Applied Technology Council
$N_{cr}$	Euler's critical load
$N_{pb,Rd}$	Yield resistance of the gross section
$N_{b,Rd}$	Buckling load

## LIST OF ACRONYMS

FCT	Fundação para a Ciência e a Tecnologia
InfraRisk-	Analysis and Mitigation of Risks in Infrastructures
PBEE	Performance-Based Earthquake Engineering
PEER	Pacific Earthquake Engineering Research
DM	Damage Measure
DV	Decision Variable
EAL	Expected Annual Loss
ATC	Applied Technology Council
HAZUS	Hazard United States
GIS	Geographic Information System
RC	Reinforced Concrete
TH	Time-History analysis
RSCCS	Regulamento de Segurança das Construções Contra os Sismos
RSEP	Regulamento de Solicitações em Edifícios e Pontes
RSA	Regulamento de Segurança e Acções para Estruturas de Edifícios e Pontes
SP	Strain Penetration
EC8-1	Eurocode 8 – Part 1
EC8-3	Eurocode 8 – Part 3
MRSA	Modal Response Spectrum Analysis
CM	Centre of Mass
EDP	Engineering Demand Parameter
SD	Significant Damage
CQC	Complete Quadratic Combination
SRSS	Square Root of the Sum of Squares
FE	Flexible Edge
SE	Stiff Edge
PGA	Peak Ground Acceleration
IP	Integration Point
FB	Force Based
DB	Displacement Based
IDR	Inter-storey Drift Ratio

PFA	Peak Floor Acceleration
RIDR	Residual Inter-storey Drift Ratio
MAF	Mean Annual Frequency
NPV	Near Present Value

# 1. INTRODUCTION

## 1.1. Motivation

The PhD thesis herein presented has been developed within the scope of the FCT PhD Program in Analysis and Mitigation of Risks in Infrastructures – InfraRisk- (<http://infrarisk.tecnico.ulisboa.pt/>). This PhD program claims as one of its main goal the analysis of the risks associated to several natural hazards, such as earthquakes and tsunamis. Catastrophic earthquake events and its cascade events, such as fire and tsunami, have extensive economic impact and are responsible for human casualties and injuries. In the last decades, earthquake disasters have caused a dramatic increase of economic losses globally. This is due to the world population growth, the development of new urban concentration in zones of high seismic hazard and the highest vulnerability of modern societies and technologies (Calvi et al., 2006). Resilience and sustainability of building stock and communities against earthquake is a global and urgent problem.

Earthquake induced damage includes direct financial loss to building properties and lifeline facilities and consequent indirect loss across regional and national communities. Additionally, all of this influences the abrupt reduction of Gross Domestic Product (GDP) for national economies. For example, After Haiti's earthquake in 2010 the country registered economic losses up to 120% of the country's GDP. In 2011 Tohoku earthquake in Japan had a significant economic impact not only in the damaged regions but also in regions outside the damaged areas due to disruptions of supply chains and domestic/international trade networks (Goda et al., 2014). Nepal's Gorkha earthquake in 2015 caused total economic loss in the order of 10 billion U.S. dollars, which is about a half of Nepal's GDP (James et al., 2015) (Goda et al., 2015). Such major events have long-term consequences as they lead to stagnation of regional and national economies.

Homeowners in disaster area suffer from loss of asset and income. The recovery can be extremely difficult especially if the economic burden falls entirely on the public financial support from governments and municipalities; a possible solution for this problem is to privatise the risk by the introduction of compulsory insurance schemes to homeowners and then export part of it to the international reinsurance market (Bommer et al., 2002). Another possibility to deal with such catastrophic events is given by integrated risk management measures, which involves the combination of "hard" risk disaster reduction measure, e.g. seismic retrofitting and upgrading, and "soft" risk reduction measure, such as insurance policies. The acceptance to adopt one of these risk mitigation measures also depends on the level of risk perception of property owners and on the type of property.

Figure 1.1 shows the significant magnitude of earthquakes catastrophes occurred in the last few decades and presents the estimated direct and insured economic losses due to earthquakes. According

to (Goda et al., 2014), the 2011 Tohoku earthquake and tsunami, the 2010-2011 Christchurch (New Zealand) sequences and the 2010 Maule (Chile) earthquake registered the highest insured loss since 1900 (exceeding 10 \$billion). From Figure 1.1, it can be observed that only a small part of direct economic losses was insured losses.

As stated before, among the various risk management measures, the transfer of risk to the insurance industry is a widespread solution in countries with high seismic hazard, especially the countries on the circum-Pacific seismic belt, the Ring of Fire. One notable example is the case of New Zealand, one of the world's forerunners in the application of seismic risk mitigation policies. Since the 40s, and after Wairarapa Earthquake, the participation to natural disaster insurance is incidental to fire insurance and is automatic/compulsory and provided to residential property owners by a government-owned *Earthquake Commission* (Earthquake Commission (EQC), 2019). Chile has one of the highest insurance penetration rate, up to 75% of commercial industry and 24% of residential buildings (Zanini et al., 2015).

In Turkey, after 1999 Izmit earthquake, the state founded the *Turkish Catastrophe Insurance Pool* (TCIP) to transfer part of the earthquake loss to the insurance industry, and its purchase is compulsory for all residential properties within municipality boundaries. European countries have different insurance schemes and penetration rates unevenly distributed among the member states. Countries with an high seismic risk, such as Italy, Portugal and Greece, show rates below 10%, despite the high maximum losses experienced within the last 20 years (Goda et al., 2014).

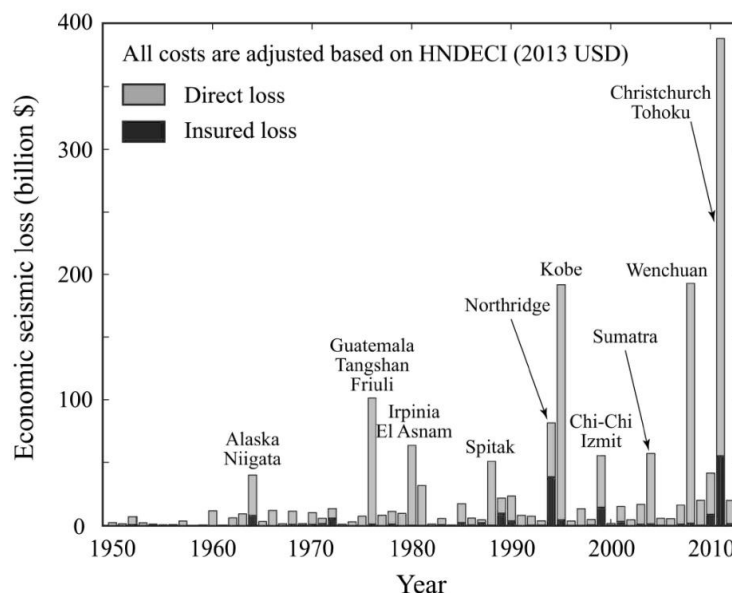


Figure 1.1 – Earthquake related economic and insurance losses (adapted from (Goda et al., 2014))

An earthquake loss model involves the combination of three main components (Figure 1.2): (i) a probabilistic seismic hazard model; (ii) an exposure model defining the spatial distribution of

elements exposed to the hazard; (iii) vulnerability characteristics of the exposed inventory (Silva et al., 2015b). The evaluation of an earthquake loss model for a region is important not only as a mean for predicting the economic impact of future earthquakes and the benefit of insuring it (risk transfer), but also for the strategic development of risk mitigation actions. Loss models capable of predicting the damage to structure and infrastructure for a given earthquake scenario can be used to produce emergency planning at urban or regional level, aiming at reducing the exposure at risk, for the calibration of seismic codes for design of new buildings and retrofitting of the existing ones, aiming at reducing the vulnerability (Calvi et al., 2006). However, risk reduction actions also include the increase in public awareness of the overall risk (Wei et al., 2015). These concepts are represented in Figure 1.2.

Attempts to establish a methodology for the seismic risk analysis of buildings and infrastructures in Europe include, for example, the Global Earthquake Model, GEM (Pinho, 2012) (Crowley et al., 2018). This initiative has the objective of developing best practices, datasets, models and tools for the seismic risk assessment through the collaboration with local experts worldwide and the development of an open source platform for the calculation of seismic hazard and risk, the OpenQuake engine (Silva et al., 2014). In Portugal, where the tectonic environment induces low to moderate seismic hazard, the vulnerable building stock lead to a significant seismic risk.

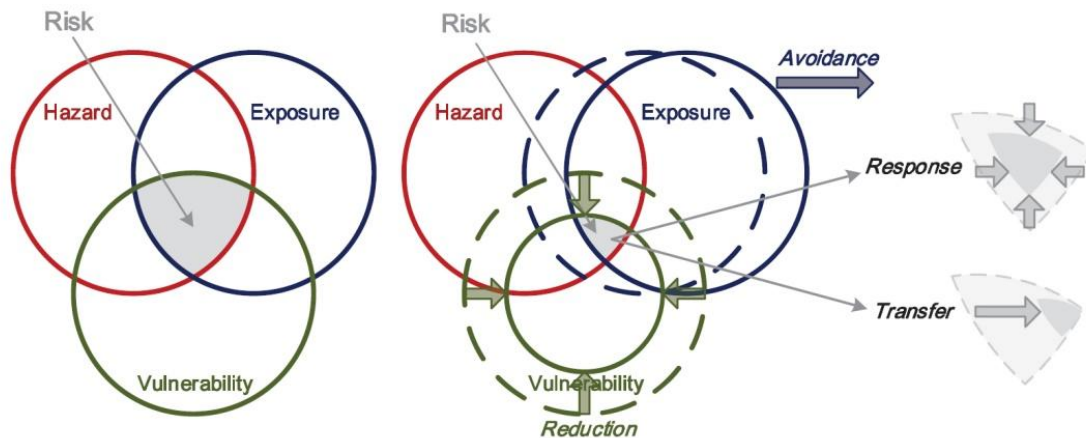


Figure 1.2 – Risk assessment model (on the left) and measures for mitigation of seismic risk (on the right) through reduction of exposure at risk (risk avoidance), transfer of risk and vulnerability reduction (adapted from (Wei et al., 2015)).

The first attempts to establish a methodology for the seismic risk analysis of buildings and infrastructures in Europe include, for example, the research projects RISK-UE (Mouroux and Le Brun, 2006) and LESSLOSS (Calvi and Pinho, 2004). In the work of (Silva et al., 2015b) the seismic risk at a national scale for Portugal was evaluated using the framework developed within GEM initiative. It combined up-to-date models for the seismic hazard, data from the last 2011 Building

Census (2011) to derive a detailed exposure model with information on the spatial distribution of buildings replacement cost and analytical vulnerability functions. It was estimated that a future seismic event, with a return period of 475 years, has the potential to produce mean economic losses to the current residential building stock in Portugal of approximately 31.8% of Portuguese Gross Domestic Product (GDP) of 2011 (reference year of the study).

Some of the main contributions in the field of vulnerability assessment in Portugal can be mentioned. Carvalho et al. (2002) derived several sets of fragility functions for each existing building typology in the country, based on the simplified approach proposed by FEMA and NIBS (FEMA, 2000). Nevertheless, the design parameters used in the construction of the capacity curves (strength coefficient, over-strength factor, elastic period and ductility factor) were calibrated for structures typically found in the United States. Silva et al. (2015a) estimated the vulnerability of typical Portuguese Reinforced Concrete (RC) buildings by employing an analytical methodology. Two-dimensional structural models were developed, thus hindering the consideration of plan irregularities, which typically involve torsional deformations. Moreover, the presence of shear walls was not considered. Martins et al. (2016) developed a detailed vulnerability model for mainland Portugal, using repair costs that are specific to the Portuguese reality. Both studies ((Silva et al., 2015a); (Martins et al., 2016)) were based on RC moment-frame systems.

This work moves from the need of reliable loss models for Portugal and the development of appropriate retrofitting interventions addressing one of the most vulnerable typology of RC buildings, i.e. RC wall-frame buildings designed and built according to old pre-seismic codes.

## **1.2. Research focus and background**

Seismic risk in Portugal has been documented over the past few years through several studies, e.g. (Mouroux and Le Brun, 2006), (Calvi and Pinho, 2004), (Silva et al., 2015b). Regions with a certain population density such as the Lower Tagus Valley (Lisbon and Setúbal districts) and the southwest of Portugal have the highest seismic hazard. Besides this, seismic risk also reflects the structural weaknesses stemming from the fact that most of the buildings in Portugal were designed without considering the seismic action. Survey information (Silva et al., 2015b) showed that the majority of existing building in Portugal were constructed prior to the 1980s with little to no consideration of modern seismic design principles.

The first Portuguese standard to explicitly consider seismic resistance was introduced in 1958 by the RSCCS, *Regulamento de Segurança das Construções Contra os Sismos* (RSCCS, 1958), while the importance of ductility in structural design was only introduced in 1983 by the RSA, *Regulamento de Segurança e Acções para Estruturas de Edifícios e Pontes* (RSA, 1983), and the REBAP, *Regulamento de Estruturas de Betão Armado e Pré-Esforçado* (REBAP 1983). Therefore, the

Portuguese building stock, which is composed of many RC structures built between 1955 and 1980, was not designed according to the current rules defined in the most recent seismic codes. In Figure 1.3 existing buildings in Portugal are disaggregated by decade of construction. It is estimated that around 50% of these buildings were constructed prior to the introduction of the current seismic code in 1983, RSA (Sousa et al., 2019).

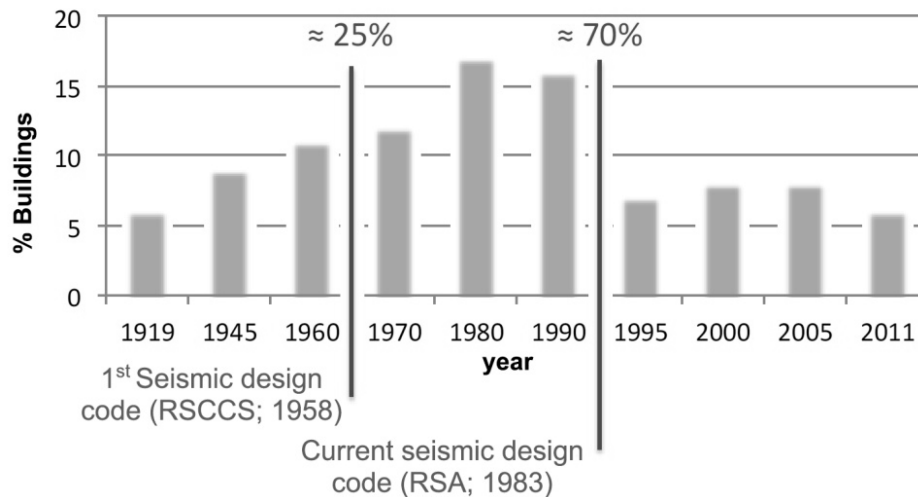


Figure 1.3 – Evolution of the construction of reinforced concrete buildings in the last century with the introduction of the seismic design code in Portugal (adapted from (Sousa et al., 2019))

Reinforced concrete framed and dual wall-frame structures represent an important fraction of the building stock in some European cities, such as Lisbon, in Portugal. Many of these were constructed without seismic provisions or based on early seismic codes (pre-1980) and present deficiencies which determine a high seismic vulnerability. Furthermore, many important cities in Europe are characterised by high seismic hazard, which, combined with a large exposure of vulnerable buildings, results in high seismic risk. The seismic vulnerability of this type of buildings was evident during the latest earthquake in Mexico (Galvis et al., 2017), where most of the collapsed building were old (pre-1985) non-ductile RC structures. Also, it was observed that up to 57% of the buildings developed a soft-storey mechanism. Due to need for structural upgrading to meet more stringent seismic design requirements in earthquake prone areas, seismic assessment and structural retrofiting is becoming more and more important and receives today considerable emphasis throughout the world.

One of the main components of a loss model is a methodology to assess the vulnerability of the building stock. The aim of a vulnerability assessment is to obtain vulnerability functions capable of describing the distribution of percentage of loss for a set of intensity measures. The various methods that have been proposed in the past for use in loss estimation can be divided into the following main categories: empirical, analytical and hybrid methods (Calvi et al., 2006).

In recent years, significant improvements have been made in the seismic performance assessment of new or existing buildings. Various analytical approaches are in development in the framework of the Performance-Based Earthquake Engineering (PBEE). It represents the effort of a new generation of seismic codes, which started with the SEOAC's Vision 2000 report (1995), were extended with the FEMA 356 (2000) and were followed by a series of ATC documents inspired by the SAC project (Cornell et al., 2002). As stated in the Vision 2000 report, PBEE can be expressed as the “*coupling of expected performance level with expected levels of seismic ground motions*”.

The main objectives of PBEE are twofold, i.e. to ensure that life-safety protection is achieved and that economic losses are reduced, designing structures to withstand minor or moderate earthquake shaking with no or low structural and non-structural damage. The necessity of defining different levels of performance for different intensities of earthquake motion was triggered by the consequences of the earthquakes of developed regions such as the California's Northridge earthquake in 1994 and the Japan's Kobe earthquake in 1995. In fact, even though the life safety objective was achieved to a certain extent, enormous economic losses followed the earthquakes (Bommer and Pinho, 2006). The principles of PBEE are relevant in any kind of setting. In fact, losses caused by earthquakes can have devastating impact especially on developing economies, as it was the case for the Kocaeli earthquake in Turkey (Bommer et al., 2002).

As opposed to older prescriptive codes, modern design codes incorporate to some degree the new principles of PBEE, prescribing different performance levels for different ground shaking intensity levels that the structures must fulfil. Focusing on the principle of PBEE, the Pacific Earthquake Engineering Research (PEER) Centre proposed a fully probabilistic framework, originally presented by Deierlein et al. (2003). The PEER-PBEE framework includes a number of stages (Figure 1.4), with hazard, structural, damage and loss analysis being conducted to provide information for a final consequence analysis of performance measures referred to as decision variables (DV), such as expected economic losses and collapse safety. As shown in Figure 1.4, the first stage is the probabilistic seismic hazard analysis, which is conducted to estimate the annual frequency of exceedance of the ground motion intensity at the site. The ground shaking at the site is parameterized in terms of an intensity measure (IM). The second stage is the structural analysis, which is evaluated through nonlinear dynamic analysis on the structural model at increasing level of ground motion intensity. The results from the structural analysis are employed to compute Engineering demand parameters (EDPs), such as peak interstorey drift demands (IDR), peak floor accelerations (PFA), etc., conditioned on the intensity measure IM. The third stage produces damage measures (DMs) using fragility functions, which are cumulative distribution functions relating the EDPs to the probability of being or exceeding particular levels of damage. In the fourth step, a loss analysis is performed on the basis of the level of damage sustained by the components. Decision variable (DVs) are produced, e.g. economic losses, based on repair and replacement cost of damaged building

components, which stakeholders can use to help them make more informed design decisions. It is worth saying that the methodology gives the frequency with which a specific performance metric will exceed various levels at a given location (many DVs depend on location, such as repair cost) (Porter, 2003).

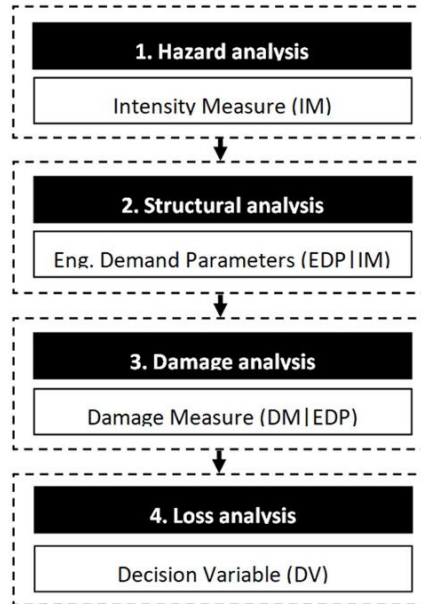


Figure 1.4 – Methodology to estimate losses in a probabilistic framework.

The PEER Framing Formula defines  $\lambda(DV)$ , the mean annual frequency of the DV exceeding a specified value, and is mathematically expressed by the triple integral given in Eq. (1.1). This expression combines the four generalized variables (IM, EDP, DM, and DV) of the performance assessment framework to describe the outcome in a probabilistic sense (Deierlein et al., 2003):

$$\lambda(DV) = \iiint p[DV|DM]p[DM|EDP]p[EDP|IM]\lambda(IM) dIMdEDPdDM \quad (1.1)$$

This equation follows directly from the total probability theorem, where uncertainties in each aspect of the solution are described in terms of independent conditional probabilities.

An important feature of PBEE is the definition of performance metrics that are relevant to decision making for seismic risk mitigation. These metrics reflect direct economic losses (repair and restoration costs), loss in functionality (or downtime), and risk casualties (Deierlein et al., 2003). If the analysis is performed on an existing building to evaluate whether it is safe enough or has satisfactorily low earthquake repair costs, the same procedure can be applied to assess the cost-effectiveness of retrofitting measures to reduce future losses, referring to the reduction of the present value of losses as “benefit”.

The PEER framework constituted the technical basis of the FEMA P-58 methodology (ATC, 2018), developed by the Applied Technology Council (ATC) in association with FEMA with the objective of introducing performance measures that can be understood by decision makers, and relating to the amount of damage the building may experience and its consequence in terms of repair and reconstruction costs, casualties, loss of use or occupancy. It includes the development of a tool for the implementation of the methodology, i.e. the Performance Assessment Calculation Tool (PACT).

Within the politics to reduce the seismic risk and communicate the risk to stakeholders, it is worth mentioning the measures introduced in Italy. In 2017, after the destructive earthquakes that occurred in 2009 near L'Aquila, in the Abruzzo region, and 2016 in the Centre Italy, the Italian government approved the Ministerial Decree n. 58 containing the new Sismabonus (Decreto ministerial 58/2017), which includes the Guidelines for the classification of the seismic risk of buildings. The framework provided by the Guidelines allows to assess the seismic performance of the building in terms of economic losses and structural collapse capacity and to classify it, before and after strengthening, in a letter-based scale from A+ to G+. This framework is aimed at practitioners that want to assess the overall seismic performance in a simplified form and allows them to deal with the sophisticated concepts of modern seismic design such as the Expected Annual Loss (EAL) and the reconstruction cost. In Italy, despite the national debate after the economic impact of the recent major earthquakes of L'Aquila and Emilia Romagna, there is not a compulsory insurance coverage for seismic events. The Guidelines provide a tool to determine the fiscal incentive for citizens intending to retrofit their house, based on the location and typology of the building and on the reduction of seismic risk class after the interventions.

The work developed within this thesis aims at giving a contribution to the seismic vulnerability assessment of old RC buildings in Portugal, which represent about 50% of the total building stock in the country, according to the 2011 Census Survey (<http://censos.ine.pt/>). According to the author's knowledge, there are no detailed loss estimation models applied to old wall-frame RC buildings in Portugal. Therefore, this work focuses on the vulnerability assessment of wall-frame building typology with smooth steel rebars built between 1960 and 1980. Due to the lack of post-earthquake data regarding damage for this type of buildings in Portugal, an analytical methodology has been adopted herein. In this study, a fully probabilistic methodology is adopted to estimate economic losses in a case study building. This methodology is based on the PEER centre probabilistic framework. The approach incorporates different sources of uncertainties: (i) uncertainty in the seismic hazard at the site; (ii) uncertainty in the structural response; (iii) uncertainty on the fragility of individual structural and non-structural components.

### 1.3. Objectives and main contributions

The aim of this work is to propose a procedure to develop a vulnerability model for the risk assessment of a certain reinforced concrete typology, i.e. old wall-frame building typology. Namely, the following aspects will be addressed:

- 1.Characterization of the building of a typology, focusing on the main features and structural behaviour;
- 2.Definition of modelling approach and discussion on modelling issues which concern the specific typology;
- 3.Addressing various sources of uncertainty;
- 4.Analysis of the seismic safety of the building and definition of damage states and the likely collapse mechanisms when the structure reaches large levels of damage;
- 5.Definition of a methodology for the economic loss assessment of old RC buildings and definition of the vulnerability of the considered typology;
- 6.Investigation of the effectiveness of different retrofitting strategies.

The work performed to achieve the referred objectives led to the contributions presented in this thesis and to the following journal publications:

- Caruso, C., Bento, R., Marino, E. M. and Castro, J. M. (2018) ‘Relevance of torsional effects on the seismic assessment of an old RC frame-wall building in Lisbon’, *Journal of Building Engineering*. Elsevier Ltd, 19, pp. 459–471. doi: 10.1016/j.jobbe.2018.05.010.
- Caruso, C., Bento, R., Sousa, R. and Correia, A. A. (2019) ‘Modelling strain penetration effects in RC walls with smooth steel bars’, *Magazine of Concrete Research*, 71(17), pp. 894–906. doi: 10.1680/jmacr.18.00052.
- Caruso, C., Bento, R. and Castro, J. M. (2019) ‘A contribution to the seismic performance and loss assessment of old RC wall-frame buildings’, *Engineering Structures*. Elsevier, 197. doi: 10.1016/j.engstruct.2019.109369.

### 1.4. Thesis layout

The present thesis has been divided in eight different chapters. The main tasks and methodologies adopted are described next:

**Chapter 1** – The first, and current chapter provides a general introduction to several aspects addressed in the thesis and the main scope and motivation.

**Chapter 2** – The second Chapter focuses on the numerical simulation of the seismic behaviour of RC walls making use of fibre-based nonlinear beam elements. Even though it is common to assume a

perfect bond between the reinforcing bars and concrete, the relative bond-slip deformations between the two materials can contribute up to 40% of the total lateral deformation of columns when ribbed rebars are used and up to 90% when in the presence of smooth rebars. This chapter intends to be a contribution to understand the importance of these effects in old RC walls and to provide indications regarding the use of a simplified bond-slip model.

**Chapter 3** – The third chapter provides an overview of the main characteristics of reinforced concrete frame buildings built in Portugal within a specific period range, i.e. 1955-1970. It provides an overview on the characterization of the examined typology based on the documents found in the literature and City Hall: (i) description and characterization of structural elements; (ii) mechanical characterization of the materials; (iii) the identification of the main structural and construction weaknesses. A case study building is chosen and a three-dimensional numerical model is developed, taking into account its main characteristics, such as (i) smooth reinforcing bars; (ii) infill walls; (iii) limited ductility properties. Afterwards, a brief review of uncertain modelling parameters (materials properties uncertainty) is presented. Then, sensitivity analysis is used in order to point out the dependence of the seismic response parameters to several modelling variables.

**Chapter 4** – Chapter four investigates the importance of assessing the torsional effects in old RC wall-frame buildings. To this objective, the applicability of the N2 method in its original formulation (Original N2) and the Extended N2 method (specifically conceived to predict the torsional response) is analysed through a comparison with the more reliable nonlinear *Time-History* dynamic analysis. Moreover, the influence of torsion on the response parameters, namely chord rotation and shear strength is assessed. A proposal is made to evaluate the shear demand by taking into account the nonlinear behaviour of the structure.

**Chapter 5** – The fifth chapter focuses on the seismic vulnerability assessment of old RC buildings. An analytical procedure is proposed to estimate the fragility functions of non-ductile reinforced concrete walls with smooth reinforcing bars and light transversal reinforcement, taking into account the strength penetration effects. To illustrate the procedure the case study building is considered. The approach used for the seismic performance assessment adopts component-based fragility and loss functions for the damage assessment of the structural and non-structural elements, adapted to the Portuguese reality. The results provide the economic losses of the building as a function of the ground motion intensity level. Finally, capacity and fragility curves of the case study building are compared with previous studies performed on old RC buildings.

**Chapter 6** – Chapter number six takes the methodology derived in the previous chapter and apply it to compare different retrofitting strategies. Fragility and vulnerability functions are developed for this structure, before and after strengthening. The feasibility of different retrofitting strategies is

investigated in terms of economic loss and compared through a cost- benefit analysis framework for guiding decision.

**Chapter 7** – The final chapter summarizes the main conclusions of the thesis and provides guidelines for future works intended to extend and improve the subjects addressed herein.



## **2. MODELLING STRAIN PENETRATION EFFECTS IN RC WALLS WITH SMOOTH BARS**

### **2.1. Introduction**

An important number of RC frame and dual wall-frame RC structures in southern Europe were constructed before the introduction of modern seismic codes, namely before the 1980s. Considering dual wall-frame RC structures and their potential seismic vulnerability, it seems important to evaluate the validity of different numerical models that can be used to assess the seismic performance of these RC walls, in particular the ones featuring smooth rebars.

Beam-column finite elements are widely used to simulate the nonlinear response of structures. The application of such finite element formulation has proved to be adequate for frame structures, combining the accuracy in the estimation of global response parameters with an appreciable computational efficiency. However, whilst slender frame elements tend to exhibit a response dominated by their flexural component, the response of wall structures combines other types of deformation, such as shear deformations, which are difficult to be explicitly modelled with beam-column elements. In addition, limited investigation has been carried out so far to assess the contribution of strain penetration (SP) effects at the anchorage region of RC walls.

Hence, this work is focused on the numerical simulation of RC walls, with particular focus on the importance of SP effects on their seismic behaviour. This phenomenon results in fixed-end rotations at the wall-foundation interface, which can represent an important contribution to the total lateral deformation of the member. Previous studies on RC columns, e.g. Sezen and Moehle (2004) and Goodnight et al. (2015), indicate that SP deformations can contribute up to 40% of the total lateral deformation of columns when ribbed rebars are used. On the other hand, experimental tests conducted on both RC columns (Verderame et al., 2008a) and beam-column joints (Melo et al., 2011) with smooth rebars reveal that this mechanism may contribute to nearly 90% of the overall member deformation at failure. These results show that SP effects can be particularly relevant in older RC members, often characterized by inadequate detailing, insufficient anchorage lengths and/or the presence of smooth rebars. As an example of the construction practice which dates from the 1960s, Figure 2.1 (Montepio Geral, 1960) shows the foundation detailing of a RC wall in a dual wall-frame system, built in Lisbon, Portugal. The foundation system was realized with smooth reinforcing and no indications are given concerning the rebars' anchorage length, which was probably based on common-practice experience.

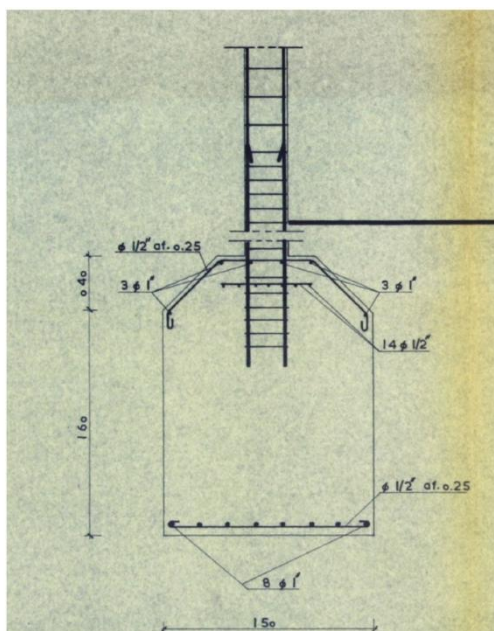


Figure 2.1 –Detailing of foundation system of an RC wall (Montepio Geral, 1690)

This study starts with a brief literature review on the use of distributed plasticity models, namely regarding the importance of shear deformations and SP effects. The consideration of different element formulations of distributed plasticity models is then analysed comparing the respective numerical response against the experimental results of a slender RC wall tested in the past by Dazio et al. (2009). Subsequently, these numerical models are used to explore the consideration of different anchorage conditions, such as rebar surface (ribbed or smooth) and different embedment lengths. Ultimately, this Chapter provides practical recommendations and simplified solutions to model the nonlinear response of RC walls, which can be used in engineering practice, when nonlinear models are used, to simulate the seismic response of existing RC buildings.

## 2.2. Modelling Issues Associated with the Numerical Simulation of RC Walls

### 2.2.1. Element Formulation

The structural response of RC walls depends largely on their geometric characteristics, namely the shear span-to-depth ratio. In general, for ratios larger than (about) 2.5, RC walls are classified as slender walls and are essentially controlled by flexural behaviour. In this case, the impact of shear deformations on global engineering demand parameters, like member forces and inter-storey drift displacements, will be typically small and can possibly be neglected. For smaller shear span ratios, walls are considered as squat and shear deformations are expected to play an increasing role in the member response (Priestley et al., 2007).

In fact, and contrarily to slender columns, whose behaviour is essentially governed by flexure, the seismic response of RC walls is more complex and their failure can be expressed through flexural, diagonal tension, diagonal compression or sliding shear failure mechanisms (Paulay and Priestley, 1992). Quasi-static cyclic tests on slender RC walls from Dazio et al. (2009) showed that the ratio of shear to flexural deformations varies between 5% and 13%. Moreover, for increasing displacement demand, the shear to flexure deformations' ratio tends to remain approximately constant if the shear capacity of the walls does not significantly degrade (Beyer et al., 2011).

The above discussion is particularly relevant when selecting the numerical tool to model these RC walls. The employment of either lumped or distributed plasticity elements results in an accurate and efficient solution to model the nonlinear behaviour of slender RC elements. However, considering their limitations to account for shear deformations, their application to walls should deserve additional attention. On the other hand, advanced modelling approaches, such as solid or shell elements, are capable to account directly for the interaction between axial force, flexure and shear, but are computationally demanding and seldom used in common engineering practice. For additional discussion, a state of the art review of different macro-modelling approaches for RC walls was presented by Wu and Lan (2016). It addresses important modelling issues, including the interaction between flexure and shear.

In this framework, reference should also be made to a study developed by Almeida et al. (2016), regarding the identification of the most suitable approach for modelling the inelastic behaviour of RC walls. In such study, shell element models were used as benchmark to assess the extent to which pure flexural models, such as beam elements, can capture the response of elements which have non-negligible shear deformations. The outcome of the work shows that, for slender walls, where a predominant flexural response is expected, the computation of global quantities, such as stiffness up to peak and force is moderately sensitive to the different modelling approaches.

Considering the above limitations, and before addressing the simulation of SP effects, the numerical response of a case-study RC wall, featuring different formulation and discretization schemes, was firstly validated through a comparison with its experimental response. This preliminary study is described in more detail in Section 2.3.2.

### ***2.2.2. Strain Penetration Effects***

RC members subjected to seismic loading can show localized relative deformations occurring between the reinforcing bars and the surrounding concrete. The transfer mechanism of rebar forces to the surrounding concrete occurs due to chemical adhesion between steel and concrete, friction at the interface between both materials and bearing actions of the ribs against the concrete (Sousa, 2015). When occurring at the connection nodes between adjacent members, these phenomena, generally

referred to as SP or bond-slip effects, lead to the development of an additional rotation at the extremity of the members due to the action of lateral loads.

This fixed-end rotation results from the spreading of rebars' strains along the anchorage region, which causes strain incompatibility between the reinforcement and the surrounding concrete. To limit these deformations, it is necessary to provide a sufficiently long embedment length ( $L_e$ ) allowing the transfer of the axial load on the rebar to the surrounding concrete through the contact surface. Whenever the embedment length is insufficient, the rebar experiences an important increase of slip, leading to a large increase of the element's base rotation or even failure of the anchorage system (Figure 2.2).

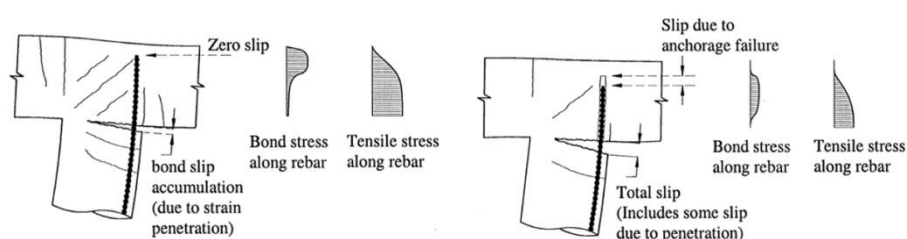


Figure 2.2 – Behaviour of anchorage region with adequate (left) and limited (right) embedment length (adapted from Zhao and Sritharan 2007)

Generally, the numerical simulation of RC structures assumes a perfect bond between the two materials. However, for increasing load demands, breaking of the bond occurs and bond-slip between reinforcing steel and surrounding concrete takes place. Even though relatively large anchorage lengths are provided, avoiding the failure of the anchorage system, these deformations can represent an important contribution to the global deformations of the members (e.g., (Filippou et al., 1983); (Sezen and Moehle, 2004); (Goodnight et al., 2015)). In older RC structures, with inadequate anchorage detailing and/or smooth rebars, with much reduced bond strength, these effects become more relevant, as noted by (Verderame et al., 2008a) and (Melo et al., 2011).

Despite the recognized contribution of SP effects to the overall member's deformations, the numerical models available to simulate these nonlinear effects are still very limited. Although these effects can be explicitly simulated in finite element software featuring highly discretized solid elements capable of describing the anchorage region (e.g., (Lowe and Moehle, 1999); (Salem and Maekawa, 2004); (Jendele and Cervenka, 2006); (Casanova et al., 2012); (Mendes and Castro, 2013)), conventional beam element formulation does not allow modelling the interface between the reinforcement and the surrounding concrete. To overcome these limitations, several studies have been conducted in recent years to develop models compatible with a beam element formulation and capable of accounting for bond-slip effects, e.g., (Sezen and Moehle, 2004) (Zhao and Sritharan, 2007) (Monti et al., 1997). Despite the number of studies developed, only a few have been incorporated in commercial software

packages used by practitioners. The interested reader can find a description of some of these models in Sousa (2015).

Considering the previous limitations, engineering practitioners often resort to simplified modelling approaches such as the elongation of the structural element by the strain penetration length or the definition of linear rotational springs at the extremities of the elements. Despite the improvements in the computed response, the former approaches present important limitations, namely the change in the elastic properties of the structure or the underestimation of the shear forces developed at the element (Sousa, 2015).

An alternative, and simpler approach, involves the modification of the reinforcing steel constitutive law. According to Varum (2003), it is possible to take into account the bond-slip effect through a correction factor ( $\lambda$ ) that modifies the constitutive law of the reinforcement. This slippage factor represents the ratio between concrete and steel strains (Equation (2.1)), and expresses the correction of the average steel strain in a RC finite element. According to this proposal, the steel constitutive law is assumed to be bilinear with elastic perfectly-plastic behaviour, as represented in Figure 2.3. In turn, Equations (2.2) to (2.4) express, respectively, the modifications in the strain, stress and modulus of elasticity of the steel, to account for the bond-slip effect (Varum, 2003) (Fernandes et al., 2007).

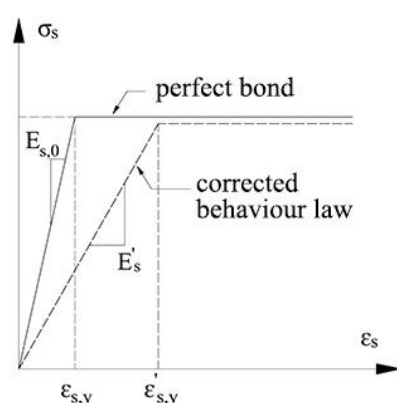


Figure 2.3 – Correction of the steel reinforcing law (adapted from (Varum, 2003))

At the current state-of-the-art, these models lack clear application guidance. Furthermore, they require additional calibration with the aim of adjusting the different parameters to alternative element typologies and anchorage conditions, such as the presence of smooth rebars or insufficient anchorage length. As an attempt to contribute to minimize these limitations, the following section presents case studies where the response of three RC walls, submitted to experimental cyclic tests, are numerically simulated considering different anchorage conditions. The outcome of these analyses provides indicative parameters to modify the reinforcing steel constitutive law in order to take into account the bond-slip effects under different loading conditions.

$$\lambda = \frac{\varepsilon_c}{\varepsilon_s} \quad (2.1)$$

$$\varepsilon'_{s,y} = \lambda \varepsilon_{s,y} \quad (2.2)$$

$$\sigma'_{s,y} = \sigma_{s,y} \quad (2.3)$$

$$E'_s = \frac{1}{\lambda} E_s \quad (2.4)$$

In the Equations (2.1) to (2.4),  $\varepsilon_c$  and  $\varepsilon_s$  are concrete and steel strains,  $\varepsilon_{s,y}$  is the steel yielding strain,  $\sigma_{s,y}$  is the steel yielding stress and  $E_s$  is the reinforcement modulus of elasticity.

## 2.3. Case studies

### 2.3.1. Description of the experimental tests

In the current study, three wall specimens analysed in previous studies were numerically modelled and subjected to pushover analysis. The characteristics of the RC wall specimens are representative of constructions without seismic detailing, with longitudinal reinforcement ratio ( $\rho_{long}$ ) smaller than 1%, a relatively low axial load ratio ( $N/A_g f_c$ ) and limited ductility properties of the longitudinal reinforcement.

The test unit WSH4 analysed by Dazio et al. (2009) is 2.00 m long and 0.15 m wide. The length of the shear span is 4.56 m for a shear span ratio of 2.3. In addition, the wall has no confining or stabilising reinforcement, i.e., it was not specifically designed for ductile behaviour. The wall specimens R1 and R2 have been tested by Oesterle et al. (1976). The horizontal length of the wall is 1.91 m and its web thickness is 0.102 m. Height of the walls is 4.57 m, for a shear span ratio of 2.4. The boundary zone of specimen R1 is not confined and the main flexural reinforcement is 1.47 % of the area of the boundary elements ( $\rho_{bound}$ ). Specimen R2 presents confined boundary elements, with 4% of reinforcement. The vertical web reinforcement ( $\rho_{web}$ ) is 0.25% of the gross concrete area of the wall section.

The details of the reinforcement (ribbed rebars) are shown in Figure 2.4 whilst Table 2.1 summarizes the information regarding the axial force and reinforcement ratios. More information about the material properties can be found in Table 2.2 and Table 2.3, for concrete and steel, respectively. A detailed description of the tests can be found in Dazio et al. (2009) for wall WSH4 and Oesterle et al. (1976) for walls R1 and R2.

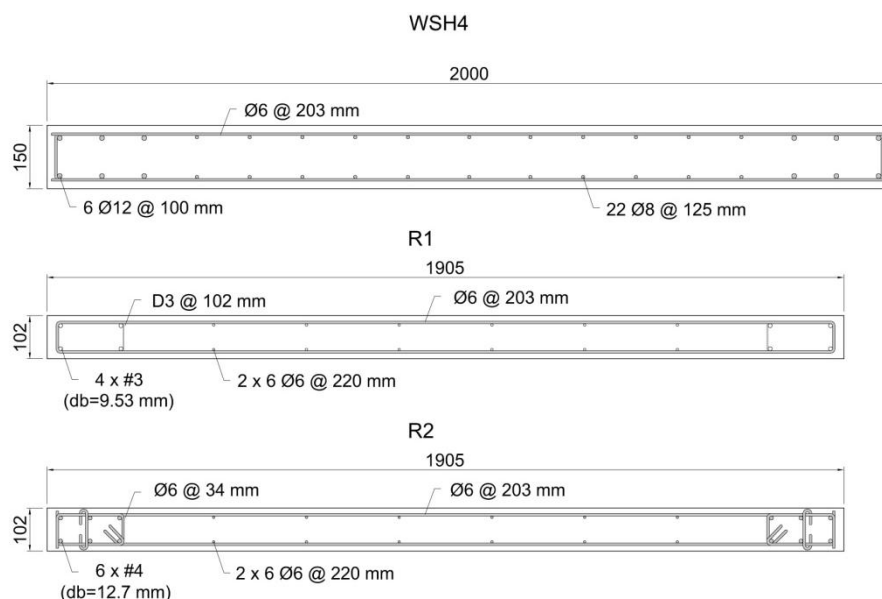


Figure 2.4 –Reinforcement layout in the plastic zone of the wall WSH4 [dimensions in mm]

Table 2.1 –Mechanical ratios of reinforced concrete wall specimens

Test unit	Axial load and ratio		Reinforcement ratios			
	$N$ (kN)	$N/A_g f_c$ (%)	$\rho_{bound}$ (%)	$\rho_{web}$ (%)	$\rho_{long}$ (%)	$\rho_h$ (%)
WSH4	695	5.7	1.54	0.54	0.82	0.25
R1	70	0.8	1.47	0.25	0.32	0.31
R2	100	1.1	4.00	0.25	0.57	0.31

Table 2.2 – Mechanical properties of concrete material

Test unit	$f_c$ (MPa)	$\varepsilon_c$ (‰)	$E_c$ (GPa)
WSH4	-40.9	-2.0	38.5
R1	-44.8	-2.0	27.8
R2	-46.4	-2.0	26.8

Table 2.3 – Mechanical properties of reinforcing steel

Test unit	$f_y$ (MPa)	$f_u$ (MPa)	$\varepsilon_{sy}$ (‰)	$\varepsilon_{su}$ (‰)	$E_s$ (MPa)
WSH4					
Ø 12	576	675	2.7	73	210000
Ø 8	584	714	2.7	79	220000
R1					
Ø 6	522	700	2.4	122	217000
# 3	513	765	2.7	98	192000
R2					
Ø 6	535	691	2.4	122	225000
# 3	450	708	2.4	123	186000

### 2.3.2. Numerical Modelling Options

Before addressing the numerical simulation of strain penetration effects, it is fundamental to guarantee that the behaviour of the wall, i.e., the response of the element above the anchorage region, can be accurately represented with the consideration of beam elements with distributed plasticity. In this section, three distinct modelling options to simulate the behaviour of the cantilever wall are presented. They differ with regard to the beam element formulation and mesh discretization.

Fibre-based nonlinear beam elements idealize a section into a number of discrete fibres to which a uniaxial material constitutive relation is assigned. These fibre sections are defined along the element length through a finite number of integration points (IPs) allowing a description of the spread of inelasticity along the element. The determination of the response parameters at the different IPs can be accomplished following force-based (FB) or displacement-based (DB) formulations, which verify the equilibrium in an exact and averaged way, respectively. In this regard, and contrarily to the FB case, where a single element with a certain number of IPs can be used to compute the element response (usually through a Gauss-Lobatto integration scheme), in the DB case, the RC member needs to be discretized in several elements. In this latter case, two IPs per element are sufficient to determine the element response if a Gauss-Legendre integration scheme is adopted.

In the present study, the RC wall WSH4 was modelled in the OpenSees platform (McKenna et al., 2000) considering 3 different formulation/discretization schemes, namely 2 FB models and 1 DB model. Although for the FB formulation 5 IPs are generally sufficient (Neuenhofer and Filippou, 1997), it has been shown that the post-peak element response is highly dependent on the number of IPs due to a numerical localization phenomenon (Almeida et al., 2016); therefore, an additional scheme with 9 IPs was also considered. Regarding the DB model, the wall was modelled with 4 elements, each of them with two Gauss-Legendre IPs.

For all the cases described above, the section of the wall was discretized in 200 fibres, which corresponds roughly to 1 fibre for each centimetre of wall length, for both cover and core. Moreover, the reinforcing steel was modelled using the uniaxial material 'Steel02' based on the Giuffrè-Menegotto-Pinto constitutive model (Menegotto and Pinto, 1973). On the other hand, the cover and core concrete were modelled using the uniaxial material 'Concrete 04', which is based on the model proposed by Popovics (1973). The mechanical properties of the confined concrete were determined according to Mander et al. (1988), with a geometrical effectiveness coefficient of confinement  $C_e = 0.5$  (Almeida et al., 2016).

A comparison of the shear force-top displacement curves presented in Figure 2.5 shows a good agreement between the numerical and experimental results for wall WSH4. Up to peak strength, the numerical predictions are very similar and are in line with the experimental results. Nonetheless, the model using FB elements appears to provide a better estimation of the peak strength than the model

employing DB elements, which shows an overestimation of the maximum lateral resisting force. After the peak strength, the predictions with the different modelling approaches diverge due to numerical localization, wherein curvatures concentrate at the most stressed sections of the elements (Calabrese et al., 2010).

Overall, and despite the potential limitations in the use of beam elements to model RC walls, highlighted in section 2.1, the results obtained indicate that the application of these models appear to produce reliable and acceptably accurate predictions of the behaviour of these RC walls. Based on the results obtained, the investigation of the importance of SP effects in old RC walls presented in the following section is conducted considering the numerical model featuring one force-based element with 5 IPs, for all the test units.

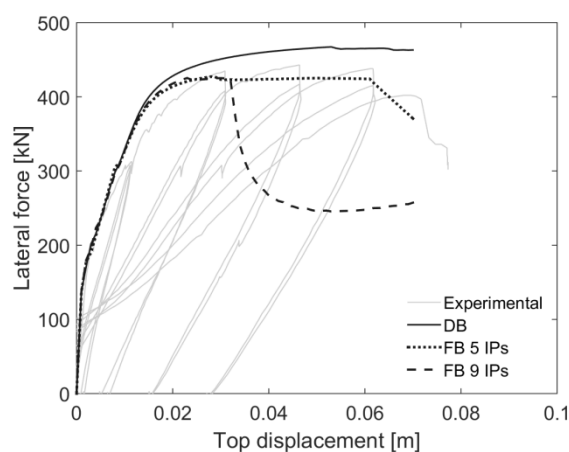


Figure 2.5 – Shear force-top displacement for the RC wall specimen WSH4, considering both FB and DB formulation

## 2.4. Numerical Results

### 2.4.1. Effects for Different Anchorage Conditions

Current software packages featuring beam elements, including the one used in this study, provide limited solutions to simulate SP effects, especially under specific conditions such as smooth rebars and limited anchorage length. Hence, these effects were firstly determined considering the bond-slip model proposed by Sousa (2015).

In addition to the geometrical and mechanical properties of the anchorage region of the elements, this model explicitly simulates the physical phenomena associated with strain penetration effects for a wide variety of anchorage conditions such as concrete strength, embedment length, rebar surface characteristics, rebar yielding or cyclic degradation, among others.

Devised to work as a zero-length element located at the extremity of the structural member, this model replicates the cross-section of the adjacent RC member, and the embedded length of each

cross-section's rebars is represented through a number of integration points (IPs) distributed along its anchorage region. These IPs feature independent bond stress-slip constitutive relations based on the model proposed in Model Code 2010 (fib, 2013), whereas both equilibrium and compatibility are enforced at every IP through an iterative procedure. A schematic representation of the model components is presented in Figure 2.6.

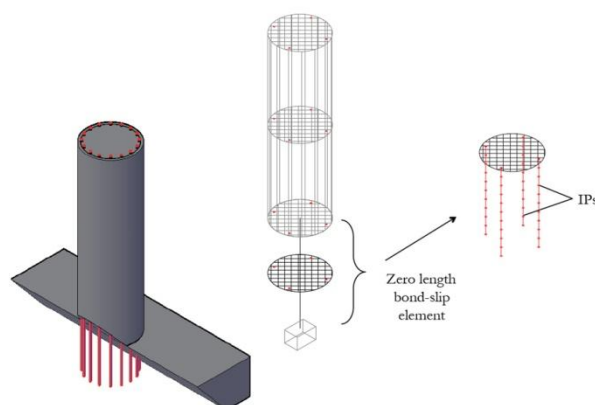


Figure 2.6 – Schematic representation of the different components of the bond-slip model by Sousa (2015) (adapted from Sousa (2015))

Once the moment-rotation relation associated with the bond-slip effects at the base of the RC wall is determined, a monotonic (tri-linear) law was adjusted to the computed response in order to calibrate the nonlinear rotational springs (Figure 2.7) to be assigned at the base of the RC wall element modelled in OpenSees. The numerical simulation of the wall specimens was conducted considering moment-rotation relationships that describe the bond-slip effects at the base of the wall corresponding to different rebars (ribbed and smooth) and embedment lengths, given in terms of bar diameters ( $d_b$ ). Table 2.4 summarizes all the considered anchorage conditions.

Table 2.4 – Anchorage conditions considered

	Rebars	$L_e$
Case 1	Ribbed	30 $d_b$
Case 2	Smooth	30 $d_b$
Case 3	Smooth	50 $d_b$
Case 4	Smooth	100 $d_b$
Case 5	Smooth	150 $d_b$
Case 6	Smooth	200 $d_b$

It should be mentioned that, for the case of ribbed rebars, the effect of bond stress reduction due to cyclic degradation was included, while this effect was neglected for the case of smooth rebars. Considering the absence of ribs in the rebars, it is expected that most of the bond force results from adhesion and friction between the reinforcement and the surrounding concrete. Consequently, it is not

expected that the anchorage system exhibits meaningful bond degradation due to cyclic loading (Sousa, 2015).

The results presented in the Figure 2.7 show that, for the case of smooth rebars, the anchorage system can only withstand a fraction of the maximum bending moment developed for the case with ribbed rebars. Given the absence of ribs, the bond stress is significantly lower and the rebars cannot sustain large anchorage forces. The decrease in anchorage strength becomes more pronounced as the embedment length is reduced. If this length becomes too short, the bond forces developed along the embedment length become insufficient to sustain the yielding force of the rebar and, consequently, the moment capacity of the wall can be considerably reduced. It is worth mentioning that while for the anchorage region with ribbed rebars an embedment length of  $30 d_b$  is sufficient to develop the maximum bending moment capacity of the anchorage system, for the case of smooth rebars an embedment length of  $200 d_b$  was considered in order to obtain the maximum bending moment capacity.

For wall specimen WSH4 (Figure 2.7a), the combination of smooth rebars with  $30 d_b$  of embedment length led to a reduction on the bending moment capacity to about half the one sustained with adequate bond conditions, i.e., ribbed rebars with an embedment length of  $30 d_b$ . For wall specimens R1 (Figure 2.7b) and R2 (Figure 2.7c) this reduction is even more important. The combination of smooth rebars with  $30 d_b$  of embedment length led to a reduction on the bending moment capacity to about a third and a fifth of that sustained with adequate bond conditions, respectively for test units R1 and R2.

Once the monotonic response of the anchorage system is determined for the five different anchorage conditions considered (Table 2.4), simplified tri-linear moment-rotation relationships were adjusted to the numerical results (Figure 2.7). As noted before, these relations are to be assigned to zero-length elements that, in turn, will be defined at the base of the wall element. These new models, defined in OpenSees, were submitted to nonlinear static (pushover) analysis in order to evaluate the changes in the global behaviour resulting from the consideration of the SP effects with different anchorage conditions. The results obtained, expressed in terms of base shear-top displacement, are presented in Figure 2.8, for wall specimens WSH4 (Figure 2.8a), R1 (Figure 2.8b) and R2 (Figure 2.8c).

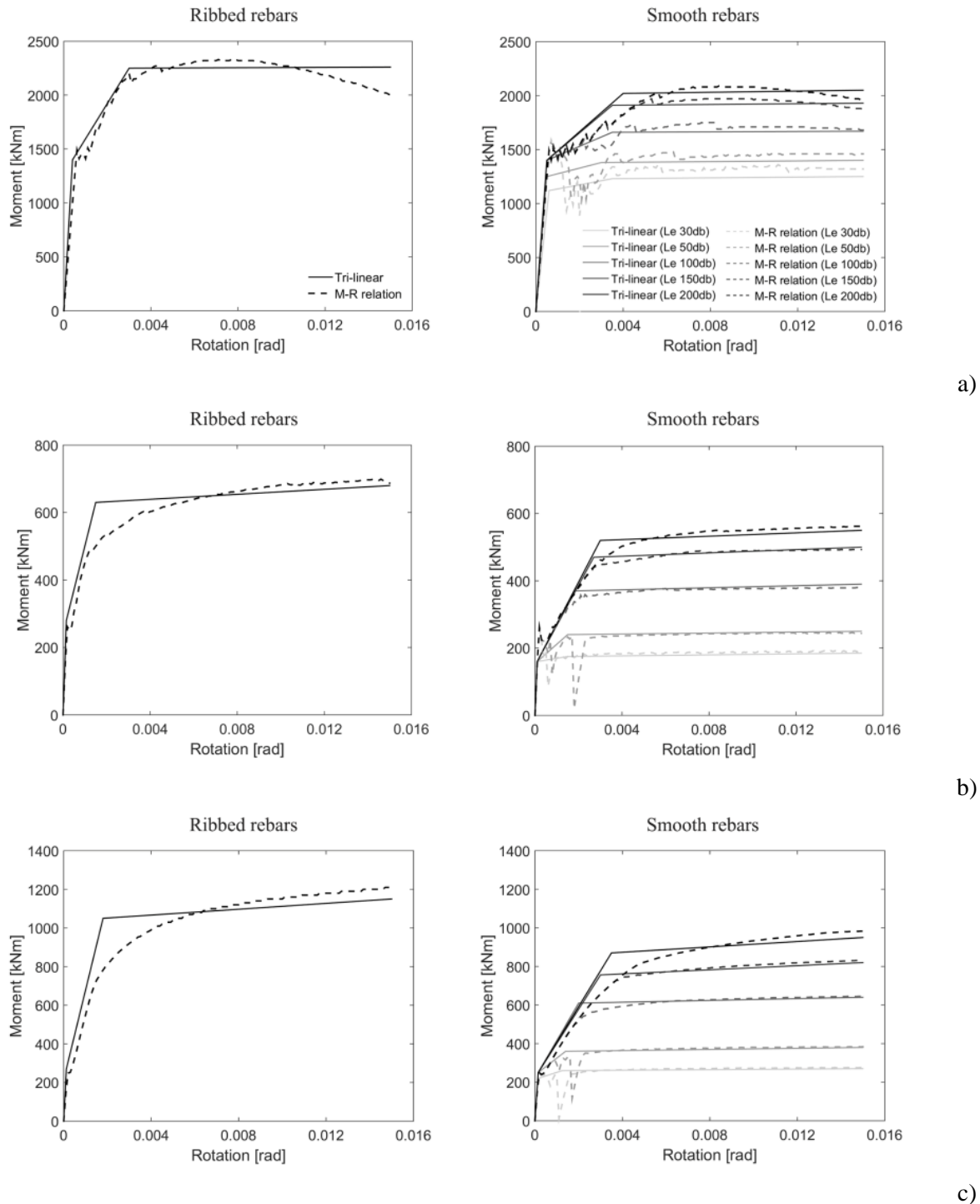


Figure 2.7 – Moment-rotation (M-R) relation for ribbed and smooth rebars with different embedment length for the RC wall specimens WSH4 (a), R1 (b) and R2 (c)

The results presented in Figure 2.8 show that the consideration of SP effects lead to an increase of the overall flexibility of the walls. This expected consequence can be noted in a softer capacity curve of the models with SP effects with respect to the one with fixed-base conditions (i.e., without SP effects). Furthermore, in the models featuring smooth rebars with different embedment lengths (i.e.,

from  $Le = 200 d_b$  to  $Le = 30 d_b$ ), the RC walls present also a reduction in the shear strength, as the embedment length of the rebars decreases.

Still with respect to Figure 2.8, it should be noted that, despite the strength of the anchorage system with smooth rebars and  $Le = 200 d_b$  is lower than the one with ribbed rebars with  $Le = 30 d_b$  (see Figure 2.7), it is still sufficiently large to sustain the maximum flexural moment that the wall can develop. For this reason, the maximum shear force in the wall is very similar for both cases.

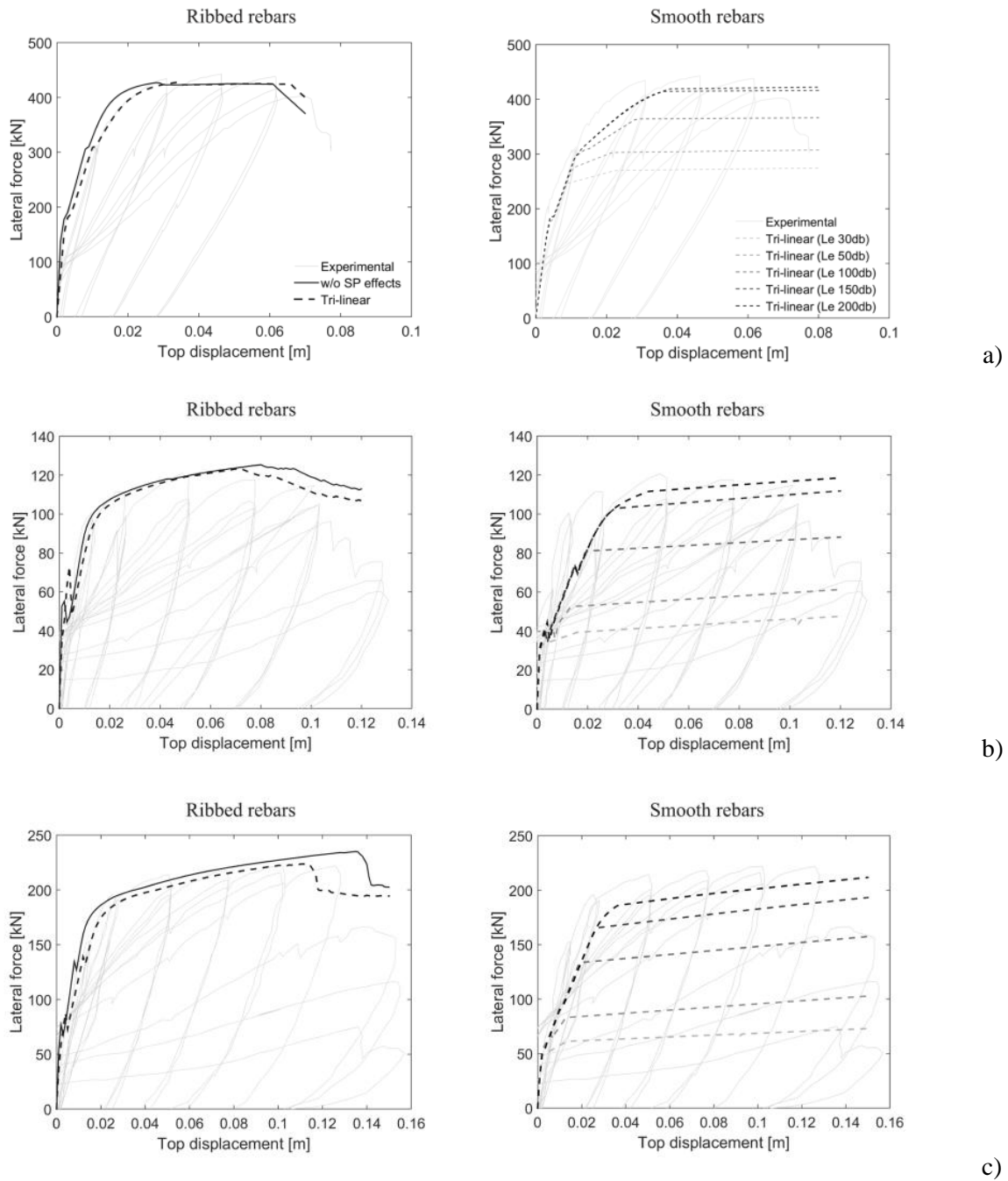


Figure 2.8 – Shear force-top displacement relations for ribbed and smooth rebars with different embedment length for the RC wall specimens WSH4 (a), R1 (b) and R2 (c)

### 2.4.2. Calibration of Reinforcement Properties to Account for SP Effects

The results presented in the previous section demonstrate the importance of incorporating the SP effects in seismic analyses, particularly for structures with smooth rebars. Considering the limitations in the numerical models available to simulate these effects, this section presents the results of a calibration procedure carried out to establish reference reduction values for the Young's Modulus and the maximum stress of the reinforcing steel.

In order to estimate the reduction of the rebar's capacity, a constant averaged bond stress is considered along the total anchorage length. Taking in consideration the geometrical characteristic of the rebars (the area  $A_s$  and the perimeter  $P$ ) and the maximum constant averaged bond stress  $\tau_{max}$ , it is possible to evaluate the maximum steel stress  $f_s$  developed for different embedment lengths, through equilibrium considerations between the force in the rebar  $F_{y,max}$  and the anchorage force  $F_a$ :

$$F_{y,max} = F_a \quad (2.5)$$

$$A_s f_s = PL_e \tau_{max} \quad (2.6)$$

The value of  $\tau_{max}$  adopted follows the one suggested in Model Code 2010 (fib, 2013). For the case of smooth rebars:

$$\tau_{max} = 0.2\sqrt{f_{cm}} \quad (2.7)$$

where  $f_{cm}$  is the mean value of the concrete compressive strength in MPa.

The application of this procedure leads to reductions of  $F_{y,max}$  that ranged from 0 to 80% of the expected rebar strength. These values are summarized in Table 2.5 together with the values of the reduction of Young's Modulus obtained for all cases.

The results show that the response of the model with the calibrated parameters (SP model) is in line with the one obtained considering a rotational spring with a tri-linear relation. Nonetheless, the responses in the post-peak branch present some important differences. This is essentially because the model with the tri-linear rotational spring accounts for the SP deformations throughout the entire response of the wall, i.e., both at the linear and nonlinear regime, whilst the reduction in the Young's Modulus increases the wall flexibility only up to yielding of the rebars. This effect can be appraised in the larger lateral displacement of the wall when the strength decreases abruptly (Figure 2.9). In the presence of smooth rebars (Figure 2.9), the anchorage system becomes even more flexible, reducing the strength demand in the wall for the same level of lateral top displacement and precluding the wall to reach its maximum lateral strength. In these cases, the wall will eventually fail due to failure of the anchorage system.

Table 2.5 –Summary of the percentage reduction for the Young's modulus ( $E$ ) and the maximum strength ( $F_{y,max}$ ) of the reinforcing steel

Test unit	Ribbed rebars		Smooth rebars	
	Red. of $E$	Red. of $F_{y,max}$	Red. of $E$	Red. of $F_{y,max}$
WSH4				
$Le = 200 d_b$	-	-	50%	-
$Le = 150 d_b$	-	-	50%	5%
$Le = 100 d_b$	-	-	50%	20%
$Le = 50 d_b$	-	-	50%	50%
$Le = 30 d_b$	30%	-	50%	60%
R1				
$Le = 200 d_b$	-	-	50%	-
$Le = 150 d_b$	-	-	50%	10%
$Le = 100 d_b$	-	-	50%	30%
$Le = 50 d_b$	-	-	50%	60%
$Le = 30 d_b$	20%	-	50%	80%
R2				
$Le = 200 d_b$	-	-	50%	-
$Le = 150 d_b$	-	-	50%	10%
$Le = 100 d_b$	-	-	50%	30%
$Le = 50 d_b$	-	-	50%	60%
$Le = 30 d_b$	25%	-	50%	80%

## 2.5. Conclusions

This chapter presents a numerical study addressing the behaviour of RC walls, in particular, the importance of strain penetration effects in the seismic behaviour of these elements. For this purpose, three slender RC walls experimentally tested in the past were used as benchmark for which different anchorage conditions were considered.

The quantification of the SP effects was firstly determined with an explicit bond-slip model capable of accounting for different properties of the anchorage region. Once the moment-rotation relationships were determined for different rebar types (ribbed and smooth) and anchorage lengths, these relations were incorporated through zero-length elements at the base of the model of the wall.

The results of the pushover analyses carried out showed that the consideration of SP effects introduces a non-negligible flexibility at the base of the walls which becomes more relevant as the anchorage conditions deteriorate, namely with the consideration of smooth rebars and reduced anchorage lengths. Moreover, when in presence of reduced embedment lengths, the lateral strength of the wall can be significantly compromised due to failure of the anchorage system.

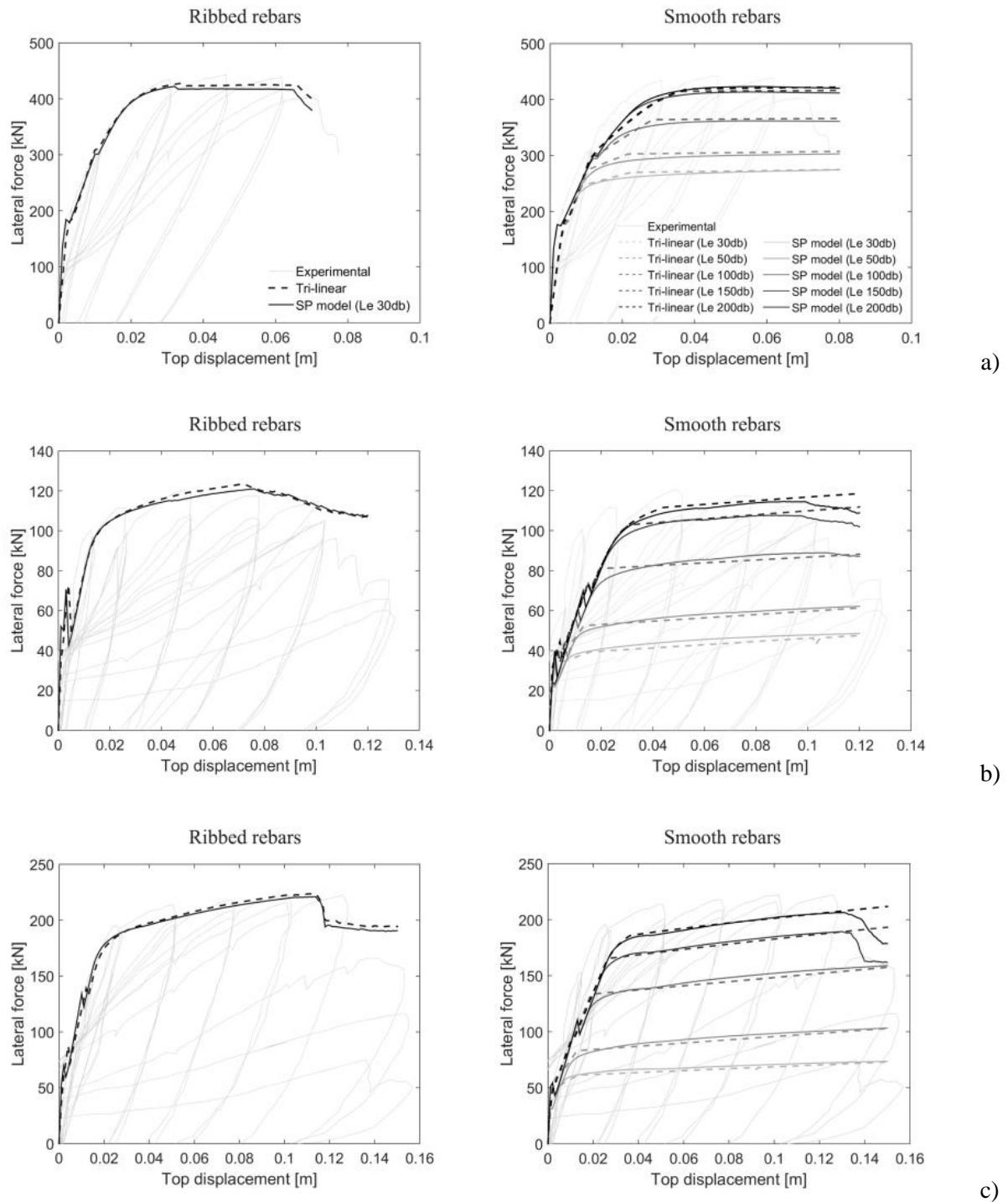


Figure 2.9 – Comparison of the shear force-top displacement relations wall WSH4 (a), R1 (b) and R2 (c), considering the cases of ribbed and smooth rebars with different embedment length, considering the model with calibrated reinforcement parameters (SP model) and the one considering a rotational spring with a tri-linear relation

The results allowed to define indicative values that can be used to reduce the Young's Modulus and the maximum strength of the rebars in order to implicitly account for such effects in numerical analyses in a very expedite manner. Hence, it was observed that, for ribbed rebars with appropriate embedment length, the reduction in the Young's Modulus should be in the order of 20% to 30%,

whilst in the presence of smooth rebars this value should increase to values in the order of 50%, regardless of the embedment length. In what concerns the rebars' strength, this value is naturally dependent on the embedment length, and may need to be reduced to values in the order of 80% of its expected value. Appropriate general expressions to estimate this parameter for different anchorage lengths were presented in this chapter. With the present study, the author intend to propose general reference values for modelling RC walls with similar characteristics.



### **3. SEISMIC ASSESSMENT OF AN EXISTING OLD FRAME-WALL RC BUILDING IN LISBON**

#### **3.1. Introduction**

Existing RC frame and dual wall-frame buildings designed before the introduction of modern seismic codes represent a significant percentage of the cities' building stock in many countries all over the world. Provisions for seismic design of structures and detailing of members resembling those stipulated in modern codes were not introduced until recently in most European countries. In Portugal, the first design codes that explicitly consider provisions for the seismic action date from 1958 (RSCCS, 1958) to 1961 (RSEP, 1961). However, such recommendations were over simplified and did not impose adequate seismic performance requirements. The importance of ductility in structural design was only introduced in 1983 by a new and more demanding code which is still in use nowadays (RSA, 1983).

Assessment methodologies have evolved significantly and methodologies based on deformation have been implemented in alternative to methodologies based on strengths (Priestley et al., 2007) (Calvi, 2013). Due to need for structural upgrading to meet more stringent seismic design requirements in earthquake prone areas, seismic assessment and structural retrofitting is becoming more and more important and receives today considerable emphasis throughout the world. In response to this need, efforts had been devoted to the study of RC buildings (frame and wall-frame structures) built between 1960 and 1980 (i.e. during this transition phase of seismic regulation codes) in the city of Lisbon, Portugal. These buildings represent a high percentage of the city building stock, and up to 49% of the Portuguese building stock (Silva et al., 2015a). In this study, a specific subcategory of buildings is selected within the RC buildings, which are referred to as RC wall-frame buildings and have the following characteristics: (i) 8 to 12 floors; (ii) an open ground storey and infills in the upper storeys; (iii) columns with rectangular cross-section mainly with the same strong axis orientation; (iv) eccentric RC core walls. This work presents the seismic assessment of a case study building with the aim of detecting and quantifying the expected deficiencies of this subcategory of RC buildings. A 3-D model of the building is developed using the OpenSees software (McKenna et al., 2000). The main features of the building are replicated in the model, such as (i) infill masonry walls and RC walls, (ii) smooth plain reinforcing bars, (iii) low dissipative behaviour of structural members due to inadequate reinforcement detailing. The model is calibrated through comparison of the results of ambient vibration tests.

It is acknowledged that many aspects of the seismic assessment process of existing structures can have a significant impact on the evaluated performance. Large source of uncertainties lies in the characterization of the ground motion but also in the definition of the building modelling parameters.

In view of the previous consideration, this chapter addresses the sensitivity of the seismic response parameters to uncertain modelling variables of the case study building. Current seismic codes do not consider explicitly the use of sensitivity analysis for the assessment of existing structure, that is on the contrary an important tool due to the aleatory and epistemic uncertainties involved. Previous studies have confirmed this issue and pointed out the importance of appropriately characterizing and propagating uncertainties in performance-based earthquake engineering. Liel et al. (2009), addressed the assessment of collapse risk of RC moment frame building including building designed according to outdated codes, showing that the modelling uncertainties increase the dispersion in the response fragility and disregarding them was un-conservative in most cases.

A number of studies on the use of sensitivity analysis were developed in which nonlinear static analyses are used to perform the seismic assessment of structures instead of the more demanding nonlinear dynamic ones. In (Haddad et al., 2017) sensitivity analysis was proposed as a tool to clearly point out the most important parameters to set an accurate investigation plan and to proceed to the seismic assessment according to a full probabilistic approach. A simplified approach involving a reduced number of nonlinear static analyses was proposed ( $2N+1$ , where  $N$  is the number of parameters). Its feasibility was verified by comparison with the results obtained from fragility curves built with the execution of a large number of nonlinear static analyses on models generated using Monte Carlo simulations. In (Celarec et al., 2012) the sensitivity of the seismic response parameters to the uncertainty modelling variable of the infills and RC frame was assessed using a simplified nonlinear method for the seismic performance assessment of the buildings. Uncertainties in the input parameters of infilled RC structure, e.g. structural component strength and stiffness, were considered.

Sensitivity analyses provide a straightforward method for interrogating the effects of modelling uncertainties on response quantities of interest. In this study, the effect of each random variable on the structural response is determined by varying a single modelling parameter and re-evaluating the structure's performance. The numerical investigation on the non-linear seismic behaviour of the building is carried out by means of static pushover analyses, within the N2 spectral assessment framework (Fajfar, 2000). Evaluation of the response parameters is based on performance-based assessment procedures and structural safety assessment procedures proposed in Part 3 of Eurocode 8 (EC8-3) (CEN, 2010) for the case of the reinforced concrete. With the results of the sensitivity analysis, it will be possible to identify the input parameters that have the greatest impact on the structural response. On the other hand, it will be also possible to integrate, in a more efficient way, the propagation of uncertainties in the probabilistic assessment of the structural collapse.

This chapter starts with the characterisation of old RC buildings (Section 3.2), followed by a description of the building typology chosen as the case study (Section 3.3). Afterwards, in Section

3.4, the seismic assessment of the building based on the N2 method procedure is performed and the results of sensitivity analyses are discussed.

### 3.2. Characteristics of Old RC buildings

In this study, RC frame and RC wall-frame buildings built between 1960 and 1980 in the city of Lisbon, Portugal, are identified in the Alvalade district, in Lisbon. This area resulted from an expansion plan of the city promoted by the municipality in 1944, and presents an elevated percentage of this type of buildings. In the work of Jarimba (2016), documents concerning 1693 buildings in this area were consulted, carrying out a careful survey of characteristics and relevant structural information and shown in Figure 3.1. A large number of buildings were identified as mixed masonry-RC (known as “placa”) buildings and few buildings as belonging to the “gaioleiro” typology (URM buildings). 17.4 % of buildings were identified as belonging to the RC frame or wall-frame building typology. In Figure 3.1, the buildings classified as "placa or concrete" correspond to buildings whose typology was difficult to classify due to the scarce amount of available information and the impossibility of visiting the site. The buildings identified as “concrete” refer to buildings built outside the period considered, i.e. they were built before or after the time range 1960-1980.

From the RC frame building typology built in the period between 1960 and 1980 some characteristics were identified (Jarimba, 2016): (i) the use of brick masonry infill walls; (ii) the use of infills of brick masonry internal walls; (iii) as for the pavement, it was found a prevalence of RC flat slabs and a minor quantity of precast slabs and void slabs; (iv) the increase in the number of levels of the buildings (the majority of RC buildings have between 5 and 9 levels, followed by buildings with 10 to 11 levels and buildings with up to 4 levels).

As previously stated, a high percentage of RC frame structures are deficient in terms of seismic resistance. Seismic rehabilitation efforts are required for this typology. The major causes of collapse in older, non-ductile buildings are the following (Ramirez and Miranda, 2012):

- these buildings were designed without considering appropriate seismic design criteria and without taking into account the effects of torsional vibrations;
- these buildings are more susceptible to beam–column joint shear failure, which may result in loss of vertical carrying capacity;
- column hinging is more likely to occur because no minimum strong column–weak beam ratio was considered in the design of these buildings;
- concentration of lateral deformation can lead to brittle shear brittle failure of columns and RC walls with low confinement and tie reinforcement;

- large lateral deformation can be developed due to bond-slip mechanism, increased by the presence of smooth rebars and rebars with small embedment length.

In the following, a brief review of the main characteristics in terms of material properties of the building typology is presented, focusing on the code provisions up to the present day.



Figure 3.1 – GIS data-base and thematic maps with identification of the Alvalade district

### 3.2.1. Mechanical properties of materials

The gradual change of material properties of the building stock in Portugal can be analysed together with the succession of the building codes. The first regulations including requirement for reinforced concrete properties date to 1918 (“Regulamento para o emprego do beton armado” 1918) and 1935 (RBA 1935), imposing a minimum mean value of the compressive strength ( $f_{cm}$ ) at 28 days of 120 kgf/cm<sup>2</sup> and 180 kgf/cm<sup>2</sup>, respectively (Table 3.1). In the code of 1967 (REBA, 1967) the concept of classes of concrete resistance was introduced, each one defined by the characteristic compressive strength ( $f_{ck}$ ) from approximately 18 to 40 MPa (B180/B225/B300/B350/B400). After the 80s, and with the introduction of new codes, i.e. RSA and Part 1 of Eurocode 2 (EC2-1) (CEN, 2001a), the concrete classes were adjusted to the international units (MPa) and extended to concrete classes B55

( $f_{ck} = 55$  MPa) and C90/105, respectively. In Table 3.1 the codes are listed in chronological order together with a summary of the main properties of the concrete.

Table 3.1 – Evolution of material properties associate to building codes

Code	Concrete	Steel
<i>Regulamento para o emprego do beton armado</i> (1918)	$f_{cm} \geq 120$ kgf/cm <sup>2</sup> ( $\approx 12$ MPa)	$f_{su} \geq 3800$ kgf/cm <sup>2</sup> ( $\approx 373$ MPa) $f_{sy} \geq f_{su}/2$ $\varepsilon_u = 22\%$
RBA (1935)	$f_{cm} \geq 180$ kgf/cm <sup>2</sup> ( $\approx 18$ MPa)	$f_{su} \geq 3700$ kgf/cm <sup>2</sup> ( $\approx 363$ MPa) $f_{sy} \geq 0.6 f_{su}$ $\varepsilon_u = 24\%$
REBA (1967)	B180/225/300/350/400 $f_{ck}$ 180 – 400 Kgf/cm <sup>2</sup> ( $\approx 18 - 40$ MPa)	A24/A40/A50 /A60 smooth or ribbed $f_{syk} = 24/40/50/60$ kgf/mm <sup>2</sup> $\varepsilon_u = 22/14/8/8\%$
REBAP + RSA (1983)	B15/... B55 $f_{ck}$ (MPa)	A235/A400/A500 $f_{syk} = 235/400/500$ MPa $\varepsilon_u = 24/14/12\%$
EC2 – 1 (2004)	C12/15; ... C90/105 $f_{ck}$ (Mpa) cylindric/cubic	S400/S500/S600 $f_{syk} = 400/500/600$ MPa $\varepsilon_u \geq 7.5\%$

Reinforcing steel bars play a key role in reinforced concrete structures. It is a construction material whose properties must be known to the users before being applied for design or assessment purposes. For RC buildings constructed in the 50s and the 60s in southern European countries up to 98% and 80% respectively of steel bars used in constructions were smooth (Verderame et al., 2011). In Portugal, a fraction of RC buildings was built with smooth (plain) bars with a lower resistance of the steel, up to the 70s (Silva et al., 2015a). Related to the mechanical characteristics of steel bars, the regulations of 1918 and 1935 required an ultimate strength ( $f_{su}$ ) greater than 3800 kgf/cm<sup>2</sup> and 3700 kgf/cm<sup>2</sup> for smooth reinforcing bars and a high ductility defined by the ultimate strain ( $\varepsilon_u$ ). The steel yield stress ( $f_{sy}$ ) was defined as a function of the ultimate strength. In the regulation of 1967 (REBA 1967) the steel resistance classes A24, A40, A50 and A60 were introduced, each class defined by a characteristic yielding tensile strength ( $f_{yk}$ ). Additionally, two types of bars were introduced, i.e. smooth and ribbed. In REBA, steel classes A24 and A40 (just for the cold formed case) were contemplated with smooth or ribbed surface. Later, with the introduction of the regulation dated 1983, i.e. REPAB (1983) applied together with RSA (1983), and EC2-1 (CEN 2004), the resistance classes were modified to A235/A400/A500 and S400/S500/S600, respectively (Table 3.1). It is worth noting that in REBAP only reinforcing steel A235 is contemplated with smooth or ribbed surface.

Only few experimental tests have been developed in the past in old smooth reinforcing steel bars. On the other hand, the results of tests performed in the period between 1960 and 1970 have been collected in Italy (e.g. (Verderame et al., 2011)). In Italy, the use of ribbed rebars was introduced for the first time in 1957, with the Circular 23 May 1957 No 1472, and the definitive transition to bars with improved adherence was defined only in 1972. The Circular introduced steel classes Aq.42, Aq.50 and Aq.60 characterized by yield strength not inferior to 23, 27 and 31 kgf/mm<sup>2</sup>, respectively, ultimate strength within 42-50, 50-60, 60-70 kgf/mm<sup>2</sup> and ultimate strain not inferior to 20%, 16% and 14%.

Experimental tests on smooth rebar specimens in Portugal was performed by Caruso and Bento (2019). The specimens were provided from an existing building, i.e. a high school located in Lisbon dating from the 60s. Tensile testing of three steel specimens were performed following the European Standard EN 10002-1 (CEN, 2001b). A tensile test machine and a video extensometer were used to record the stress-strain relationship of the steel bars. Figure 3.2 shows the Specimen 1 at different elongation stages (Figure 3.2a) and the stress-strain relationship (Figure 3.2b).

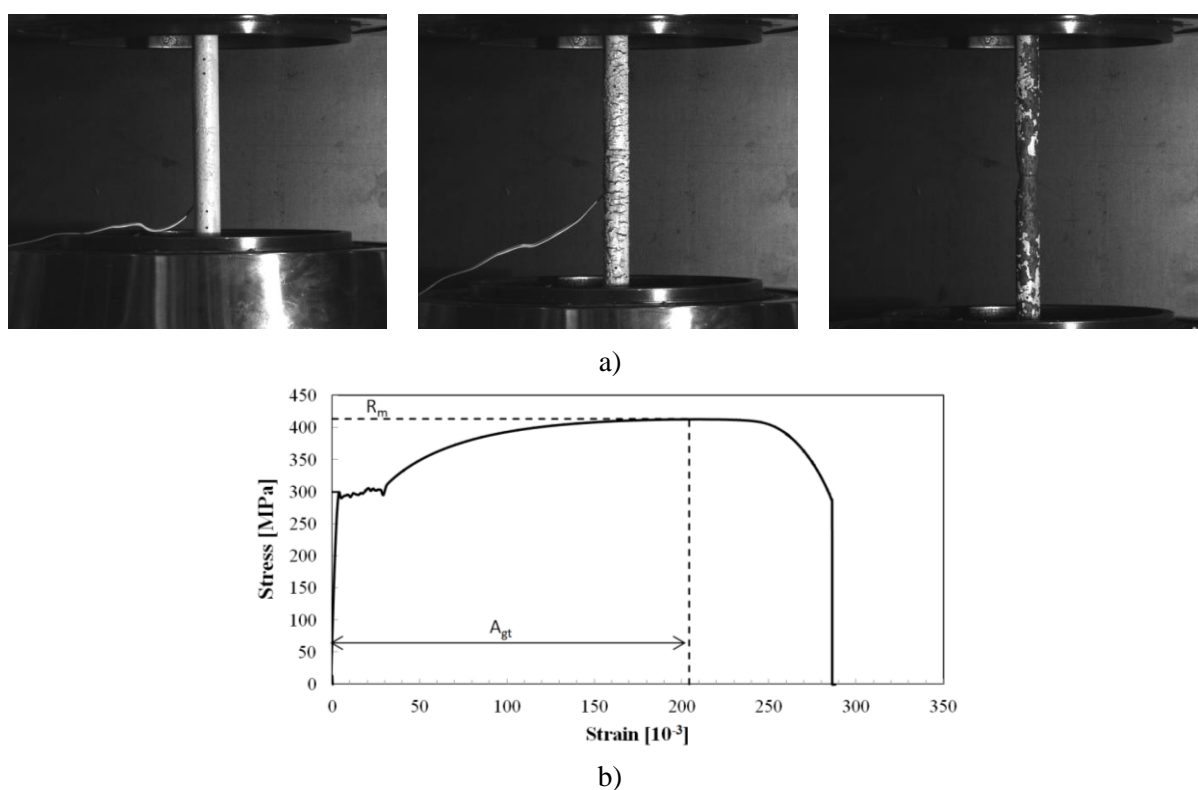


Figure 3.2 – Elongation stages (a) and stress-strain relationship (b) for specimen 1.

The results of the tensile tests showed that the steel rebars are characterised by high tensile strength and high ductility, with ultimate strains  $\varepsilon_u$  ( $A_{gt}$ ) up to 24.1%. The mechanical properties of the steel smooth bars experimentally tested present similar values to those defined in the Portuguese regulation

REBA for the A24 steel rebars and to the Italian Aq. 42. More details on the tests set up and results can be found in Caruso and Bento (2019).

### 3.3. Case study

#### 3.3.1. Case study RC wall-frame building

A case study belonging to the typology of RC wall-frame buildings built within 1960 and 1980 in Lisbon (Portugal) is selected for this study. The building is located between Av. do Brasil and Rua Aprígio Mafra that was designed and built in the 1960's (Figure 3.3). Total building height is approximately 27 m (Figure 3.4). The building is an eight-storey RC building (ground floor plus seven storeys above ground). All storeys feature the same height, 3.0 m, except the ground floor which is 3.6 m high.



Figure 3.3 – Location of the building within Avenida do Brasil and Rua Aprígio Mafra

The urban planning of *Avenida do Brasil* marks the end of a certain type of urban intervention in consolidated areas of the city of Lisbon, whose guiding principles were based on the "Athens Charter" principles established by Le Corbusier in 1943. In particular, special attention was given to the separation of traffic (motorized and pedestrian) and health requirements (sun light, clean air and green areas). These principles were applied to the layout of the buildings, positioned perpendicularly to the axis of the avenue on a green platform, in order to provide the facades with equal conditions of sun exposure. The building belongs to a period of modern architectural design that was strongly encouraged around the world since the first half of the 20<sup>th</sup> century and is characterized by the common application of "open floors" or "pilotis" (structure with an open ground storey and infills in the upper storeys) and free façade. The principle of free design of the façade, which consisted in separating the structural function of the structure from its exterior shell, resulted in exterior masonry infills with large openings ((Figure 3.4) to (Figure 3.6)), such as the long window of the living room (with 3.70 meters).

This building belongs to a set of eight similar parallel residential buildings with eight storeys, organized in two housing layouts: five buildings with two “T4” apartments (four bedrooms and a living room) and three buildings with four “T2” apartments (two bedrooms) per floor. The model building belongs to the second configuration, with four “T2” apartments (Figure 3.5). Each apartment includes two types of access: the main entrance via the lift and the “service” access, through the stairs. The ground floor includes an apartment for the caretaker of the building and an area identified in the project as "prams storage" (Figure 3.6). The top floor includes a laundry washing and drying area for each apartment.



Figure 3.4 – Views of the building in Av. do Brasil and front view of the building

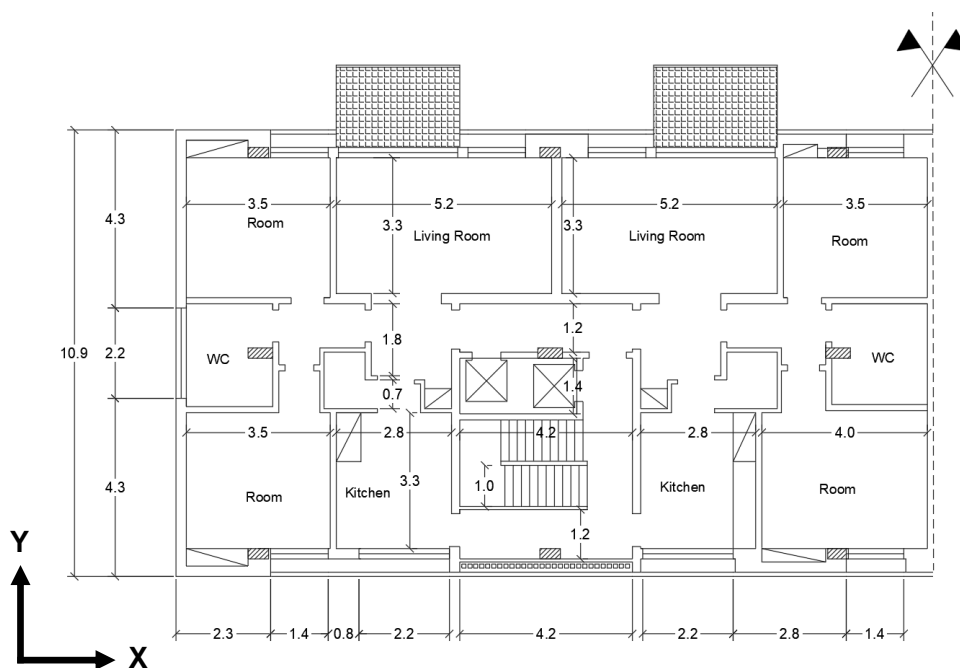


Figure 3.5 – Plan of the building floors 1-7 (adapted from Montepio-Geral, 1960) (dimensions in [m])

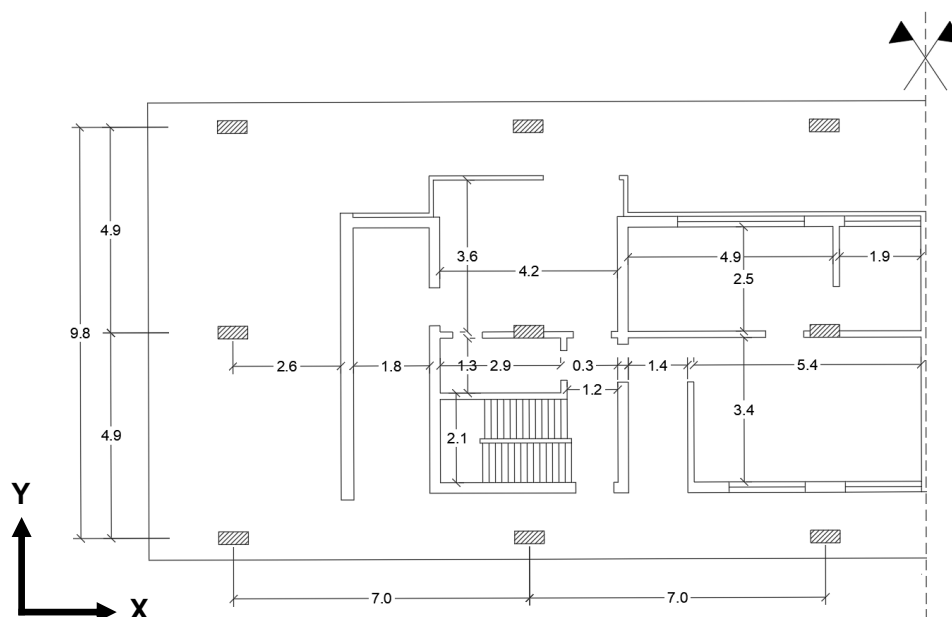


Figure 3.6 – Plan of the ground floor (adapted from Montepio-Geral, 1960) (dimensions in [m])

### 3.3.2. Structural Design Options

The structure features three main RC frames in the longitudinal (X) direction (facades direction) carrying gravity loads and beams framing eccentrically from the columns in the transverse (Y) direction (Figure 3.7). Its plan dimensions are 36.80 m in the X-direction and 10.85 m in the Y-direction. It also includes two stair and lift cores and interior masonry walls. One of the peculiarities of this project lies in the distribution of the columns, all oriented with their strong axis orthogonal in the X direction. However, the two stiff RC cores ensure an acceptable rigidity in the transverse (Y) direction. The structure is symmetric with respect to the Y direction and moderately asymmetric along the X direction.

For the computation of the mass of the structure, the definition of dead and live loads is carried out. The dead load comprises the self-weight of the RC structure while other dead load includes finishing, such as coatings (wood or ceramic tiles) and partition masonry walls. Given the lack of information in the original drawings, the live loads are defined according to Part 1 of Eurocode 8 (EC8-1) (CEN, 2004) as  $2 \text{ kN/m}^2$ . The total mass of the building amounts to 3,677 ton. The floor masses and the moments of inertia of mass about the centre of mass are equal to 443 ton and  $54341 \text{ ton} \cdot \text{m}^2$  for the bottom storey, and 456 ton and  $53,700 \text{ ton} \cdot \text{m}^2$  for the other storeys.

The building was designed according to the old Portuguese codes for reinforced concrete and for earthquake resistant design, the RSCCS, introduced in 1958. Seismic loads were defined as horizontal static forces equivalent to the inertia forces due to the earthquake and were obtained by multiplying the mass of the structure by a seismic coefficient. The base shear coefficient for the case study building is equal to 0.1, corresponding to seismic Zone A of the old 1958 RSCCS code. Thus, the

design base shear can be estimated as 3552.8 kN, which corresponds to 10% of the total weight of the building, which amounts to 35527 kN. The safety checks of the structural members were purely force-based, consisting in the comparison of internal force demands with the member resistance. In the design of the RC frames, the structural actions (dead load, imposed loads, shrinkage, temperature variations and seismic load) were combined according to the regulation, in order to obtain the most unfavourable loading scenario. Thus, for the case study building the horizontal forces are resisted in the longitudinal X-direction by the RC frames and in the transverse Y-direction by the RC walls of the stairs and lift core (Figure 3.8). All the details about the sectional properties and reinforcement of columns and RC walls are reported in Annex A.

The building was designed with lightened slabs of “Tijomel-P12” bricks completed with distribution reinforcement to ensure a proper load distribution (Figure 3.9). The foundations of the RC frames were designed with simple reinforced concrete footings, according to the required dimensions, in which the joints of the frames are supported (Figure 3.10).

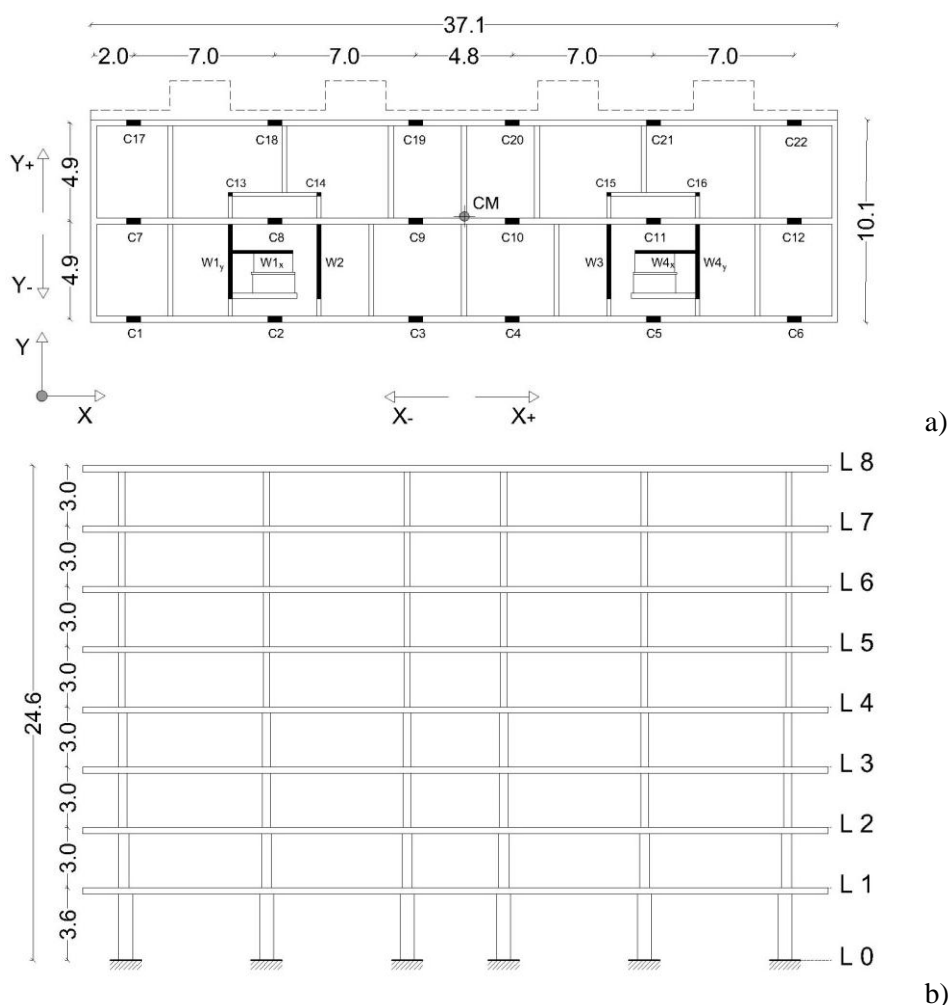


Figure 3.7 – Case study building, dimensions in [m]: (a) structural plan layout, (b) elevation in Y-direction.

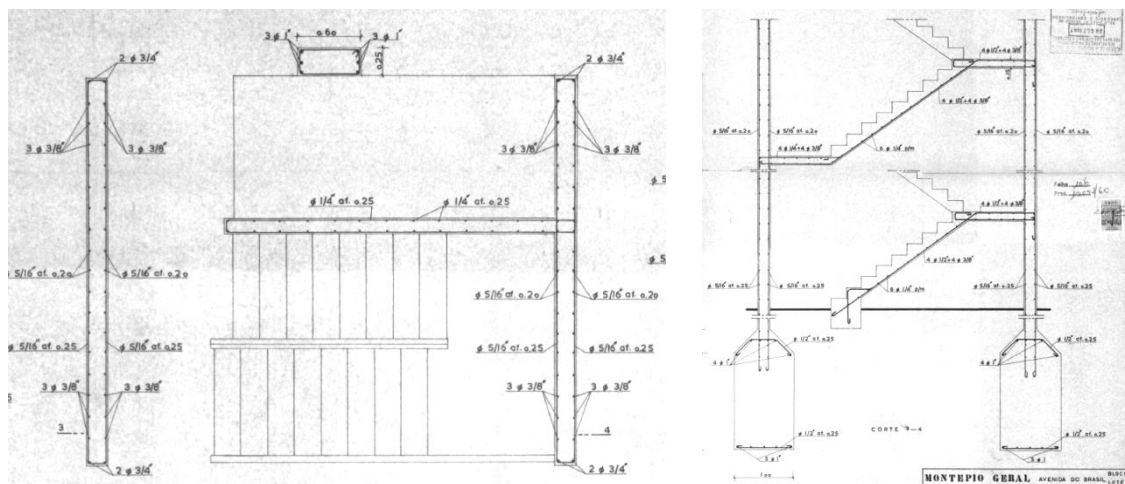


Figure 3.8 – Detail of the reinforced concrete core and RC walls

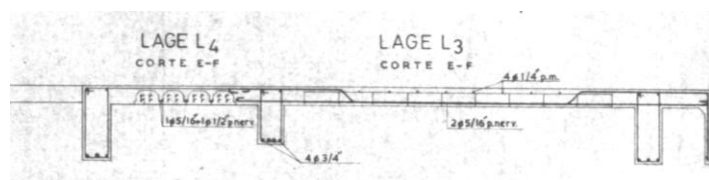


Figure 3.9 – Detail of the lightened slab

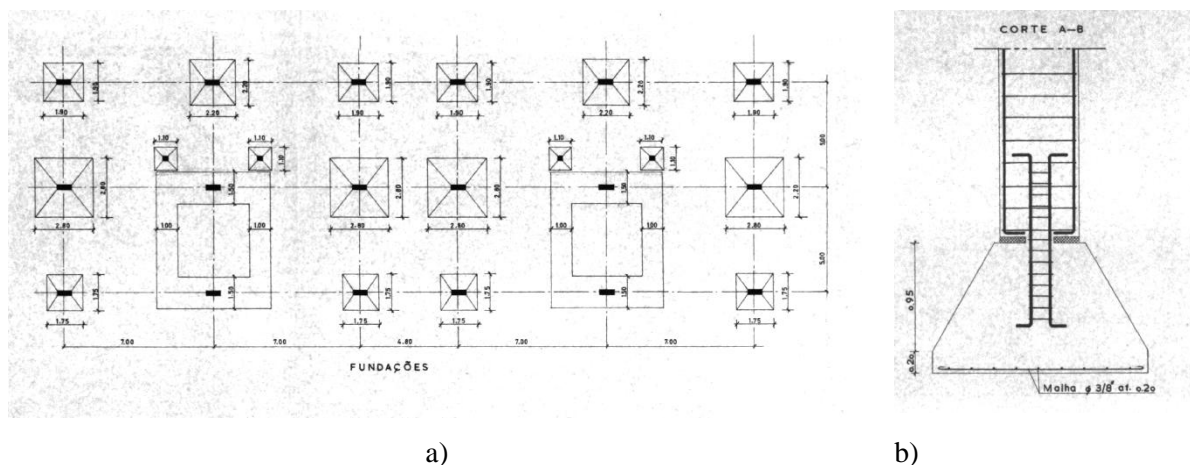


Figure 3.10 – (a) Plan of the foundation; (b) detailing of foundation system of a RC column (Montepio Geral, 1690). Dimensions in [m]

From a preliminary assessment of the building, some inadequate reinforcement detailing conditions can be noticed:

- the size of the columns changes in each floor, since only the vertical loads were considered in the design. Consequently, there is a strong reduction in the stiffness of the columns in the upper storeys, creating a relevant vertical irregularity;
- RC elements are characterized by smooth longitudinal reinforcing bars, which increases the bond-slip effect and the fixed-end rotation at the elements' base;

- according to modern standards (e.g. EC8-1) to ensure a ductile behaviour of the RC walls, the reinforcement details should be characterized by confined boundary elements and adequate levels of horizontal ratios. However, RC walls designed according to older codes, such as this case study, do not feature these characteristics.

Dimensions and reinforcement properties of the two T-shaped RC walls (Wall 1 and Wall 4 in Figure 3.7) in the X and Y direction, are presented in Table 3.2, where  $\rho_{long}$  is the longitudinal reinforcement ratio and  $\rho_h$  the horizontal reinforcement ratio. As stated before, and as shown by the calculation notes of the building, the structure was designed to resist the horizontal loads by the longitudinal frames (X) and by the RC walls in the transversal (Y) direction. This explains the different amounts of longitudinal and horizontal reinforcement in the shear walls.

Appendix A presents the information about RC elements (columns, RC walls and beams), in terms of reinforcement and cross-sectional area.

Table 3.2 – Summary of T-shaped walls' properties

Wall		Dimension (m)	$\rho_{long}$ (%)	$\rho_h$ (%)
W1 <sub>y</sub> - W4 <sub>y</sub>	L0 - 1	0.25 x 4.00	0.65	0.16
	L 1 - 2	0.25 x 4.00	0.35	0.16
	L 2 - 8	0.25 x 4.00	0.27	0.16
W1 <sub>x</sub> - W4 <sub>x</sub>	L 0 - 1	0.15 x 3.00	0.18	0.17
	L 1 - 8	0.15 x 3.00	0.18	0.17

### 3.3.3. Structural modelling

The seismic analysis of the buildings requires the development of nonlinear numerical models as effective tools for the assessment of the structural behaviour. In this work, a 3-D numerical model of the case-study building was developed in OpenSEES (McKenna et al., 2000). In the model, force-based beam-column element and fibre modelling approach are employed for beams, columns and shear walls. The sectional analysis is performed by discretizing the sections into fibres. Cover and core concrete were modelled using the uniaxial material 'Concrete 04', which is based on the model proposed by Popovics (Popovics, 1973). The steel constitutive law was modelled using the uniaxial Giuffre-Menegotto-Pinto model (Menegotto and Pinto, 1973), 'Steel02'. Table 3.3 provides a summary of the mean values of the materials' properties, namely the compressive maximum strength ( $f_c$ ), strain at maximum strength ( $\epsilon_c$ ) and modulus of elasticity ( $E_c$ ) for concrete and the yield strength ( $f_y$ ), ultimate strength ( $f_u$ ), ultimate strain ( $\epsilon_{su}$ ) and modulus of elasticity ( $E_s$ ) for steel.

Table 3.3 – Summary of material properties

	$f_c$ (MPa)	$\varepsilon_c$ (‰)	$E_c$ (GPa)	
Concrete	40.0	2	30.0	
	$f_y$ (MPa)	$f_u$ (MPa)	$\varepsilon_{su}$ (‰)	$E_s$ (GPa)
Steel	370.0	370.0	240	210.0

The materials properties of the building are derived according to the regulation in force in the period 1950 – 1980 and based on the statistical distribution of each material's property derived from the Portuguese building stock (Silva et al., 2015a). According to the original technical notes of the building, the reinforced concrete compressive strength at 28 days is 300 kgf/cm<sup>2</sup> ( $\approx$  30 MPa). In this work, and according to expert opinion, a mean value of 40 MPa is assumed, higher than the 28-day strength, considering that past cements were coarse-grained and took longer to fully hydrate. The main difficulty resulted in defining reliable mean values of yield strength of the steel reinforcing bars. This limit depends on the scarce amount of laboratory tests performed especially on smooth reinforcing steel bars used for constructions dating 1950 – 1970 in Portugal. In fact, most of the available experimental results are based on A400 and A500 steel classes, as defined by REBAP, the Portuguese code dating 1983. Carvalho and Coelho (2001) proposed for European and Mediterranean buildings the mean yielding strength of 344.3 MPa. In this study, the value of 370 MPa is used, based on both the information available in old codes and on the results of the statistical campaign conducted by Verderame et al. (2011). The mechanical properties adopted for the steel have been confirmed also on the experimental campaign conducted by Caruso and Bento (2019) and presented in Section 3.2.1.

The floor systems consist of lightened slabs supported by beams in both directions. Considering that the slabs have a much higher in-plane stiffness in comparison to the out-plane stiffness and that there is not significant stiffness discontinuity in the structural system, it is decided to neglect the in-plane flexibility of the lightened slab. Therefore, in the model, the RC frames are connected by means of rigid diaphragm at each floor level and the masses are concentrated at the CM of each floor. It is important to note that the results of the analysis are conditioned by this modelling decision.

In the model, only nonlinear behaviour in flexure is considered. The shear capacities of the most critical elements are accounted for in the assessment stage and in post-processing phase on the results data, where the shear strength of the critical elements was compared with shear demand. A wide column model is assumed for the T-shaped wall. Force based nonlinear beam column elements are used to model web and flange of the wall, each element located at the centre of wall axis. The connection to the frame structure and within web and flange of the T-shape is obtained with horizontal rigid links. In Beyer et al. (2008) it is commented that the link spacing should not be too large in order to limit effects of parasitic bending moment. Link spacing of the order of one fifth of the design shear span or half of the wall length (assumed as the larger of the web and flange length)

are suggested. In this study, the rigid links are positioned at floor level, which roughly correspond to that order of length. The horizontal links are assigned a torsional flexibility as proposed in Beyer et al. (2008).

The main features of the building are replicated in the model, such as the infills and the smooth reinforcing bars, typical of structures built in the 60s. Infill walls can have a beneficial effect on the structural response, when they are distributed regularly and do not cause shear failures of columns. Instead, negative effects can arise from an irregular distribution of infills in plan and elevation. A soft-storey collapse mechanism may occur in infilled structures when the infills are not present in one storey, e.g. at the bottom storey (first storey mechanism). Different studies have shown the importance of taking into account the presence of the infills in the numerical model (e.g., (Favvata et al., 2013) (Choudhury and Kaushik, 2018)) and developed tools to simulate the in-plane and out-of-plane behaviour (e.g. (Furtado et al., 2016)).

In this study, the infill panels are modelled by means of two diagonal struts which can only carry axial compression, placed between the beam–column joints. The equivalent connecting strut only transmits forces directly to the node, which is a limitation of this simplified model. A quadrilinear force-displacement relationship was assumed for the diagonal strut (Figure 3.11), as proposed in (Dolšek and Fajfar, 2008) and (Celarec et al., 2012). The first branch, which corresponds to the linear elastic behaviour up to the first cracking of the infill, is characterized by the elastic stiffness ( $K_{el}$ ) and shear cracking strength ( $F_{cr}$ ):

$$K_{el} = \frac{G_w A_w}{h_w} \quad (3.1)$$

$$F_{cr} = \tau_{cr} A_w \quad (3.2)$$

where  $A_w$  is the cross sectional area of the infill panel,  $G_w$  is the elastic shear modulus of the wall,  $h_w$  is the clear height of the infill panel and  $\tau_{cr}$  is the shear cracking stress. The second branch, corresponding to the beginning of crushing, is characterized by a value of the maximum strength given by:

$$F_{max} = 1.30 \cdot F_{cr} \quad (3.3)$$

The third branch of the envelope is the post-capping degrading branch, which runs from the maximum strength to the residual strength ( $F_{res}$ ). Its stiffness ( $K_{deg}$ ) depends on the elastic stiffness and on the value of a degrading coefficient. The fourth branch of the envelope is the horizontal branch corresponding to the residual strength, which is assumed to be equal to 2% of the maximum strength. A reduction coefficient is adopted to consider the influence of the openings in the infills as in Fardis (2009). In this study, mean values of 0.28 MPa and 1240 MPa are adopted for the cracking stress and

the shear elastic modulus, respectively (Celarec et al., 2012). The infills are modelled in the exterior frames along the X direction and in the central internal frame in the Y direction. The exterior panels in the Y-direction are not considered since they are not aligned with the columns. The panels are distributed along the height of the building, except in the ground storey, that is an open storey.

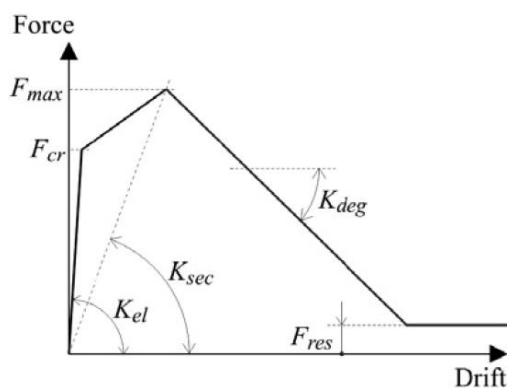


Figure 3.11 – Schematic quadrilinear force-displacement relationship of the compressed diagonal struts (adapted from (Celarec et al., 2012)).

As for the smooth rebars, even though it is common to assume a perfect bond between the reinforcing bars and concrete, neglecting the relative bond-slip deformations, strain penetration (SP) deformations can contribute up to 40% to the total lateral deformation when deformed rebars are used and up to 90% when plain rebars are present. In this study, a simple approach involving the reduction of the Young's Modulus and maximum strength of the reinforcing steel is used to simulate the increase in member flexibility due to strain penetration effects. Based on the results of Chapter 1, and on the characteristics of the reinforcing bar of the case study building, it is chosen to reduce by 40% the Young Modulus of the rebars of the RC walls at the ground storey only, while the maximum strength, which is directly related to the embedment length of the rebars, is reduced by 30%. It should be noted that, for the case study building, this approach involves only the RC walls, but has no impact on the columns-base modelling. In fact, after analysing the original drawings (Figure 3.10), there is no evidence that the foundations of the columns were modelled to withstand bending moments, therefore the columns have been considered pinned at the base.

#### 3.3.4. Dynamic properties

It is worth noting that the numerical model of the structure is validated through ambient vibration tests performed by Ferreira (2016), and an error lower than 10% between the measured and the model frequencies in the X and Y directions is obtained. The elastic properties of the building in terms of periods and modes of vibration obtained with the numerical model and ambient vibration tests (in-situ) are presented in Table 3.4.

The results obtained with the numerical model as well as those obtained by ambient vibration tests show that the analysed building consists, in basic terms, of a torsionally uncoupled system. In fact, one translational mode along each of the two principal axes of resistance and one torsional mode can be clearly detected. As it can be seen, for the structure the second and third modes are associated with deformations in the longitudinal (X) and transverse (Y) directions, respectively, while the first mode is rotational (r).

Table 3.4 – Periods of vibration and frequencies of the first 3 modes of vibration

Mode	Numerical model		In-situ	
	Period (s)	Frequency (Hz)	Period (s)	Frequency (Hz)
1	0.91 (r)	1.09 (r)	-	-
2	0.90 (X)	1.11 (X)	1.05 (X)	0.95 (X)
3	0.87 (Y)	1.15 (Y)	1.00 (Y)	1.00 (Y)

### 3.4. Sensitivity analysis and seismic performance assessment

Given that a fully exhaustive (i.e. deterministic) knowledge of an existing building in terms of geometry, detailing and properties of the materials is realistically impossible to achieve, a sensitivity analysis is proposed as an effective tool: (i) to clearly point out the influence of each uncertain parameter on the structural response; (ii) to set the base for an effective investigation plan to improve the knowledge of the building; (iii) to evaluate the essential parameters to pass to a verification based on a full probabilistic approach (Haddad et al., 2017).

Relevant uncertainties concerning the structural knowledge can be distinguished in:

- factors that can be considered known in deterministic terms, or with a negligible margin of uncertainty. For these factors a single value is adopted for all the analyses;
- factors affected by aleatory uncertainty, generally associated with the intrinsic variability of property of the structure. These factors are modelled using random variables;
- factors affected by epistemic uncertainty, associated with a lack of knowledge of the structure or mechanical behaviour of its component elements. These factors can be modelled in some cases by continuous random variables, when the uncertainty concerns the quantification of a model's parameter, or by means of the logic tree technique, when the knowledge defect requires the consideration of alternative models (CNR-DT 200, 2013).

In this study uncertainties related to the material properties and the characteristics of the reinforcing bars (i.e. the embedment length) are considered and modelled by continuous random variables, characterized by a probability density function  $f(x)$ .

A basic type of deterministic sensitivity analysis is used, comprising  $2N+1$  models, where  $N$  is the number of aleatory variables. Each of the  $2N$  models is formed by varying one random variable to its

16th or 84th fractile while considering the mean values of the others. One additional analysis is performed setting each input variable to the best-estimate (mean) value.

In this work, sensitivity analysis is used to measure the sensitivity of the limit-state top displacement and corresponding Peak Ground Acceleration (PGA) to the input variables which contribute to it. Seismic safety of the building is assessed comparing, for each structural element, the seismic demand, calculated in terms of deformation and strength, with the corresponding capacity. The deformation capacity of columns and walls is estimated in terms of chord rotation,  $\theta$ , according to Equation A.1 of EC8-3; the shear capacity is obtained with the expressions provided by EC8-3, Equation A.12 for the shear strength, as controlled by the stirrups, and Equation A.15 for the shear strength corresponding to failure by web crushing. EC8-3 provides capacities at the element level rather than global level.

It is worth noting that several uncertainties lie in the definition of the plastic rotation (Romão et al., 2009) (Araújo and Castro, 2016) and shear strength of RC members (several models exist in the literature, leading to significantly different outcomes (Del Vecchio et al., 2017)).

The variability of the output variable peak ground acceleration with respect to the variability of each input variable is calculated as follows:

$$\Delta a_{g,i} = \frac{100(PGA_{i,j} - PGA_{bm})}{PGA_{bm}} (\%) \quad (3.4)$$

where  $PGA_{i,j}$  is the value of the output variable computed for the variation of the  $i$ th input variable to the  $j$ th fractile (i.e. 16th or 84th), whereas  $PGA_{bm}$  corresponds to the value of the output variable estimated for the base model (i.e., the model with the variables set to their mean values).

#### 3.4.1. Parameters of sensitivity analysis

To address the seismic assessment of the building, the following modelling parameters are identified as source of uncertainty: (i) the concrete compressive strength ( $f_c$ ), (ii) the steel yield reinforcement ( $f_y$ ), the reinforcing bars' embedment length ( $L_e$ ), the shear elastic modulus of the infill walls ( $G_w$ ). The value adopted for the modelling parameters together with their lower and upper limit values and coefficients of variation (CoV) are summarised in Table 3.5. Lognormal distributions are assumed for the random variables.

For the concrete compressive strength,  $f_c$ , a CoV of 40% is adopted, due to the uncertainty in quality controls. With respect to the infill walls, a full correlation is assumed for the mechanical characteristics of hollow clay brick panels. Hence, the elastic modulus of the infills is assumed to be equal 3.33 times the value of shear modulus  $G_w$ , according to the Italian standards (CNR-DT 200, 2013), whereas the shear cracking stress,  $\tau_{cr}$ , is assumed as linearly dependent on  $G_w$ .

As discussed in Section 3.3.3, the embedment length at the anchorage region,  $L_e$ , affects the maximum strength of the steel bars of the RC walls at the ground storey. The embedment length  $L_e$  is expressed in terms of the longitudinal bars diameters and, according to the original drawings of the building, ranges from 30 to 80 diameters ( $d_b$ ) for a mean value of 50 diameters, which correspond to reductions of the steel strength of 60%, 0% and 30% respectively.

Table 3.5 – Parameters of sensitivity analysis

Parameters	Mean value	Lower limit	Upper limit	CoV
$f_c$	40 MPa	24 MPa	56 MPa	0.40
$f_y$	370 MPa	333 MPa	407 MPa	0.10
$G_w$	1.24 GPa	0.744 GPa	1.74 GPa	0.40
$L_e$	50 $d_b$	30 $d_b$	80 $d_b$	0.40

### 3.4.2. Ageing effects

Ageing effects are particularly important for old buildings that are reaching or have already reached the end of their design life. Even though the ageing process is often neglected in seismic design and assessment of building structures, aggressive environmental conditions can cause different types of structural damage such as corrosion or material fatigue and lead to extensive deterioration of the mechanical properties of the structural elements. In (Celarec et al., 2011) the effect of environmental corrosion on the seismic behaviour of RC buildings was investigated and a simplified procedure for seismic performance evaluation with consideration of degradation over time was presented. It was shown that, due to the effect of corrosion, the structural capacity in terms of the maximum base shear and the maximum roof displacement of a case study building built in the 1950-1960 decrease over time.

In the context of this thesis, corrosion effects are analysed and taken into account in the structural model of the building by decreasing the diameter of the reinforcement bars and the concrete cover of the structural elements, as suggested in (Celarec et al., 2011). Due to the architectural configuration of the building (open ground storey and free façade - Figure 3.5 and Figure 3.6), which was very common in the period in which the structure was designed, only the columns of the ground storey are exposed to the unfavourable environmental conditions and present, to some extent, the effect of corrosion. After performing pushover analyses of the building, it was observed that the influence of these effects on the structural capacity, are almost negligible. For this reason, although recognising the importance of verifying the influence of these effects on the structural response, it was decided not to take this phenomenon into account for the case study building.

### 3.4.3. Results and discussion

In order to evaluate the seismic capacity of the structure and to check the seismic safety of the building, nonlinear static analyses are performed based on the procedure prescribed in EC8-3. The seismic safety is assessed by comparing the demand with the capacity at the significant damage (SD) limit state, which, according to the National Annex of EC8-3 (NP EN 1998-3 2017), is the limit stated to be verified for buildings belonging to importance class II. Lateral forces are applied for the pushover analysis in the form of modal proportional load patterns. The loads are applied independently in the two X and Y directions, in the positive (+) and negative (-) senses. It is worth noting that, due to symmetry in the X direction, the results obtained for the positive and negative senses are equivalent.

The limit state displacements of the structure for the SD limit state are determined through the N2 method (Fajfar 2000), the nonlinear static procedure prescribed by EC8-3. To define the seismic action, the EC8-1 elastic response spectrum for soil type B is adopted. Thus, according to the Portuguese National Annex of EC8-1 (NP EN 1998-1 2010), the seismic action is represented by a ground motion with a return period of 475 years and a peak ground acceleration of 0.153 g for seismic action Type 1. Although the National Annex of EC8-3 recommends lower return periods of seismic action for the seismic assessment of existing structures, in the context of this work this option is not considered; nevertheless, this choice does not change the final general outcomes. In addition to the pushover analyses of the reference structural models, 8 pushover analyses are performed to compute the sensitivity of the seismic response parameters to the four input random variables set to their 16<sup>th</sup> or 84<sup>th</sup> fractile.

The most representative pushover curves are depicted in Figure 3.12 for the X direction and in Figure 3.14 for Y direction and for the (+) and (-) signs of loading, together with the limit state displacement values corresponding to shear failure (SF) and flexural failure (FF) of columns and walls. In the figures the results are presented in terms of top displacements ( $d$ ) and maximum base shear ( $V$ ) for the cases of the base model and for the maximum positive and minimum negative variations of the described parameters resulting from variations of the random variables to their 16<sup>th</sup> and 84<sup>th</sup> fractile.

In the X direction, the period of the structure is mostly influenced by the infill walls, and then by the shear modulus  $G_w$  parameter (Figure 3.12). In fact, the infill walls contribute to increase initial stiffness of the pushover curves, even though the maximum strength is unaltered. The maximum value of the strength is slightly influenced by the concrete strength  $f_c$  (Figure 3.12) and the steel yielding strength  $f_y$ . The pushover curves are practically unaffected by the embedment length  $L_e$ . This is because the RC walls, that are the only elements involved by the reduction of the embedment length, have a partial contribution to the total lateral strength of the building for this direction of loading (X direction), which is mostly provided by the columns.

The uncertainty in the parameter  $f_c$  has the greatest impact on the output variable PGA of the flexural failure mode of all elements and the shear failure mode of the columns. This is well shown in the diagrams presented in Figure 3.13, which display the sensitivity of the PGA to the input variables (see Equation (3.4)), respectively for flexural and shear failure modes, in columns and RC walls. The PGA decrease by about 30%, if  $f_c$  is set to its 16th fractile for the case of the flexural failure of the columns. The steel yield reinforcement  $f_y$  influence mostly the PGA associated to the shear failure mode of the RC walls. The PGA increases up to about 20%, if the variable is set to its 84th fractile and decrease of about 18% if set to their 16th percentile.

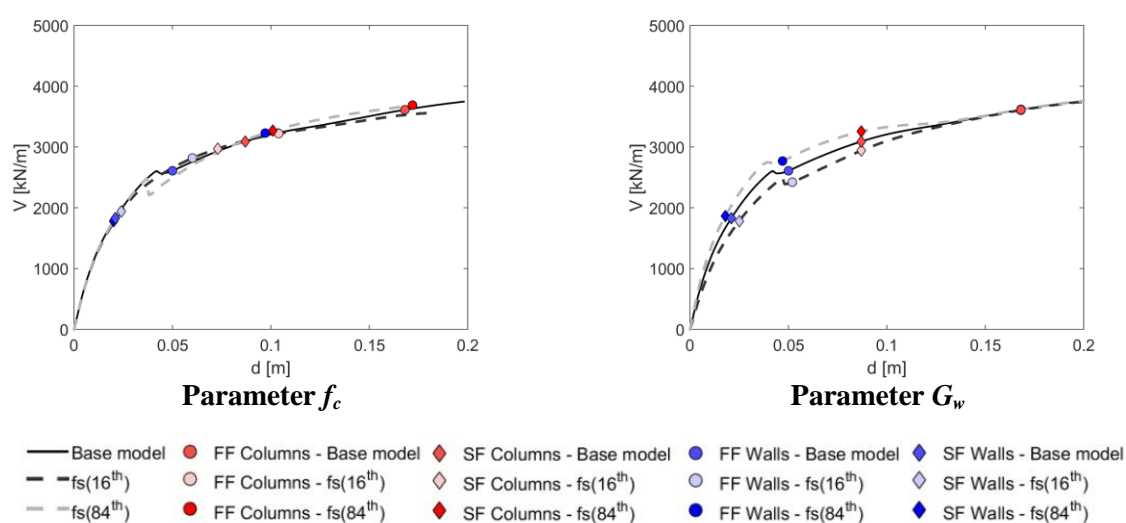


Figure 3.12 –Pushover curves for X direction (base model and models with parameters set at 16th or 84th fractiles) and top displacements-base shear for flexural failure (FF) and shear failure (SF).

In the positive Y (+) direction, the infills slightly influence the initial stiffness of the pushover curves. Changing  $f_y$  and  $L_e$  to the 16th or 84th fractile influences both the maximum base shear of the pushover curves and the top displacement capacities (Figure 3.14), whereas the initial stiffness is practically the same as that obtained for the base case model. The 16th value of the fractile corresponds to an inferior maximum strength of the pushover curves for both random variables  $f_y$  and  $L_e$ . The opposite effect is obtained for the 84th fractile. This result was expected, as the embedment length  $L_e$  directly influenced the lateral strength of the RC walls that are the main resisting system for this direction of loading, whereas the columns are very flexible in this direction, because their flexural resistance is mobilised in turn of their weak axis and also due to the fact that there are no beams framing into the columns (see Figure 3.7). The sensitivity of the limit-state peak ground accelerations to the random variables is presented in the diagrams shown in Figure 3.13 for columns and RC walls, respectively. The inelastic limit-state top displacements of the RC walls at shear failure is proportional to the variation of parameter  $f_y$ . The variation of  $f_y$  from its mean to its 84th fractile increase the PGA at the shear failure mode by at least 25% in the RC walls (Figure 3.13).

The pushover curves for the negative Y (-) direction are shown in Figure 3.14. The variables  $G_w$  and  $f_c$  have a small effect on the maximum shear strength, which is mostly affected by the random variables  $L_e$  and  $f_y$ , as evident from pushover curves (Figure 3.14). The sensitivity of the peak ground acceleration, is presented in the diagrams shown in Figure 3.13 for the four random variables. Similarly, to the positive Y direction, the random variable  $f_y$  has the biggest impact on the limit-state peak ground accelerations, while the variables  $f_c$  and  $G_w$  have a much lesser impact on the failure modes.

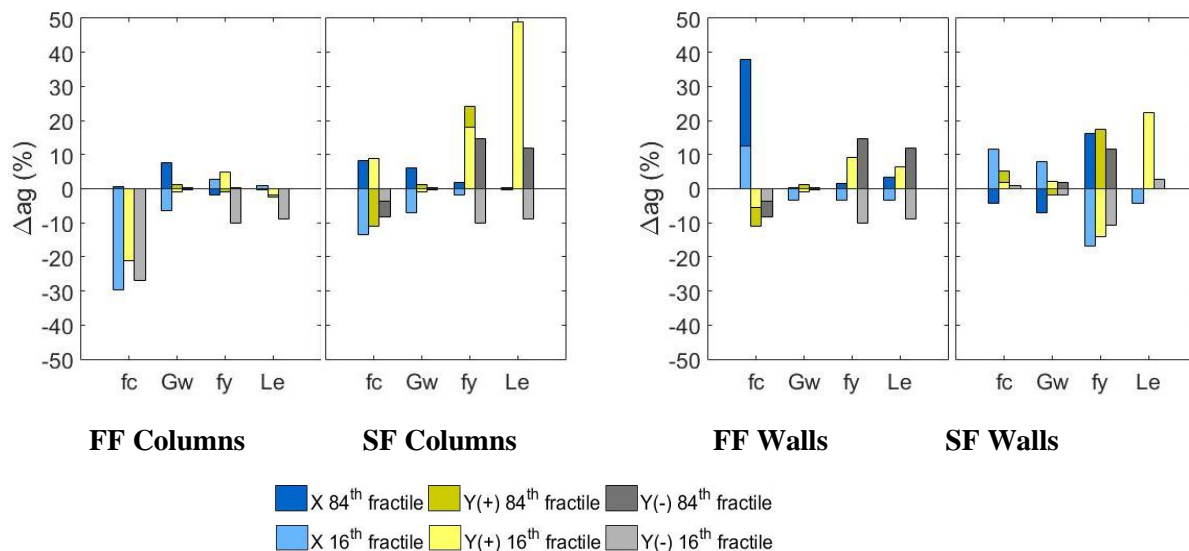


Figure 3.13 – Variation of peak ground acceleration for parameters uncertainties corresponding to flexural failure (FF) and shear failure (SF) in columns and walls and for all directions of loading.

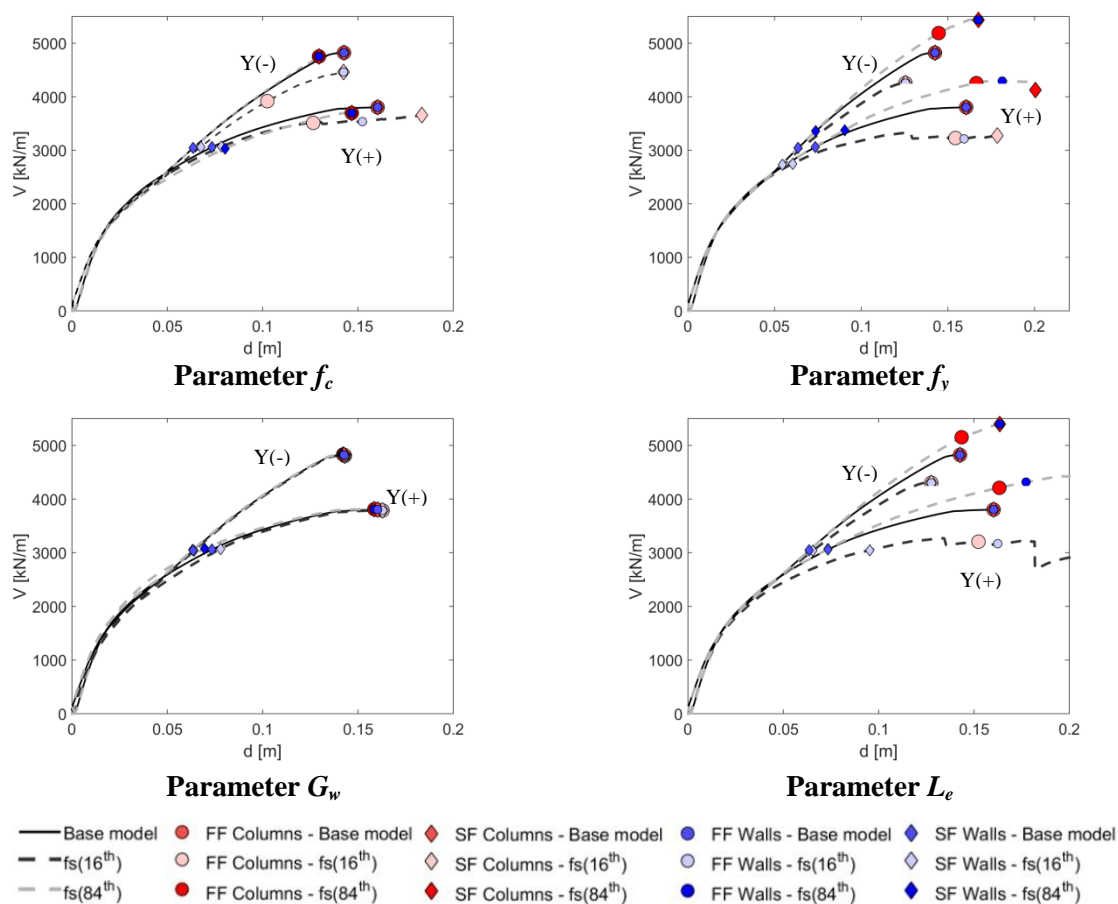


Figure 3.14 – Pushover curves for Y direction (base model and models with parameters set at 16<sup>th</sup> or 84<sup>th</sup> fractiles) and top displacements-base shear for flexural failure (FF) and shear failure (SF).

Finally, it is clear that  $f_y$  and  $L_e$  are the variables that most affect the seismic performance of the building, especially for the shear failure of the RC walls, for all directions. The variable  $f_c$  is the parameter that most affect the flexural performance of columns and walls in all directions.

### 3.5. Conclusions

In this chapter, a numerical model of the case study is developed. This building is representative of a specific building class, i.e. the RC wall-frame buildings, designed and built within 1960 and 1980. The numerical model takes into account the main properties of the building, such as (i) smooth reinforcing bars; (ii) infill walls; (iii) limited ductility properties. A simplified bond-slip model is adopted to consider the strain penetration effects in RC walls with smooth bars.

Then, sensitivity analysis is used in order to point out the dependence of the seismic response parameters to several modelling variables on a case study RC wall-frame building structure, with the main objective of integrating in a more efficient way the propagation of uncertainties in the structural assessment of a specific subcategory of RC buildings.

It is evident that the parameter that mostly influences the initial stiffness of the pushover curves is the infills elastic modulus  $G_w$ , especially in the X direction. The results presented show that the consideration of the SP effects through the embedment length of the rebars  $L_e$  leads to a reduction of the overall shear strength as the embedment length of the rebars decreases. This is particularly evident in the Y direction, where the horizontal load is mostly carried by the RC walls. Therefore, it is important to consider the uncertainty in this parameter, as it affects the seismic response.

The uncertainty in the parameter  $f_c$  has the greatest impact on the output variable peak ground acceleration for the flexural failure mode for all directions of loading (Figure 3.13). The uncertainty in the parameters  $f_y$  has the greatest impact on the output variable peak ground acceleration for the shear failure mode of the columns and RC walls in the X direction and in the positive and negative Y directions (Figure 3.13).

In the next chapters, it is intended to derive vulnerability curves for the case study building to deeply characterize the seismic performance of the structure, incorporating new source of uncertainty, such as the seismic demand at the site, governed by the hazard function, and the record-to-record variability described by a set of records.



## 4. RELEVANCE OF TORSIONAL EFFECTS ON THE SEISMIC ASSESSMENT OF OLD RC FRAME-WALL BUILDINGS

### 4.1. Introduction

Torsional effects may significantly affect the seismic response of a building and the distribution of damage throughout the structure. This problem is particularly important for existing RC frame and wall-frame buildings designed before the introduction of modern seismic codes which provide specific design criteria to account for torsional effects. Due to need for structural upgrading to meet more stringent seismic design requirements in earthquake prone areas, seismic assessment and structural retrofitting is becoming more and more important and receives today considerable emphasis throughout the world. This Chapter presents the seismic assessment of the case study RC frame-wall building presented in Chapter 3 with the aim of detecting and quantifying the expected deficiencies of this typology of buildings with focus on the torsional response. The structure is symmetric with respect to the Y direction and moderately asymmetric along the X direction (Figure 3.7). However, an accidental mass eccentricity was assumed, which amounted to 5% of the plan dimensions in each of the two horizontal directions, as suggested in EC8-1 (4.3.2 *Accidental torsional effect*) in order to account for uncertainties in the location of masses.

In Anagnostopoulos et al. (2015) a comprehensive literature review of earthquake induced torsion in buildings is presented, including the existing procedures for the seismic capacity assessment of asymmetric buildings. Nonlinear static procedures (e.g. (Peter Fajfar, 2000); EC8-1) have proven to be effective in predicting seismic response of low-rise regular buildings and planar frames. Problems arise when dealing with plan-asymmetric buildings which exhibit torsional response. Generally, these methods cannot capture the torsional effects and the real structural response. Some efforts have been made to overcome these limitations towards a more accurate prediction of the structural response. Chopra and Goel (2002) developed the so called Modal Pushover Analysis with reference to planar frames. Later, the method was extended to 3-D symmetric or asymmetric structures (Reyes and Chopra, 2011). Fajfar et al. (2005) proposed a procedure based on pushover analysis of the 3-D structure, combined with an elastic dynamic modal analysis to determine, through correction factors, the influence of torsion mode on the deformation in plan. Then, the procedure was adapted to consider higher mode effects also in elevation, enabling the analysis of plan-asymmetric medium- and high-rise buildings (Kreslin and Fajfar, 2012). New procedures for extending pushover analyses to 3-D asymmetric structures can be found in some other papers, e.g. (Bhatt and Bento, 2011), (Bosco et al., 2012).

In this chapter, the Original N2 method (Fajfar, 1999) and its extension to structures whose response is affected by higher modes, both in plan and elevation, (Extended N2 method) (Kreslin and Fajfar,

2012) are applied to the case study, a real existing building structure and the results are compared with the ones from nonlinear Time-History (TH) analysis. The seismic behaviour of the case study building is assessed with particular focus on the effects of torsion on the distribution of deformations and damage in plan and in elevation. A proposal is made to predict the amplification due to torsion on the shear demand of the RC resisting elements when the structure is excited in the inelastic range of behaviour.

The chapter begins with the description of the seismic assessment procedures used, including a brief review of the Extended N2 method and the proposal of a new procedure for shear demand prediction (Section 4.2). In Section 4.3, the seismic assessment of the torsional behaviour of the building is performed and the results are discussed.

## **4.2. Seismic response assessment procedures**

This section describes the procedures adopted for the seismic response assessment of the RC wall-frame building considered in the study. The torsional response of the structure is evaluated by means of nonlinear static method and by nonlinear Time History (TH) analysis. The first part of this section is dedicated to a brief review of the Extended N2 method. Then, the seismic action is defined and the selection of ground motions for the TH analysis is presented.

### ***4.2.1. Application of the Extended N2 method***

The Extended N2 method is applied to assess the seismic response of a structure and to analyse to which extent the torsional behaviour affects unfavourably the response parameters. The Extended N2 method combines the results of a pushover analysis with those of a Modal Response Spectrum Analysis (MRSA), which accounts for the higher mode effects, in both plan and elevation, on the distribution of deformations. This method is widely recognised as a valid tool for seismic assessment of buildings as it is simple in application and provides a fair prediction of the displacement demands. However, it may predict too conservatively the shear demand of resisting elements. Concerning the estimation of the torsional component of the structural response, it is worth mentioning that this method assumes that MRSA generally provides conservative estimates of the torsional effects (Fajfar et al., 2005) (Kreslin and Fajfar, 2012). Higher mode effects in both plan and elevation are considered through the application of correction factors that are used for the adjustment of results obtained by conventional pushover analysis. The use of the Extended N2 method is also supported by the European seismic code. EC8-1 (4.3.3.4.2.7 Procedure for the estimation of the torsional effects) (CEN, 2004) includes guidelines for the determination of torsional effects of torsionally flexible structures based on the application of MRSA. These guidelines are conceptually close to the Extended N2 method. In fact, it is stated that “for such structures, displacements at the stiff/strong side shall be

increased, compared to those in the corresponding torsionally balanced structure” and “this requirement is deemed to be satisfied if the amplification factor to be applied to the displacements of the stiff/strong side is based on the results of an elastic modal analysis of the spatial model.”

In the Extended N2 method, two types of correction factors are considered: the correction factors for displacements due to torsion and correction factors for storey drifts due to the contribution of higher mode effects in elevation. In order to evaluate the coefficients that consider the effects of torsion in plan, the roof displacements at different locations are determined by pushover analysis and elastic modal response spectrum analysis. All the results (from both pushover and MRSA) are normalized by the roof displacements at the centre of mass (CM). The correction factors are defined as the ratio between normalized roof displacements obtained by MRSA and by pushover analysis. If the correction factor is lower than 1.0, then the value of 1.0 is used, i.e. no de-amplification due to torsion is allowed. It is assumed that the torsional correction factors are independent of the floor level, so the same value should be used for the adjustment of the pushover results at any floor in elevation. For the evaluation of the correction factors that account for higher mode effects, firstly the results (displacements and storey drifts at the CM in each storey) obtained by MRSA are normalized in such a way that the roof displacement at the CM is equal to the target displacement. Then, the correction factors are determined as the ratio between the normalized results obtained with MRSA and the absolute values of the results obtained by pushover analysis. If this ratio is greater than 1.0, then the correction factor is equal to this ratio, otherwise it amounts to 1.0. The values of the correction factors depend on the floor level, but are constant at each individual storey, i.e. they do not depend on the position in plan. The evaluation of the correction factors is defined in more detail in (Kreslin and Fajfar, 2012).

#### ***4.2.2. A proposal for shear demand prediction***

In order to account for the torsional behaviour of the building by the Extended N2 method, all the relevant engineering demand parameters (EDPs) obtained with pushover analyses should be multiplied by correction factors. The relevant EDPs are the deformations of ductile elements and the internal forces of the brittle ones (Fajfar et al., 2005). However, since the structure yields, the amplification of internal forces imposed to brittle elements/mechanisms due to torsion is not equal to that used for the displacements. An example is the shear demand of columns and shear walls of RC frame-wall buildings. In this study, a proposal is made to account for the amplification due to torsion on the shear demand imposed on the RC elements, taking into consideration the inelastic behaviour of the structure. The amplification of the shear demands through a direct application of the correction factor would lead to an overestimation of the shear demand.

Figure 4.1 schematically describes the procedure proposed to estimate the shear demand imposed on the member, column or wall, for a given seismic intensity level. Firstly, the target displacement ( $d_t$ )

obtained with the N2 method is determined for the balanced model (Figure 4.1a). To this target displacement corresponds a shear demand  $V_i$  of a member (column or wall). The balanced model can be obtained by moving the CM to the same location of the centre of rigidity or by restraining the deck rotation. Then, the target displacement is multiplied by the torsion correction factor,  $f$ , corresponding to the location in plan of the column/wall under investigation. The shear demand  $V_i'$  of this element is found in correspondence of this increased displacement on the pushover curve  $d_t'$  (Figure 4.1b).

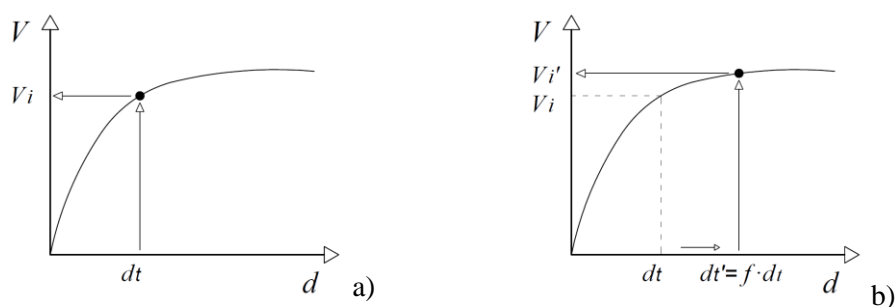


Figure 4.1 –Amplification of the shear demand of the member (column or wall): (a) shear demand of the member of the balanced model and (b) increased shear demand of the member due to torsion.

It is clear that, in the elastic range of behaviour, the result obtained with the proposed method coincides with that obtained by simply multiplying the shear force for the amplification factor ( $V_i = V_i'$ ), as originally proposed by the Extended N2 method. Instead, if the structure has been pushed in the inelastic range of behaviour, the proposed method allows to take into account the yielding experienced by the structural members and the consequent reduction of stiffness and redistribution of internal forces, by drawing the shear demand directly from the results of the pushover analysis.

#### 4.2.3. Analysis procedures

The target displacements of the structure are determined with the Original N2 method (Peter Fajfar, 2000) (Fajfar, 1999), the nonlinear static procedure prescribed by EC8-3. For the Pushover analysis, a displacement control strategy is used. The imposed displacements are applied using a displacement-control integrator, where the load factors are scaled to reach the desired displacement. This method is the most efficient when dealing with a strength-degrading system. “Modal” proportional load patterns are applied independently in the X and Y directions and in positive and negative senses.

To define the seismic action, the EC8-1 elastic response spectrum for soil type B is adopted. The Significant Damage (SD) limit state is considered for the seismic assessment. Thus, according to the Portuguese National Annex of EC8-1, the seismic hazard is represented by a ground motion with a return period of 475 years and a PGA of 0.153 g for seismic action Type 1, which corresponds to the most severe seismic action for the case study building.

The seismic performance evaluation is conducted based on the assessment procedures prescribed in EC8-3 which, in simple terms, consist of comparing chord rotations and shear demands with the

values of ultimate chord rotation and shear strength defined in the European code. For the calculation of the capacities of ductile or brittle elements, mean properties of the materials are used. In the calculation of the strength capacity of brittle primary seismic elements, the material strength is divided by the partial safety factor of the material, as defined in EC8-1, i.e. 1.5 and 1.15 for concrete and steel, respectively. As for the confidence factor, they are taken as equal to 1.0, assuming full knowledge of the structure.

#### 4.2.4. Ground motion record selection

The main results obtained by means of the Original and the Extended N2 method are compared with the results obtained with TH analysis, which is recognized as the most reliable analysis procedure to assess the seismic performance of structures, particularly in the case of irregular ones.

For the TH analyses, a group of 30 real ground motion records was selected using the SELEQ tool (Macedo and Castro, 2017) following the methodology proposed in (Araújo et al., 2016). Each record has two horizontal components and is scaled to match the elastic acceleration response spectrum corresponding to the SD limit state (Figure 4.2).

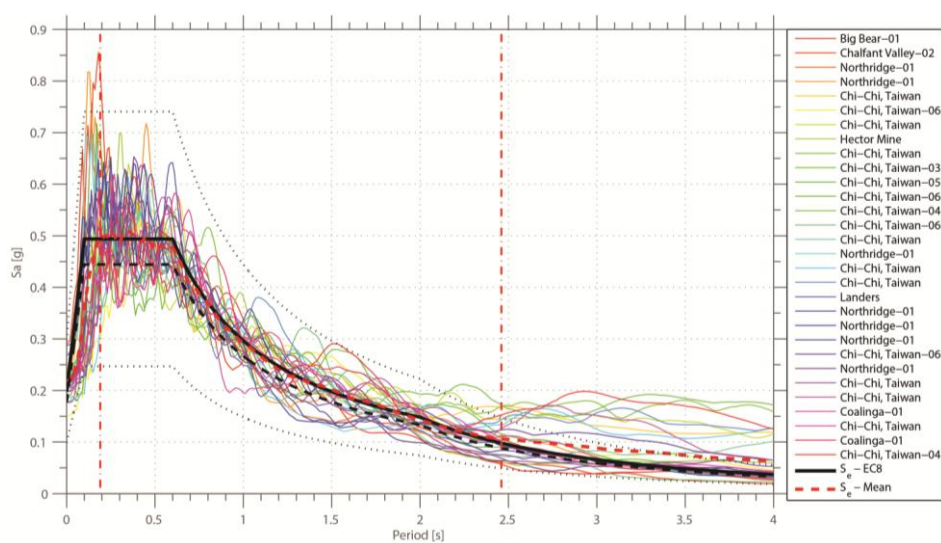


Figure 4.2 – Individual acceleration response spectrum of each of the 60 signals and corresponding average.

A MRSA of the model is performed. The sum of the effective modal masses for the modes of vibration considered contributes to 95% of the total mass in each direction. The complete quadratic combination (CQC) rule is used for the combination of the different modes. The results in the two horizontal directions are combined using the square root of the sum of squares (SRSS) rule. MRSA and TH analyses are performed on a model which considers the accidental eccentricity. On the other hand, two separate pushover analyses of the 3D structural model are performed: one with CM coincident with the centre of the floor, herein after called torsionally balanced structure, and another

one which considers the accidental eccentricity (Figure 4.3). The correction factors are calculated with the results of the corresponding balanced structure, as suggested in (Fajfar et al., 2005).

For the TH analysis, an initial stiffness and mass proportional damping is considered. This choice is supported by the work of (Chopra and McKenna, 2016), where it is discussed that when a fibre model is used to model structural elements, allowing distributed plasticity, the structural response is not sensitive to the damping model. A 5% damping is assumed in the first and fifth mode, being the modes in which almost all participation mass is mobilized. For the N2 method and the response spectrum modal analyses, 5% damping was considered for the definition of the elastic response spectrum.

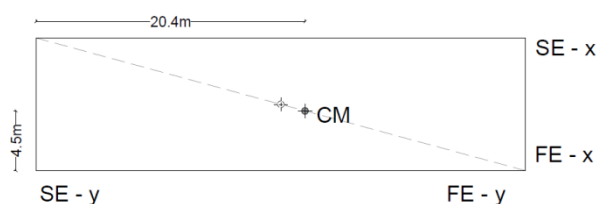


Figure 4.3 – Schematic plan of the building with the location of CM considering the accidental eccentricity

### 4.3. Discussion of the results

In this section, the higher mode effects in both plan (roof displacement) and elevation (storey drifts) are evaluated. The results are presented for the CM, for the “Flexible” Edge (FE) and the “Stiff” Edge (SE) of the building (identified in Figure 4.3), i.e., the sides where under a static lateral force through the CM the displacement due to pure torsion is added or subtracted, respectively, to the displacement due to pure translation behaviour (Anagnostopoulos et al., 2015).

The results of the application of the Extended N2 method are presented and compared with the Original N2 and the TH, this latter used as benchmark.

#### 4.3.1. Dynamic properties

The elastic properties of the building in terms of periods and modes of vibration are analysed. Table 4.1 shows the periods of the first 6 modes of vibration of the torsionally balanced structure together with the period ratios  $\Omega$ , i.e., the ratio of the translational period to the rotational period. The first mode is predominantly torsional. The second and third modes are associated with deformations in the longitudinal (X) and transverse (Y) directions, respectively, with an effective modal mass representing 70% ( $r_x$ ) and 73% ( $r_y$ ) of the total mass of the building. It is worth noting that the periods of vibration and the participating mass ratios of the building, which considers the effects of the accidental eccentricity, were close to those of the balanced structure.

It is acknowledged that the rotational response of the system greatly depends on the geometric eccentricity and the values of  $\Omega$  (Anagnostopoulos et al., 2015) (Fajfar et al., 2005) (Kreslin and

Fajfar, 2012). The case study building is characterised by period ratios  $\Omega$  of 0.96 and 0.99 in the X and Y direction, respectively, which denotes the structure as torsionally flexible ( $\Omega < 1$ ) in both directions.

Table 4.1 – Results of the modal analysis of the torsionally balanced model.

<i>Mode</i>	<i>Period (s)</i>	$\Omega$	$r_x$ (%)	$r_y$ (%)
1	0.91	1.00	2.9	0
2	0.90	0.99	70	0
3	0.87	0.96	0	73
4	0.26	0.29	2.2	0
5	0.22	0.24	0	0
6	0.19	0.21	0	1.8

#### 4.3.2. Determination of the target displacement

Figure 4.4 shows the pushover curves, i.e. base shear ( $V$ ) versus top displacement ( $d$ ) at the centre of mass, for the X and Y directions and for the (+) and (–) sign of loading (see Figure 3.7). For the X direction, the results in the two senses of loading are identical (Figure 4.4a), as the structure is symmetric with respect to the Y axis. The pushover curves shown in the figure are determined with a modal load pattern. In the TH analysis, the components of the ground motion were scaled for different levels of PGA, i.e. 0.0765g (50%), 0.115g (75%) and 0.153g (100%), leading from moderate to large inelastic deformations in the building. The results of the conventional pushover analysis are compared with the mean response determined by TH on the structure with eccentricity, for:

- 1) maximum top floor displacement  $d_{max}$  versus maximum base shear in each direction independently of time at which they occur ( $V_{max}$ );
- 2) maximum top floor displacement  $d_{max}$  vs the base shear  $V(d_{max})$  attained at the same instant of  $d_{max}$  (spot as  $V(d_{max})$ );
- 3) maximum top floor displacement  $d_{max}$  vs the maximum base shear attained in the time interval [-1 sec; +1 sec] from the instant when  $d_{max}$  is attained (identified as “Interval” in Figure 4.4).

The target displacements by the N2 method for the PGA prescribed in Lisbon for SD limit state are depicted as a cross in Figure 4.4. They amount to 0.108 m for the X direction, 0.120 m and 0.115m for the –Y and +Y directions, respectively. These values are about 15% larger than the mean value of the nonlinear time history analysis at a level of PGA of 0.153g.

The reason why the results of the conventional pushover analysis on the balanced structure are compared with the mean response determined by TH on the structure with eccentricity is that the pushover of the building with eccentricity (Ecc N2) fails completely in predicting the torsional response, as it will be showed in the next Section. Therefore, the results of this analysis are not considered. The comparison with the balanced structure gives a good approximation in terms of maximum shear strength and top floor displacement.

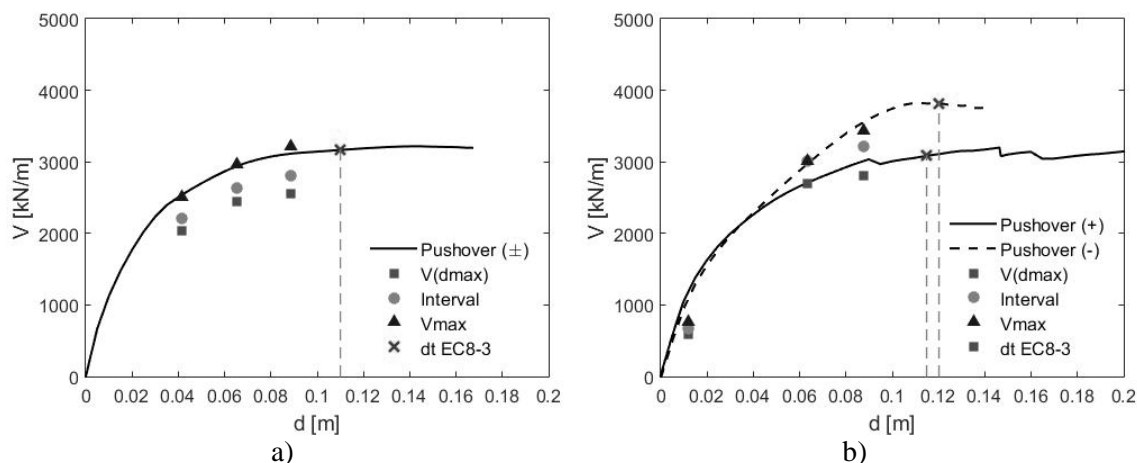


Figure 4.4 – Pushover curves in X (a) and Y directions (b).

#### 4.3.3. Assessment of the torsional response

In order to evaluate the torsional effects caused by the seismic action, the in-plan distribution of roof displacements is determined by MRSA and TH analysis. The MRSA and TH analysis are performed on the model which considers the accidental eccentricity. Then the results are normalized by the roof displacement at CM. The normalized roof displacements of MRSA provide the torsional correction factors of the Extended N2. Hence, the curve of the in-plan distribution of roof displacement determined by the results of MRSA represents the effect of the torsional component on the seismic response of the building as predicted by the Extended N2. In Figure 4.5, Figure 4.6 and Figure 4.7 the normalized roof displacements  $u/u_{CM}$  are shown for the Extended N2 and TH analysis at increasing ground motion intensities. An excellent agreement is obtained between the results of Extended N2 and the results of the TH analysis for the lowest level of PGA (Figure 4.5). The prediction of the torsional component provided by MRSA becomes conservative for larger values of PGA. These results confirm the assumption that led Kreslin and Fajfar (2012) to the formulation of the Extended N2 method, i.e. MRSA provides “at least” a conservative estimation of the torsional response of building in the inelastic range of their behaviour.

In the Y direction, the Extended N2 method gives torsional amplification of displacements both on the stiff and flexible edge of the structure. This behaviour is typical of torsionally flexible buildings, as shown in a parametric study conducted by (Fajfar et al., 2005). The amplification due to torsion decreases in the inelastic range especially on the stiff side (Figure 4.7). On the flexible side, the estimate of the torsional effects obtained by the Extended N2 method is reasonably accurate, when compared with the TH analysis. On the stiff side, instead, the Extended N2 method is generally more conservative. The normalized displacements in the X direction show a torsional amplification smaller than 5%, both on the stiff and flexible side. In fact, the structure is moderately asymmetric for this direction of loading, but the in-plan length in the orthogonal direction is small (about 1/3 of the other). Hence the side displacement due to the rotation, which is proportional to the distance of the side from

CM, is small too. It is worth to note that a simple pushover analysis with lateral loading at the CM of the building with accidental eccentricity (EccN2) fails completely in predicting the torsional response, especially the amplification of displacements in the stiff side.

The Extended N2 method provides for all the cases herein considered, conservative results and from good to fair estimates of the effect of torsion on the displacement demand of the case study building. Hence, in the following sections the method is applied to perform the seismic assessment of the case study building.

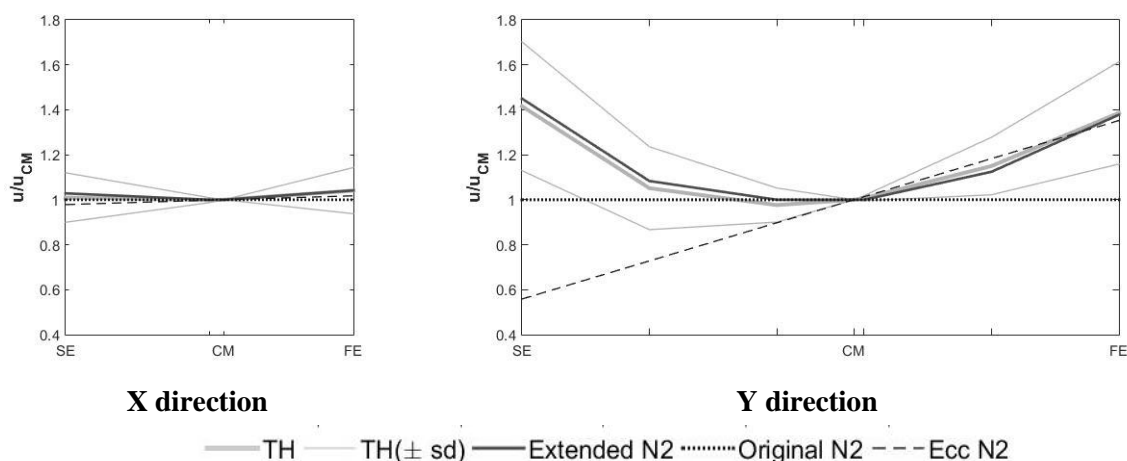


Figure 4.5 – Normalized roof displacements ( $u/u_{CM}$ ) in the horizontal plane for X and Y direction at 0.0765g

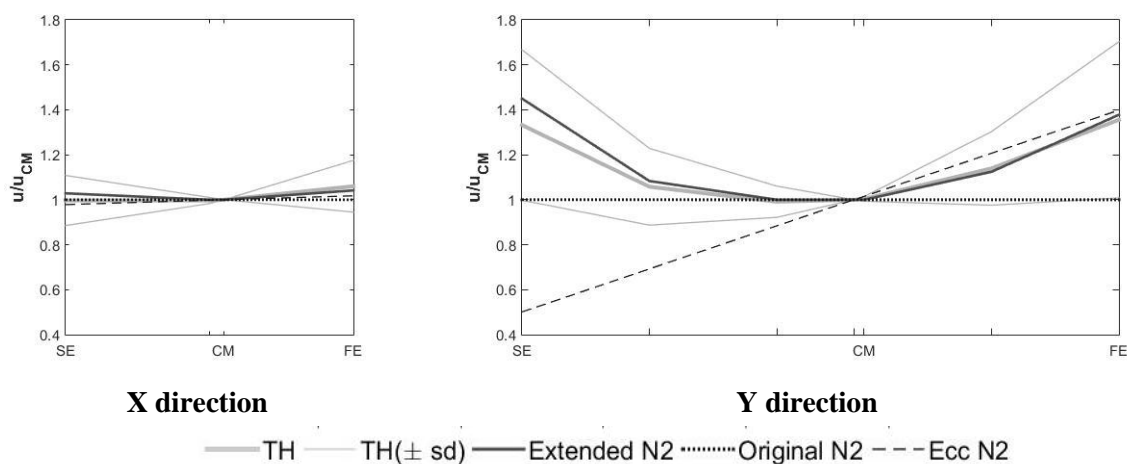


Figure 4.6 – Normalized roof displacements ( $u/u_{CM}$ ) in the horizontal plane for X and Y direction at 0.115g

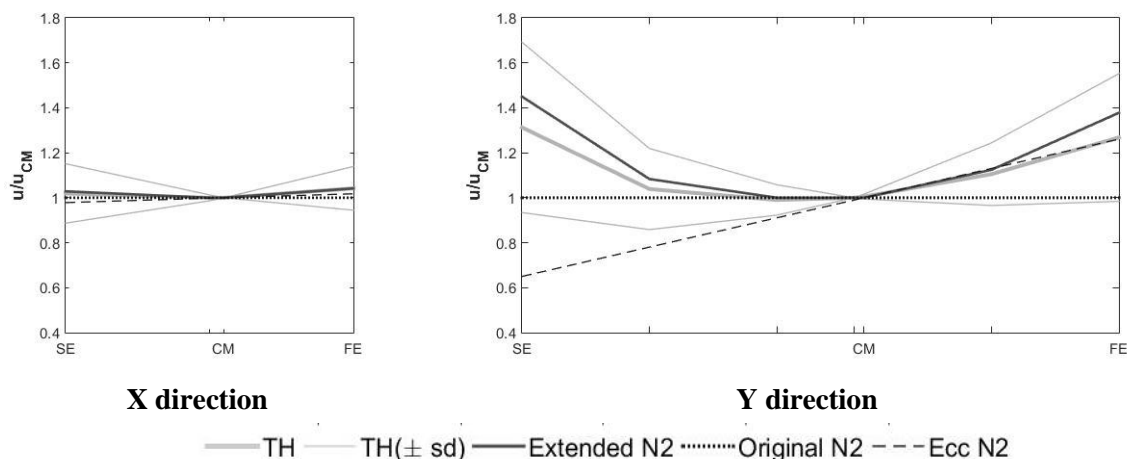


Figure 4.7 –Normalized roof displacements ( $u/u_{CM}$ ) in the horizontal plane for X and Y direction at 0.153g

#### 4.3.4. Application of Extended N2 method for the evaluation of storey drifts

Figure 4.8 and Figure 4.9 show the storey drift ratio (storey drift / storey height). The results are obtained for the target displacement at the SD limit state, corresponding to a seismic action of 0.153 g. The results comprise the storey drift ratios at the CM, SE and FE edge of the building with accidental eccentricity, obtained by the TH and the Extended N2. In the same figure the storey drift ratios of the torsionally balanced building obtained by the Original N2 are also represented. For the pushover analysis, a modal proportional load pattern is used, based on the fundamental mode shape in the X and Y direction, respectively. The N2 quantities were calculated for two horizontal directions and, for each direction, the envelope of the results obtained for two signs of loading was determined. The Extended N2 estimates were obtained multiplying the pushover results by the correction factors, to take into account both the influence of the higher mode effects in elevation and the torsional behaviour.

By analysing the deformation profiles, it is noted that the global behaviour of the structure in the X direction (Figure 4.8) is controlled by the longitudinal frames, which are composed by the columns and the RC walls, while in the Y direction (Figure 4.9) the structure is mainly controlled by the behaviour of the RC walls. From the results obtained, it is evident that the higher mode effects are important especially for the upper part of the building. In the X direction (Figure 4.8) the effects of torsion are small. In fact, the results obtained by Original N2 method for the torsionally balanced building and those obtained by the Extended N2 method taking into account the accidental eccentricities are close to each other. Furthermore, the results obtained by the N2 method are within the range of the mean and mean  $\pm$  standard deviation (sd) values determined by TH. In the Y direction (Figure 4.9), the results show that the Extended N2 method is able to represent the amplification of displacements due to torsion along the height of the building in the stiff and flexible edge. However,

due to larger target displacement (as shown in Figure 4.4), all the results obtained with the Extended N2 are about 20% larger when compared to the mean value of the nonlinear time history results.

The comparison shows that all the estimates obtained by the Extended N2 method are conservative when compared to the mean value of the TH. In spite of the overestimation of the target displacement, the pushover analysis with lateral loading at the CM displaced by the accidental eccentricity (Ecc N2) underestimates the storey drifts at the stiff edge, leading to non-conservative results (Figure 4.9).

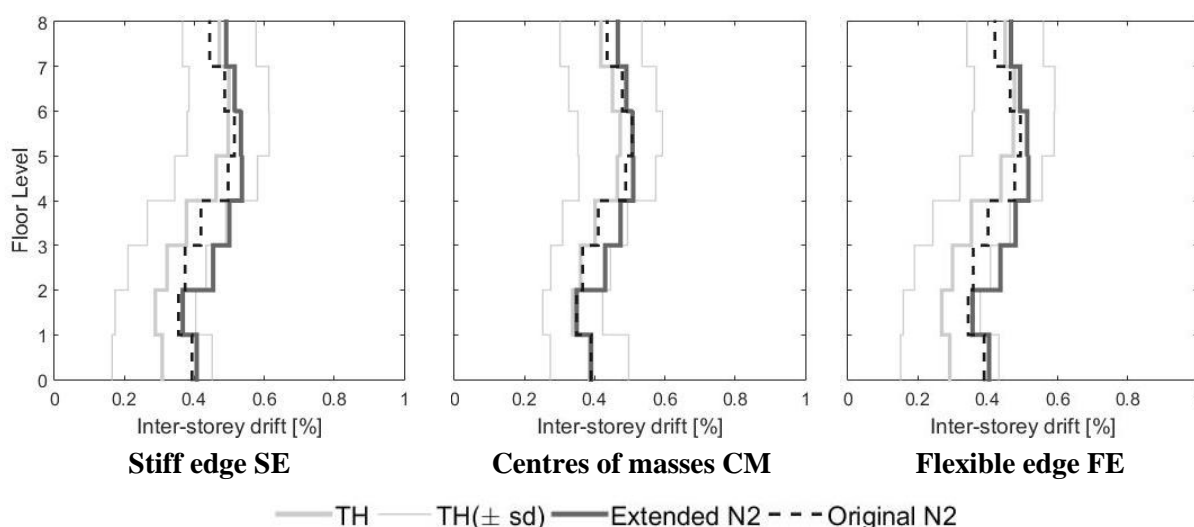


Figure 4.8 – Storey-drifts at the SE, at the CM and at the FE for the X direction.

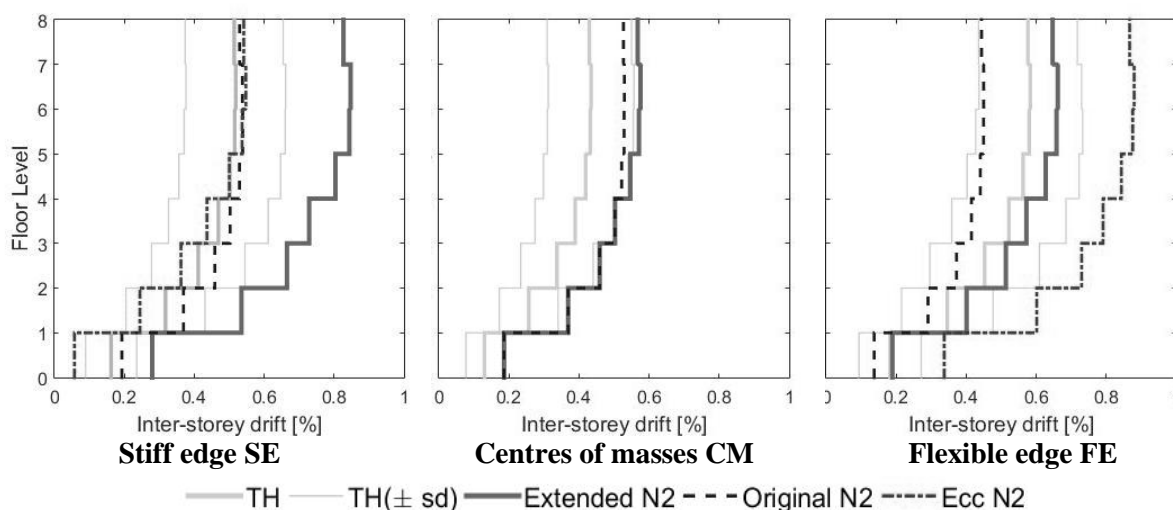


Figure 4.9 – Storey-drifts at the SE, at the CM and at the FE for the Y direction.

#### 4.3.5. Application of Extended N2 method for the evaluation of shear demand

The amplification of shear demand is performed with the approach proposed in Section 4.2.2. At the target displacement, in fact, the structure is no longer in the elastic range of behaviour. Multiplying it by the correction factors would lead to overestimate the shear demand. In this study, it is proposed to consider the shear demand at a step on the pushover curve increased by the correction factor. In this

way, the nonlinearity of behaviour can be taken into account. Figure 4.10 and Figure 4.11 show the shear demand in the RC walls obtained with the Extended N2 and with the proposed method, and compared with the results of the TH analyses.

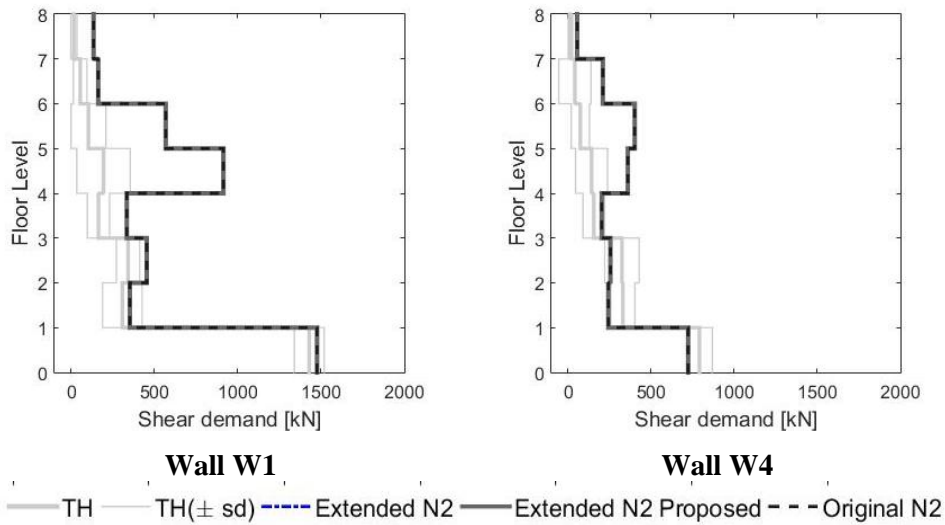


Figure 4.10 – Shear demand for the shear walls W1 and W4 in the X direction.

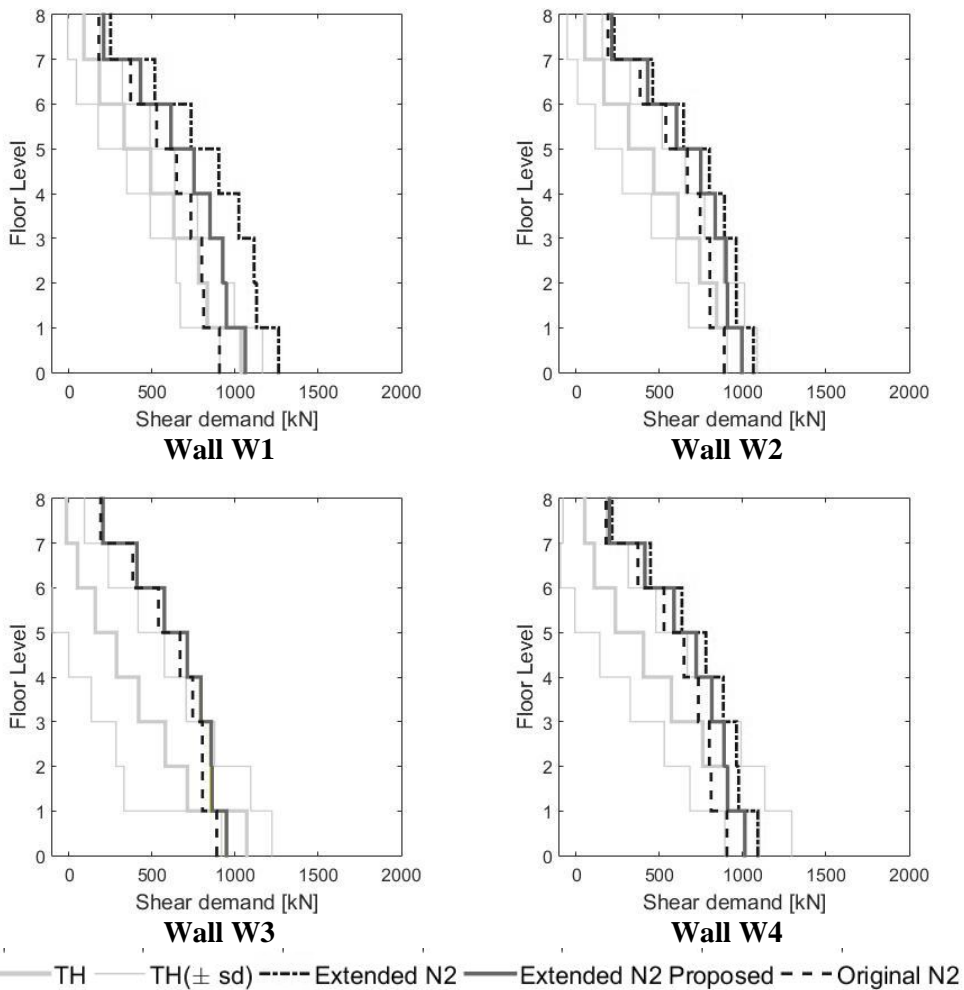


Figure 4.11 – Shear demand for walls W1, W2, W3 and W4 in the Y direction.

The results in the X direction (Figure 4.10) show that the higher shear demand is concentrated at the ground floor, whereas in the Y direction (Figure 4.11) the shear force varies gradually along the height. In the X direction, the correction factor due to torsion are almost negligible, as the structure's rotation is very small. Moreover, the shear demand corresponds to the maximum shear of the walls' response, therefore no amplification of the action is applied due to torsion. In the Y direction (Figure 4.11) it is showed that amplifying the shear demand by simply multiplying it by the correction factor leads to conservative results (e.g. in wall W1), whereas with the proposed method the results are much closer to those obtained with TH analysis.

#### 4.4. Seismic safety - Deformation capacity and shear strength

The seismic safety of the building is assessed comparing, for each structural element, the seismic demand, calculated in terms of deformation and strength, with the corresponding capacity. The deformation capacity of columns and walls is estimated in terms of chord rotation,  $\theta_{um}$ , according to Equation A.1 of EC8-3; for the walls the value of the ultimate rotation  $\theta_{um}$  is multiplied by 0.58 (CEN, 2010). EC8-3 provides correction coefficients for members with smooth longitudinal bars. In this case, the ultimate chord rotation should be multiplied by 0.8, with this factor including the reduction factor accounting for the lack of seismic detailing. If the longitudinal bars are lapped starting at the end section of the members, other coefficients should be adopted. The chord rotation capacity corresponding to SD limit state ( $\theta_{SD}$ ) is taken as 3/4 of the ultimate chord rotation  $\theta_{um}$ , as prescribed by EC8-3.

The shear capacity is obtained with the expressions provided by EC8-3; Equation A.12 for the shear strength, as controlled by the stirrups  $V_{Rd,s}$ , and Equation A.15 for the shear strength corresponding to failure by web crushing. For the estimation of the shear capacity, the RC walls were assumed as primary seismic elements. Due to the low amount of horizontal reinforcement (Table 3.2), in this study the shear resistance as controlled by the stirrups,  $V_{Rd,s}$ , is the most demanding parameter for the vertical elements.

In Table 4.2 the shear demand  $V_d$  and capacity  $V_{Rd,s}$  corresponding to the SD limit state (0.153 g) are provided for some of the most critical elements, i.e., for wall 1 in the X and Y direction and wall 4 in the X direction, at the base (L0 in Figure 3.7). In the table, the value of the shear resistance is evaluated as a function of the compression axial load and the ductility demand.

Table 4.2 –Shear demand and resistance for walls W1 and W4.

Wall	Level	$V_d$ [kN]	$V_{Rd,s}$ [kN]
W1 <sub>y</sub>	L 0	838	780
W1 <sub>x</sub>	L 0	1330	379
W4 <sub>x</sub>	L 0	247	222

Figure 4.12 and Figure 4.13 present the location of the plastic hinges, defined as the end of the member where yielding has taken place. The figures present the ratio of the chord rotation demand over the ultimate chord rotation capacity at the SD limit state at the end sections of the columns. Values of demand-to-capacity ratios smaller than 1 in Figure 4.12 and Figure 4.13 refer the ends of the members that have yielded but can still sustain plastic deformation before failure. These ratios are considered assuming that no shear failures occurred.

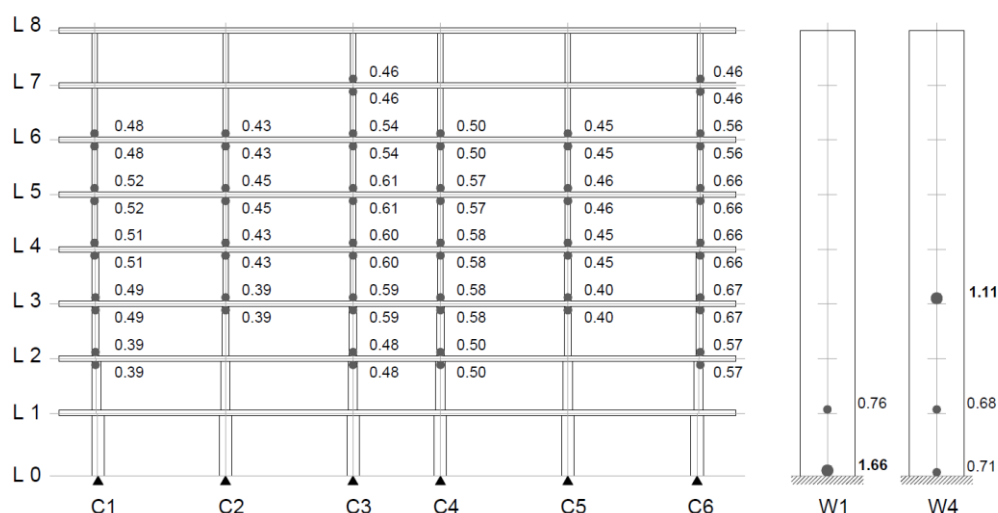


Figure 4.12 –Locations of the plastic hinges and demand/capacity ratios in the X direction for the frame in the FE and the RC walls in the same direction.

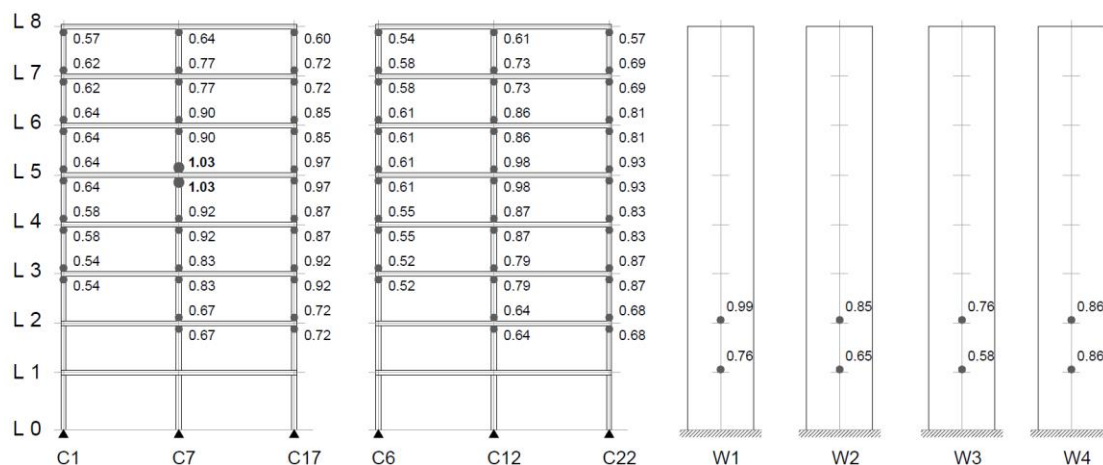


Figure 4.13 – Locations of the plastic hinges and demand/capacity ratios in the positive Y direction for the frames in the SE and FE and the RC walls in the same direction.

Figure 4.12 shows the demand/capacity ratios at the FE and for the shear walls in the X direction. Figure 4.13 shows the demand/capacity ratios at the SE and FE and for the shear walls in the Y direction. The flexural demand to capacity ratio in Figure 4.12 indicates that the capacity of all the elements of the frame is greater than the demand corresponding to the input ground motion. The most

critical elements are the two RC walls in the X direction, where the chord rotation demands are larger than the capacities (demand to capacity ratio higher than 1), while the frames have a higher deformation capacity. In the Y direction (Figure 4.13), the demand/capacity ratio is higher than 1 at the fifth level (L 5) of the central frame. The demand/capacity ratio is higher throughout the structure, when compared to the X direction. In fact, in this direction the flexural resistance of the columns is mobilised in turn of the weak axis and also there are no beams framing into the columns.

In Figure 4.14 and Figure 4.15 the pushover curves are depicted together with the target displacements and the top displacement corresponding to Shear Failure (SF) and Flexural Failure (FF) of columns and walls, respectively for the X and positive Y directions.

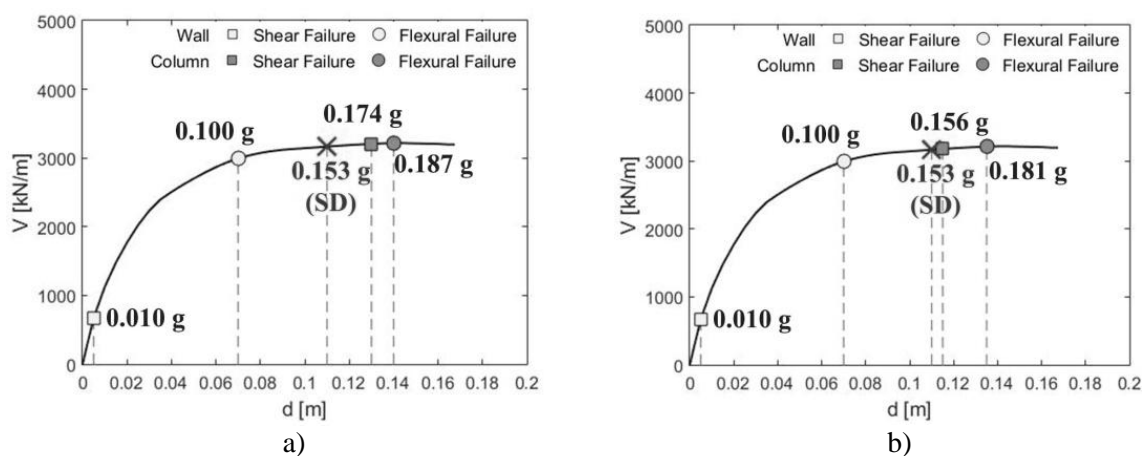


Figure 4.14 –Pushover curves for X direction. Target displacement and flexural and shear failure are indicated considering (a) and not considering (b) the torsional response.

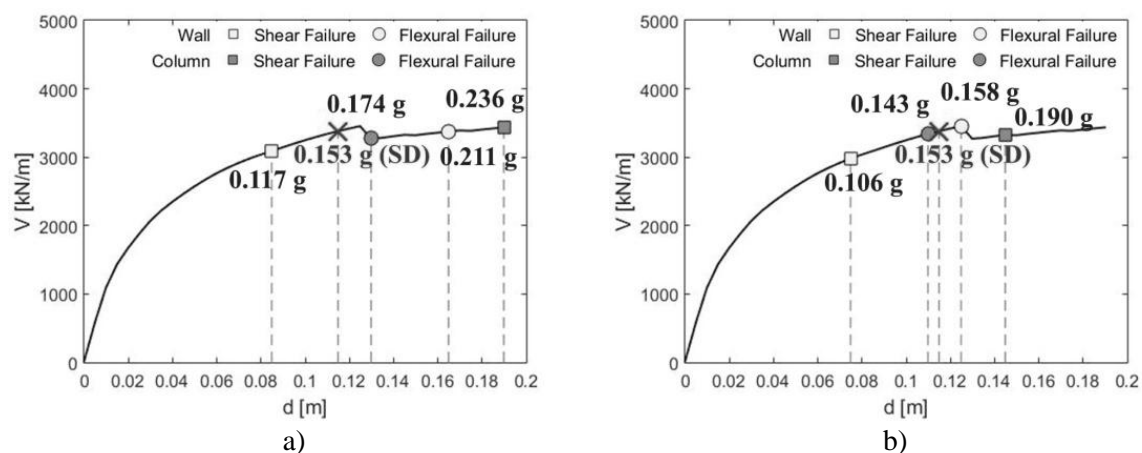


Figure 4.15 –Pushover curves for positive Y direction. Target displacement and flexural and shear failure are indicated (a) considering and (b) not considering the torsional response.

First the results related to the torsionally balanced structure determined by the Original N2 are shown (Figure 4.14a and Figure 4.15a) and then the results of the structure with accidental eccentricity determined by the Extended N2 (Figure 4.14b and Figure 4.15b). It is observed that the most severe

failure mode of the building corresponds to the shear failure (brittle failure mechanism) of the RC walls in both X and Y directions, while the columns have a fair flexural behaviour.

In the X direction, the torsional effect does not have influence on the seismic safety verification. The shear failure of the wall is reached for a very low value of the PGA, equal to 0.010 g, less than 10% of the design PGA. As stated before, this result is due to the very low amount of horizontal reinforcement (see Table 3.2).

In the Y direction, the torsional effects lead to flexural failure in columns and shear failure of the walls at an earlier stage (Figure 4.15b). The first flexural mechanism forms in columns at the roof displacement  $d = 0.111$  m, which corresponds to a PGA of 0.143 g (Figure 4.15b). Several columns in the exterior frames fail soon after the failure of the first column. The brittle failure is reached in walls at 0.075 m (PGA = 0.106 g).

It is possible to conclude that torsional effect worsens the behaviour of the structure in the Y direction, considering both the flexural behaviour of the columns and the shear failure of the RC walls. But because the worst condition is in the X direction, the PGA which leads to the failure of the structure is not varying with the consideration of the torsional effects.

#### 4.5. Conclusion

This chapter investigates the seismic performance and the importance of torsional behaviour of a specific typology of old RC wall-frame buildings which is very common in Lisbon. To this objective, the applicability of the N2 method in its original formulation (Original N2) and the Extended N2 method (specifically conceived to predict the torsional response) were analysed through a comparison with the more reliable nonlinear *Time-History* dynamic analysis. Moreover, the influence of torsion on the response parameters, namely chord rotation and shear strength was assessed.

It was possible to observe that the Extended N2 method provides a conservative estimate of the structural response in comparison with nonlinear *Time-History* analysis. However, its application is essential for predicting the torsional response of a torsionally flexible building, for which the Original N2 method does not provide accurate estimates.

A proposal was made to evaluate the shear demand by taking into account the nonlinear behaviour of the structure. It was found that the shear demand evaluated by multiplying it by correction factor (as suggested by Extended N2 method) provides a conservative estimate in comparison to TH analysis. It is suggested to apply this proposal to other types of buildings in order to confirm the obtained results.

The torsional behaviour worsens the seismic response of the structure, particularly when the earthquake acts in the Y direction (longer and asymmetric direction), leading to flexural failure in

columns and brittle failure in RC walls for values of PGA significantly smaller than those obtained for the torsionally balanced structure. Conversely, the torsional response has a small impact when the earthquake actions is applied in the X direction, corresponding to the shorter dimension in plan.

The present chapter showed that, due to the very low amount of horizontal reinforcement of the RC walls, shear failure develops in the building for a very low value of the PGA. This result expresses a very important deficiency of the building, independently from the consideration of the torsional effects.



## **5. A CONTRIBUTION TO THE SEISMIC PERFORMANCE AND LOSS ASSESSMENT OF OLD RC WALL-FRAME BUILDINGS**

### **5.1. Introduction**

Seismic vulnerability evaluation of existing buildings and the application of adequate retrofitting solutions is key to reduce the levels of physical damage, loss of life and the economic impact of future seismic events.

Earthquake economic loss estimation is an effective tool to provide owners and stakeholders with useful information to support decisions related to risk mitigation actions. In the framework of performance-based earthquake engineering (PBEE), the probabilistic estimation of monetary losses can be used as a meaningful metric of the building's seismic performance.

There are few studies in the literature concerning the development of loss estimation models for old reinforced concrete (RC) buildings in Portugal. Carvalho et al. (2002) derived several sets of fragility functions for each existing building typology in the country, based on the simplified approach proposed by FEMA and NIBS (FEMA, 2000). However, the design parameters employed in the development of the capacity curves (strength coefficient, overstrength factor, elastic period and ductility factor) were calibrated for structures typically found in the United States. Silva et al. (2015) (Silva et al., 2015a) estimated the vulnerability of typical Portuguese reinforced concrete buildings by employing an analytical methodology. Two-dimensional structural models were developed, thus hindering the consideration of plan irregularities, which typically involve torsional deformations. Moreover, the presence of shear walls was not considered. Martins et al. (2016) developed a detailed vulnerability model specific for mainland Portugal, using repair costs that are specific to the Portuguese reality. Both studies focused on RC frame systems.

Several methods are currently available for seismic loss estimation. They range from regional loss estimation methods, developed for large building portfolios, e.g. HAZUS (FEMA, 2015), to component-based loss estimation methods, which attempt to predict losses by estimating the earthquake damage to each component in a building, e.g. FEMA P-58 (ATC, 2018). In Europe, the research community is working towards the development of a uniform European risk model which will be shared through the OpenQuake platform developed by the GEM. The project involves the collection of European fragility and vulnerability functions in a database and the development of new structural fragility and vulnerability models for building typologies that have not been subject of investigation in the past (Silva et al., 2014) or that required further study.

The Pacific Earthquake Engineering Research (PEER) Centre framework, originally developed to assess seismic risk, includes a loss estimation methodology based on the principle of Performance-

Based Earthquake Engineering (PBEE). The procedure includes estimation of economic losses in four stages (Figure 1.4): (i) probabilistic seismic hazard analysis, which requires the consideration of an intensity measure (IM); (ii) structural analysis, aiming at computing engineering demand parameters (EDPs) such as peak inter-storey drift demands, peak floor accelerations, etc., conditioned on the intensity measure, (iii) damage analysis, which produces damage measures (DMs) using fragility functions; (iv) loss analysis, which consists on the calculation of probabilistic system performance measures, referred to as decision variables (DVs), conditioned on damage, such as economic losses.

Recent studies adopted the framework outlined in FEMA P-58, conceptually similar to the PEER-PBEE framework, to estimate economic losses of a set of reinforced concrete moment-resisting frame buildings, representative of older non-ductile structures, e.g. (Cardone and Perrone, 2017a) (Romano et al., 2018) (O'Reilly et al., 2018).

In this work, a specific loss estimation methodology, based on the PEER-PBEE approach, is proposed (Section 5.2) to estimate economic losses of old RC buildings. Focusing on the wall-frame building typology, the different steps of the procedure are described in detail and illustrated with the case study described in Section 3.3 of Chapter 3. The buildings of this typology, which were designed before the introduction of modern seismic codes (pre- 1980), are characterized by non-ductile behaviour and insufficient seismic detailing, e.g. (i) smooth longitudinal reinforcing bars; (ii) columns and RC walls with low confinement and tie reinforcement (lower than 1%); (iii) beams framing eccentrically to the columns. Due to the lack of data regarding post-earthquake damage for these types of buildings in Portugal, an analytical methodology is adopted.

The procedure adopted for the loss analysis makes use of the efficiency and accuracy of the component based-fragility function approach to assess damage in structural and non-structural elements. The expected level of damage for a given ground motion intensity is estimated through the employment of numerical modelling and nonlinear response-history analysis.

Specific tools for loss assessment of old RC buildings are already available in the literature (e.g. (Aslani and Miranda, 2005)). Fragility and loss functions for structural and non-structural elements were developed based on laboratory tests performed on specimens with design details representative of pre-70s RC buildings ((Cardone, 2016) and (Cardone and Perrone, 2015)). Even though experimental tests on RC walls with light horizontal reinforcement and ribbed rebars are available in the literature (e.g. (Oesterle et al., 1976); (Dazio et al., 2009); (Greifenhagen and Lestuzzi, 2005)), to the best of the authors' knowledge, no experimental data is available for RC walls with smooth reinforcing bars. For this reason, an analytical methodology is proposed herein and adopted to derive fragility functions for this type of structural elements (Section 5.3). In Section 5.4, the procedure adopted for the estimation of repair and replacement costs required for individual structural and non-structural elements is presented, along with the proposal of some unit costs for the Portuguese

building stock. The work closes with an application of the loss estimation methodology to a case study building (Section 5.5). Different repair techniques are considered, based on the extent of damage in the various components, for which repair costs associated to the Portuguese reality are considered. Economic losses are estimated based on the contribution of three components: losses associated to damage on structural and non-structural components, losses resulting if the building collapses and losses resulting from having to demolish the building due to excessive residual drifts. Finally, in Section 5.6, the results in terms of capacity and fragility curves of the case study building are compared with previous studies performed on old RC buildings.

## **5.2. Methodology for loss assessment**

In this section, the procedure for seismic performance and loss assessment of old RC wall-frame buildings is presented. The main described stages correspond to the ones identified in Figure 1.4.

### **5.2.1. Hazard Analysis**

Firstly, the probabilistic seismic hazard analysis should be conducted to estimate the site's seismic hazard curve,  $\lambda_{sa}$ , i.e. the mean annual frequency of exceeding a specific ground motion intensity level. It is suggested to use the pseudo-spectral acceleration,  $Sa(T_1)$ , as the intensity measure (Kohrangi et al., 2016). The conditioning period  $T_1$  should be the average of the first mode building vibration periods in X and Y directions,  $T_1 = (T_{1x} + T_{1y})/2$ , as proposed by FEMA P-58 for assessing the response of 3D buildings.

### **5.2.2. Structural Analysis and Engineering Demand Parameters**

For the structural analysis, a multiple stripe analysis (MSA) is proposed, which consists of performing nonlinear response-history analyses at discrete IM levels using different sets of ground motion records for a range of IM levels. The ground motions for each IM level are selected using a conditional mean spectrum (CMS) (Baker, 2011) as the target spectrum, which provides the expected (mean) response spectrum conditioned on the occurrence of a target spectral acceleration value at the period of interest.

For old RC wall-frame building structures, as with other structural systems, different engineering demand parameters should be adopted, namely the inter-storey drift ratio (IDR), the peak floor acceleration (PFA) and the residual inter-storey drift ratio (RIDR).

### 5.2.3. Damage Analysis

#### *Damage to structural components*

To identify the level of damage on structural elements, component-based fragility functions are used, which represent the probability of attaining a given level of damage for a given level of the relevant EDP. For this building typology only damage to vertical elements, i.e. columns and RC walls, is considered. In fact, for the typology of buildings object of this study, damage in beams is far less common than in columns and its impact on global stability is minimal (Fardis, 2009).

Four different damage states (DS) have been defined for non-ductile reinforced columns related to the observed damage in the components, i.e., DS1 (Light Damage), DS2 (Moderate Damage), DS3 (Severe Damage) and DS4 (Collapse). The four damage states correspond to different actions to repair the structural elements. Restoring structural damage aims to re-instate original characteristics that may have degraded. Repair is generally sufficient when such deterioration or damage is minor to moderate, provided that a necessary global upgrading of earthquake resistance is provided elsewhere (Fardis, 2009). The DS and the corresponding repair actions are discussed in more detail in the following paragraphs.

DS1 corresponds to the formation of light visible cracking which is characterised by a crack width smaller than 0.3 mm. Repair actions associated with this damage state consist of applying a surface coating on the concrete surface for moisture protection.

DS2 involves crack widths between 0.3 mm and 2.0 mm. Cracking is more extensive compared to the light cracking damage state. The repair action associated with this damage state consists of epoxy injection into the cracks. If properly carried out, injection fully reinstates the continuity of the material and, hence, the tensile strength and cohesion across the crack.

DS3 corresponds to spalling of cover concrete, possible crushing of concrete and possible buckling of rebars. Repair of columns or walls may comprise one or more of the following actions (Fardis, 2009): (i) replacement of reinforcing bars that have fractured or suffered visible buckling; (ii) removal of any loose concrete surrounding a rebar that is broken or has buckled, or has been partially exposed owing to spalling or disintegration of concrete, and replacement with epoxy or cement based concrete; (iv) Injection of cracks.

For RC walls at DS3, repair of the damaged zone is followed by concrete jacketing of the structural element. Different procedures can be adopted for the execution of RC jacketing, depending on whether it is used for repair or strengthening purposes (Júlio et al. 2003). If strengthening is intended for a damaged and/or deteriorated element, this process must be preceded by a repairing operation.

The fourth damage state (DS4) in non-ductile RC columns and walls is characterised by shear failure or loss of vertical carrying capacity. If there is no possibility to redistribute the vertical load to other members, this damage state can lead to a local collapse or, eventually, global progressive collapse of the building structure. Thus, at DS4 the structural vertical element is deemed to have collapsed. Repair actions are no longer viable.

### ***Fragility functions for RC columns***

Drift-based fragility functions are adopted for RC columns. They represent conditional probabilities of reaching or exceeding a damage state knowing that the element has been subjected to a specific level of inter-storey drift. For the definition of drift-based fragility functions of the columns, fitted lognormal cumulative distributions functions of the inter-storey drift are used.

Fragility functions selected for this methodology are derived based on the results of the study of (Aslani and Miranda, 2005). In that study, a database was collected from an experimental research conducted on 92 non-ductile RC column specimens. The results of the experimental studies were used to establish levels of lateral deformations associated with the four damage states previously described. According to the study of (Aslani and Miranda, 2005), the median inter-storey drift ratios associated to DS1 and DS2 are equal to 0.35% and 0.71%, respectively, and the values of dispersion ( $\sigma_{Ln IDR}$ ) are equal to 0.37 and 0.44, respectively. The median inter-storey drift ratios at DS3 and loss DS4 were derived using closed form analytical expressions and are given, respectively, by Equations (5.1) and (5.2):

$$\overline{IDR}_{DS3} = \frac{1}{0.26 \left( \frac{N}{A_g f'_c \rho_h} \right) + 25.4} \geq \frac{1}{100} \quad (5.1)$$

$$\overline{IDR}_{DS4} = \frac{1}{0.2 \left( \frac{N}{A_g f'_c \rho_h} \right) + 4.6} \leq \frac{1}{10} \quad (5.2)$$

where  $N$  is the axial load at the time of shear failure,  $A_g$  is the column gross section area,  $f'_c$  is the nominal concrete compressive strength,  $\rho_h$  is the transverse reinforcement ratio (the smallest along the height of the element) computed as  $A_{st}/bs$ , where  $A_{st}$  is the transverse reinforcement area in the direction of loading,  $b$  is the column width and  $s$  is the tie spacing.

The dispersion  $\sigma_{Ln IDR_{DS3}}$  of the inter-storey drifts at which shear failure occurred was assumed constant and equal to 0.55 (Aslani and Miranda, 2005). The dispersion at DS4 is given by Equation (5.3).

$$\sigma_{Ln IDR_{DS4}} = 0.68 \exp \left[ - \frac{29.4}{\left( \frac{N}{A_g f_c' \rho_h} \right)} \right] \geq 0.1 \quad (5.3)$$

### ***Fragility functions for RC walls***

An analytical methodology is proposed in Section 5.3 of this chapter to produce fragility parameters for RC walls with smooth reinforcing bars and light horizontal reinforcement.

#### ***5.2.4. Loss Analysis***

The total expected loss in a building as a function of the ground motion intensity,  $IM$ , can be calculated as the sum of three components: (i) losses resulting if the building collapses,  $E[Loss|C]$ , (ii) losses associated with repairs given that the structure has not collapsed ( $NC$ ) at a given ground motion intensity,  $E[Loss|NC \cap R, IM]$ , and (iii) losses resulting from having to demolish the building due to excessive residual drifts,  $E[Loss|NC \cap D]$ . The following equation is used to develop the building-specific relationship that relates ground motion intensity to economic monetary loss:

$$E[Loss_T|IM] = E[Loss|C] \cdot P(C|IM) + E[Loss|NC \cap R, IM] \cdot \{1 - P(D|NC, IM)\} \cdot \{1 - P(C|IM)\} + E[Loss|NC \cap D] \cdot P(D|NC, IM) \cdot \{1 - P(C|IM)\} \quad (5.4)$$

where  $P(C|IM)$  is the probability that the structure will collapse under a ground motion intensity  $IM=im$  and  $P(D|NC, IM)$  is the probability that the structure will be demolished given that it did not collapse when subjected to an earthquake with intensity level  $IM=im$ . For further details on how this expression was obtained the reader is referred to (Ramirez and Miranda, 2012).

### ***Repair Losses in Structural and Non-structural elements***

The expected value of the economic loss associated to the repair of the structure is given by the sum of the losses in structural and non-structural components. The procedure for the estimation of repair costs for structural components is presented in Section 5.4, where values typical of the Portuguese reality are presented.

The expected repair loss is computed as the sum of the losses of each individual structural and non-structural component of the building. The expected loss in an individual component,  $E[Loss_i|IM]$ , can be computed using the total probably theorem as follows:

$$E[Loss_i | IM] = \int_0^{\infty} E[Loss_i | EDP_i] \cdot |dP(EDP_i > edp_i | IM)| \quad (5.5)$$

where  $E[Loss_i | EDP_i]$  is the expected loss in the  $i$ th component when it is subjected to a given level of an engineering demand parameter, and  $P(EDP_i > edp_i | IM)$  is the probability of exceeding  $edp_i$  in the  $i$ th component for a given ground motion intensity. Further explanations on the numerical procedure to compute the expected losses in structural and non-structural elements can be found in (Aslani and Miranda, 2005).

Losses associated to acceleration-sensitive non-structural components can be computed using a storey-based approach, as proposed by (Ramirez and Miranda, 2009), which requires grouping the losses per storey and pre-computing estimated damage using assumed cost distribution of the total storey value. In this study, storey damage functions and loss ratio provided by HAZUS are used. For the case-study building presented in Section 5.5, it is assumed that the total replacement value is uniformly distributed among the stories.

### ***Expected annual loss***

One of the objectives of monetary loss estimation analysis is the evaluation of the expected annual loss (EAL) of the building, which corresponds to the economic loss that, on average, can occur every year. The EAL provides quantitative information to assist stakeholders in making risk management decisions and is used in the insurance sector to calculate the insurance premium. Therefore, a reduction of EAL can, in principle, be transformed into an economic return (Calvi, 2013).

The mean annual frequency of exceeding an economic loss greater than a certain amount provides information on the likelihood of experiencing an economic loss higher than a certain amount (Ramirez and Miranda, 2009). Once the expected loss at a given intensity level has been computed, the expected annual loss is obtained by integrating over all possible intensities, as follows:

$$EAL = \int_0^{\infty} E[Loss_T | IM] \cdot d\lambda(IM) \quad (5.6)$$

where  $\lambda(IM)$  is the mean annual frequency of the ground motion intensity.

### **5.3. Analytical evaluation of fragility parameters for RC walls**

The severe damage and collapse of many reinforced concrete (RC) wall buildings in recent earthquakes (Kam et al., 2011) have shown that old RC walls did not perform as required by modern seismic codes. The low amount of transverse reinforcement and/or the absence of seismic detailing can be detrimental for the member response. Another characteristic that can affect the seismic response is the presence of smooth rebars, widely used in many European countries, including

Portugal, up to the '70s (Verderame et al., 2008b) (Silva et al., 2015a). Even though it is common to assume a perfect bond between the reinforcing bars and concrete, neglecting the relative bond-slip deformations, strain penetration (SP) deformations can contribute up to 40% to the total lateral deformation when ribbed rebars are used (Goodnight et al., 2015) (Sezen and Moehle, 2004) and up to 90% when smooth rebars are present (Verderame et al., 2008a). The results in Section 2.4 of Chapter 1 showed that the consideration of SP effects introduces a non-negligible flexibility at the base of the walls, which becomes even more relevant as anchorage conditions deteriorate (i.e. considering smooth rebars and reduced anchorage lengths). Moreover, in the case of reduced embedment lengths, the lateral strength of the wall can be significantly compromised due to failure of the anchorage system.

In the following paragraphs a numerical procedure is proposed with the aim of deriving fragility parameters for RC walls made with smooth rebars.

### 5.3.1. Modelling considerations

A parametric analysis on a case study slender RC wall is considered hereafter. The wall is representative of constructions without seismic detailing, with a longitudinal reinforcement ratio lower than 1%, a relatively low axial load ratio ( $N/A_g f_c$ ) and limited ductility. The geometric and material properties of the wall are based on the test unit WSH4 analysed by (Dazio et al., 2009).

The RC wall is modelled with a fibre-based nonlinear beam element using the open-source software OpenSEES (McKenna et al., 2000). The fibre-section elements capture the spread of yielding and cracking in reinforcing steel and concrete, avoiding the predefined cracked section stiffness and moment-curvature relationship. The cross-sectional analysis is performed by discretizing the sections into fibres. A simple approach involving the reduction of the Young's Modulus,  $E$ , and maximum strength of the reinforcing steel,  $f_{y,max}$ , is used to simulate the increase in member flexibility due to SP effects (Chapter 1). Based on the results of Section 2.4 in Chapter 1, the reduction in Young modulus is assumed as 50%. In order to estimate the reduction of the rebar's capacity, a constant averaged bond stress is considered along the total anchorage length and the force in the rebar is equal to the anchorage force, as in Equation (5.7):

$$A_s f_s = P L_e \tau_{max} \quad (5.7)$$

where  $f_s$  is the maximum steel stress,  $A_s$  and  $P$  are the area and perimeter of the bars, respectively,  $\tau_{max}$  is the maximum constant averaged bond stress for the case of smooth bars (fib, 2013).

As regards the material properties, the concrete compressive strength is taken equal to 40.9 MPa and the concrete tensile stress as 10% of the compressive strength, while the steel yield strength is 576 MPa (Dazio et al., 2009). The model in (Menegotto and Pinto, 1973) is used for defining the steel behaviour. Cover and core concrete are modelled using the uniaxial material 'Concrete 04' available

in OpenSEES, which is based on the model proposed by (Popovics, 1973). The confinement effect of the concrete core is determined according to (Mander et al., 1988) with a geometrical effectiveness coefficient of confinement  $C_e = 0.5$ , as recommended by (Priestley et al., 2007) for wall-type elements, whereas the ultimate confined concrete compression strain assumed is based on the recommendations of (Priestley et al., 1996).

### 5.3.2. Parametric investigation

In order to examine different geometrical and material parameters, which is usually impracticable in experimental tests, the numerical modelling is commonly used as a complementary approach for further studies. In the presented work, the numerical analyses are performed on the pre-calibrated model (Caruso et al., 2019) to assess the influence of various geometrical and material parameters that can affect the behaviour of the RC walls.

It is worth noting that the structural response of RC walls largely depends on their geometrical properties, namely the shear span-to-depth ratio (Paulay and Priestley, 1992). In general, for ratios higher than about 2.5, RC walls are classified as slender walls and are essentially controlled by flexural behaviour. In this case, the impact of shear deformations on global engineering demand parameters such as member forces and inter-storey drift displacements will be typically small and can possibly be neglected (Priestley et al., 2007). For smaller shear span ratios walls are considered squat and shear deformations are expected to play an increasing role on the member response (Priestley et al., 2007).

As for the geometrical parameters, some considerations can be made. For example, it is known that displacement ductility, plastic hinge rotation and ultimate drift capacities are size independent under constant shear span ratio (fib - bulletin 24, 2003). The shear span ratio has a particular influence on elastic contributions to peak displacement capacity and this could lead to a parametric dependency of ductility and drift on shear span ratio, particularly for the lightly confined sections. Furthermore, when confinement is poor, a strong dependency of deformation indices (such as yield and ultimate displacement or curvature) on the axial load ratio is expected with a marked reduction of deformability as the axial load ratio decreases (fib - bulletin 24, 2003). These parameters and the interaction between them are expected to have a strong influence on the structural behaviour of slender RC walls with low horizontal reinforcement. The study presented herein examines these effects.

Taking into account the abovementioned considerations, and after performing a preliminary sensitivity analysis, the following parameters have been considered: (i) shear span ratio, defined as the moment ( $M$ ) to shear ( $V$ ) ratio divided by the member depth ( $L_w$ ) (i.e., length of wall) ( $M/VL_w$ ); (ii) axial load ratio ( $N/A_g f_c$ ); (iii) horizontal reinforcement ratio  $\rho_{hi}$ ; (iv) normalized maximum steel

strength as a function of the embedment length,  $\rho_{Le} = f_{y,max}/f_y$ , where  $f_{y,max}$  is maximum strength of the reinforcement, and  $f_y$  is the yield strength of reinforcement. The values adopted for these parameters are listed in Table 5.1. The logic tree approach used for the combination of the parameters is shown in Figure 5.1. As regards the material properties, mean values are considered.

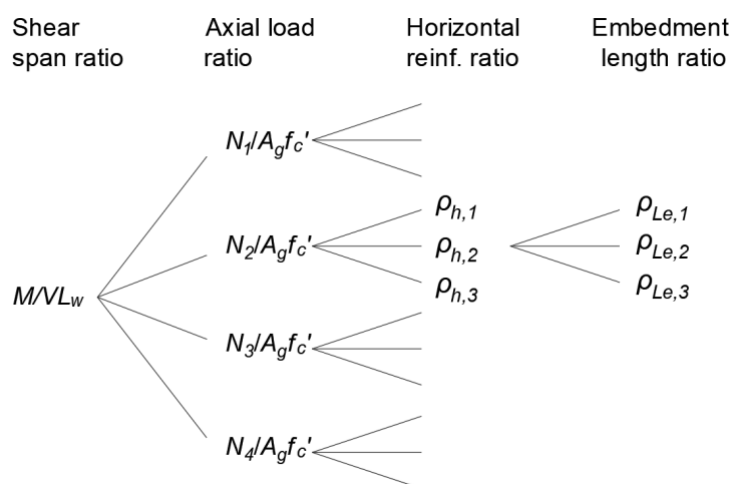


Figure 5.1 – Logic tree adopted in the parametric study.

Table 5.1 – Parameters and corresponding values considered in the study.

Shear-Span Ratio ( $M/VL_w$ )	Axial Load Ratio ( $N/A_g f'_c$ )	Reduction factor ( $\rho_{Le} = f_{y,max}/f_y$ )	Transverse Reinf. Ratio ( $\rho_h$ )
2.1	0.04	0.6	0.0009 - No conf.
2.3	0.06	0.8	0.0012
2.5	0.08	1.0	0.0020
	1.00		

### 5.3.3. Identification of damage states

In this study, four damage states (or performance levels) are considered in the performance assessment of the RC walls. The assessment is based on local EDP, i.e. material strains for flexural failure modes and internal forces for the brittle failure mechanism:

- DS1 refers to the flexural cracking of concrete and is identified as a drop of 30% of the initial stiffness of the wall.
- DS2 corresponds to the first yield, which is characterized by the occurrence of either (i) the yield strain in the rebars,  $\varepsilon_y$  ( $\varepsilon_y = f_y/E_s$ ), or (ii) by a value of concrete strain,  $\varepsilon_c$ , equal to 0.002.
- DS3 is defined at the first occurrence of either the ultimate strain in the unconfined concrete,  $\varepsilon_c = 0.004$ , at the onset of concrete spalling, or a strain in the rebar after yielding,  $\varepsilon_s$ , equal to 0.015, at the onset of 1 mm crack widths.

- DS4 is bounded by one of the following scenarios, whichever occurs at a lower value of drift: (i) the ultimate strain in the steel rebar or in the concrete is reached; (ii) occurrence of shear failure. As for the material strain limits, DS is defined as the first occurrence of either the ultimate strain of confined concrete,  $\varepsilon_{cu}$  or the ultimate strain of reinforcement, defined as 60% of the ultimate capacity to account for the effects of buckling and low cycle fatigue, as recommended by (Priestley et al., 2007):

$$\varepsilon_s = 0.6 \varepsilon_{su} \quad (5.8)$$

The ultimate concrete strain is given as:

$$\varepsilon_{cu} = 0.004 + 1.4\rho_s f_{yh} \frac{\varepsilon_{su}}{f'_{cc}} \quad (5.9)$$

where  $\rho_v$  and  $f_{yh}$  are, respectively, the volumetric ratio and the yield strength of the transversal reinforcement,  $\varepsilon_{su}$  is the monotonic steel strain at maximum strength and  $f'_{cc}$  is the compression strength of confined concrete.

Shear failure mode is identified by comparing the shear demands with the values of the shear capacity. As for the shear capacity, a detailed review of shear strength capacity models for the seismic assessment and retrofit of existing structures was carried out by (Del Vecchio et al., 2017). In particular, classical truss-based approaches, refined mechanical models and semi-empirical formulations properly calibrated for non-conforming RC elements have been surveyed. It emerged that the empirical model proposed by (Biskinis et al., 2005), which is currently suggested in EC8-3 for assessment purposes, provides accurate predictions of shear strength. This empirical model has been calibrated to a database of 239 experimental tests, including tests on rectangular and circular columns, shear walls and bridge piers failed both in shear and flexure-shear. The model provides two formulations for columns shear failure, due to diagonal tension and diagonal compression. This makes the model suitable for application in seismic assessment procedures as long as the ductility at the onset of shear failure is properly estimated. Due to this consideration, the shear strength capacity model prescribed by EC8-3 is adopted in this study.

#### **5.3.4. Analysis and discussion of the results**

Nonlinear static pushover analyses are performed on the model which takes different values of the parameters, as previously defined and according to the logic tree presented in Figure 5.1, for a total of 108 analyses. The most representative pushover curves are shown in Figure 5.2 for two values of shear span ratio and different embedment lengths and constant levels of horizontal reinforcement and axial load ratio. It is clear that higher lateral strength is obtained for lower levels of shear span ratio and also that the consideration of SP effects introduces a non-negligible flexibility at the base of the walls, which becomes more relevant as the embedment length is reduced.

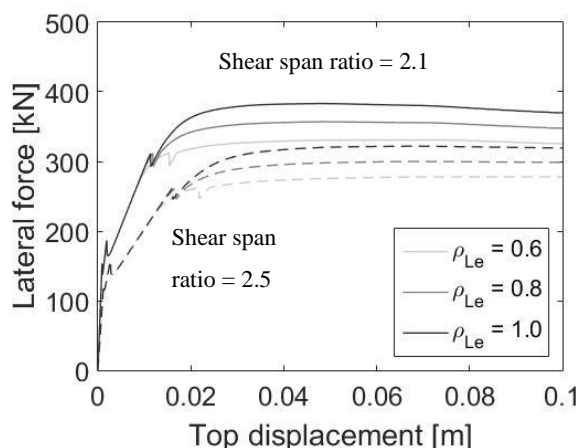


Figure 5.2 – Pushover curves with different embedment length of the rebars, for two values of shear span ratio and for specific values of horizontal reinforcement ratio and axial load ratio.

In Figure 5.3 the variation of IDR with respect to several parameters is shown for DS4. Figure 5.3a shows the variation of IDR with respect to the horizontal reinforcement ratio ( $\rho_h$ ), whereas Figure 5.3b shows the variation of IDR with respect to the axial load ratio, for constant values of horizontal reinforcement ratio ( $\rho_h$ ). Higher levels of  $\rho_h$ , therefore higher level of confinement, are reflected in higher scatter of the results. This is due to the shear capacity model employed in this study, according to which the shear resistance increases with confinement but decreases for higher levels of shear span ratios. It is worth noting that the IDR is measured at the top of the wall specimen.

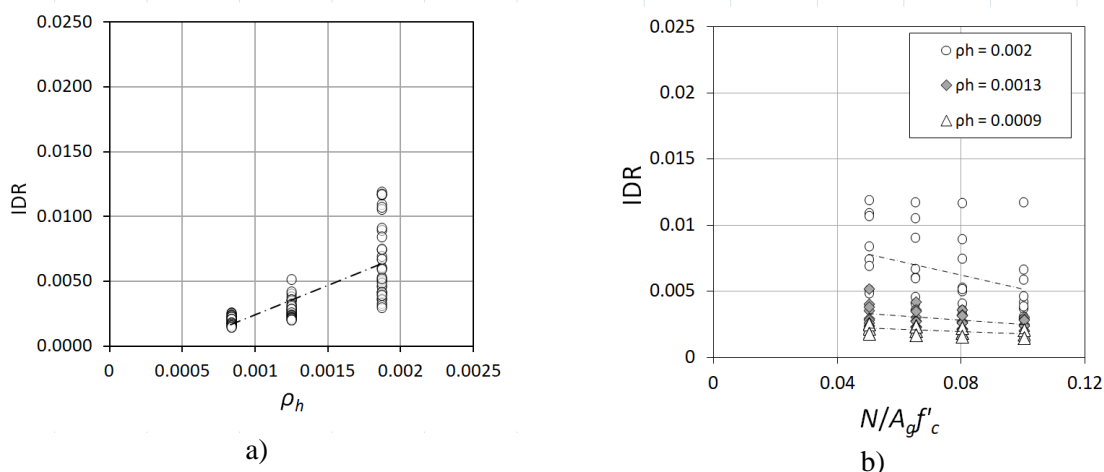


Figure 5.3 – Variation of IDR with respect to (a) the axial load ratio and (b) horizontal reinforcement for DS4.

A regression analysis is performed to fit polynomial functions that establish a relation between the IDR and the three parameters, namely the axial load ratio, the horizontal reinforcement ratio and the reduction factor of steel strength as function of the embedment length. Equations (5.10) to (5.13) have been obtained to express the median inter-storey drift ratios for DS1 to DS4, respectively. The coefficient of determination,  $R^2$ , is equal to 0.85 and 0.7 for DS3 and DS4, respectively, which

suggests a good and a moderately good correlation for DS3 and DS4, respectively. The dispersion,  $\sigma$ , is estimated as 0.20 for DS1 and DS2 and 0.35 and 0.38 for DS2 and DS3, respectively.

$$\overline{IDR}_{DS1} = 0.0013 \quad (5.10)$$

$$\overline{IDR}_{DS2} = 0.0015 + 0.05\rho_h \quad (5.11)$$

$$\overline{IDR}_{DS3} = 0.001 + 0.054\rho_h + 0.005\rho_{Le} - 0.003 \frac{N}{A_g f_c} \quad (5.12)$$

$$\overline{IDR}_{DS4} = 0.003 + 4\rho_h - 0.035 \frac{N}{A_g f_c} \quad (5.13)$$

#### 5.4. Estimation of repair and replacement costs

In this section, the procedure suggested for the estimation of costs associated with the repair and replacement actions required for individual structural and non-structural elements is presented, along with the proposal of some unit costs for the Portuguese building stock.

##### 5.4.1. Costs for repairing structural damage

The damage state in an individual structural component is defined based on specific repair and/or replacement actions that would have to be undertaken as a result of the observed damage. Economic loss is defined as the cost associated to the repair or replacement actions required for an individual component when a specific damage state has been observed in that component.

The economic losses in individual components can be normalized by dividing each repair activity by the replacement costs of each component,  $i$ . The expected normalized losses,  $E[Loss_i|DS_j]$ , at different damage states,  $j$ , are obtained as the sum of the normalized cost of repair actions required for each damage state:

$$E[Loss_i|DS_j] = \sum_{k=1}^k E[RA_k] \quad (5.14)$$

where  $E[RA_k]$  is the expected normalized cost associated with the  $k^{\text{th}}$  repair action.

Information corresponding to the cost of the repair actions for each damage state in reinforced concrete columns is presented in Table 5.2. Information about the cost of concrete jacketing RC walls for DS3 is presented in

Table 5.3. In the tables, a brief description of each repair action is presented together with the unit costs. In order to consider reliable and realistic repair costs, the CYPE database (CYPE, 2014), which contains detailed and up-to-date construction costs for the Portuguese building stock, has been utilized. Repair costs should not be estimated for the fourth damage state. This is mainly because, for the old RC wall-frame buildings, it is assumed that once DS4 is reached by any structural vertical component, at least a local collapse occurs and therefore the building needs to be replaced. For more details on the estimated cost of repairing damage at each damage state see Annex C.

Table 5.2 – Unit cost for repair action required for each damage state in reinforced concrete columns.

Damage state	Repair Actions	Unit	Unit cost [€/unit)
DS1 Light damage	Cleaning cracks' interior	m	3.64
	Patching spalled concrete with mortar mix	m <sup>2</sup>	12.10
DS2 Moderate damage	Cleaning cracks' interior	m	3.64
	Epoxy crack injection	m	88.50
	Patching spalled concrete with mortar mix	m <sup>2</sup>	12.10
DS3 Severe damage	Cleaning cracks' interior	m	3.64
	Replacement of buckled or fractured bars	m <sup>3</sup>	162.36
	Epoxy crack injection	m	88.50
	Replacement of concrete that is loose, or has spalled, or has been removed to replace bars	m <sup>2</sup>	82.86

Table 5.3 – Unit cost for repair action required for concrete jacketing of walls required at DS3.

	Repair Actions	Unit	Unit cost [€/unit)
DS3 Severe damage	Surface roughening	m <sup>2</sup>	40.52
	Bonding agent (epoxy)	kg	13.35
	Concrete	m <sup>3</sup>	111.63
	Reinforcing steel bar	kg	0.74
	Formwork	m <sup>2</sup>	10.50
	Specialised worker	h	18.05
	Regular worker	h	17.64

However, repair activities are not limited to a series of specific repair actions for each RC member but they also include a few preliminary and supplementary activities such as: (i) safety operations (installation of scaffoldings and/or work platforms, etc.), (ii) demolition activities, (iii) cleaning operations, (iv) replacement and restoration of finishes and other mechanical and electrical systems, technical costs (fees for structural engineer, project engineer, construction manager, etc.).

As highlighted in the work of (Cardone, 2016), the most important cost items are related to replace/restore activities and safety operations, which together can represent up to 50% of the total repair cost. In this study, the total repair costs for each DS are increased to account for the safety operations which are estimated as 30% of the total repair cost, as referred in (Cardone, 2016).

#### 5.4.2. Damage to non-structural components

Buildings are composed by structural (load carrying) and non-structural systems (e.g. architectural and mechanical components). In general, the structural system represents about 25-30% of the building's total value (Martins et al., 2016) (Calvi, 2013) (FEMA, 2015). The remaining cost is distributed among different categories of non-structural components. In this building typology two categories of non-structural components should be considered: drift-sensitive non-structural components, that are primarily affected by building lateral deformations, and acceleration-sensitive non-structural components, that are primarily affected by floor accelerations. The two types of EDPs considered are the inter-storey drift ratio evaluated at every storey,  $IDR_i$ , and the peak floor acceleration at every floor,  $PFA_i$ , for drift-sensitive and acceleration-sensitive non-structural components, respectively. A brief description is reported in Table 5.4 based on (FEMA, 2015) and (Cardone et al., 2018).

Table 5.4 – Classification of drift-sensitive and acceleration-sensitive non-structural components.

Type of component (EDP)	Component category	Component Description
Non-structural drift-sensitive (IDR)	Architectural	Non-bearing Walls/Partitions
		Exterior Walls
		Veneer and Finishes
		Sliding Windows
Non-structural acceleration-sensitive (PFA)	Architectural	Cantilever Elements and Parapets
		Racks and Cabinets
		Appendages and Ornaments
		Roof covering
	Mechanical and Electrical	General Mechanical (boilers, etc.)
		Piping Systems
		Elevators
		Electrical service and distribution
		Lighting system

While damage to the structural system is the most important measure of building damage affecting mostly human losses, damage in non-structural component contributes, to a large extent, to direct economic losses. The study of (Cardone and Perrone, 2017b) showed that, for old residential buildings, the contribution to repair losses is mostly characterised by damage to drift-sensitive non-structural component, e.g. masonry infills and partition walls, while the contribution of acceleration-sensitive non-structural components is practically negligible. For this reason, it is suggested to adopt component specific fragility and loss functions for drift-sensitive non-structural components and a simplified storey-based approach for acceleration-sensitive non-structural components.

In this study fragility and loss functions for masonry infill walls developed in (Cardone and Perrone, 2015) are adopted. In (Cardone and Perrone, 2015), fragility functions were derived from previous experimental tests on laboratory specimens representative of typical non-structural components of RC frame buildings built before the 70s, i.e. infills realized with solid/hollow clay brick units with lime/cement mortar, while loss functions were derived based on Italian price lists. Fragility functions were distinguished for exterior masonry walls with and without windows or French windows and interior partitions and for four discrete damage states.

Fragility and loss function parameters for masonry infills walls and partitions are presented in Table 5.5. In (Cardone and Perrone, 2015) four damage states have been defined, corresponding to: Light Cracking (DS1); Extensive Cracking (DS2); Corner crushing (DS3); Collapse (DS4). It is worth noting that DS4 corresponds to the in-plane or out-of-plane (whichever occurs first) global collapse of the wall. For the partitions, DS3 = DS4. The last columns of Table 5.5 represents the normalized repair cost ratios,  $L_i$ , at the 50<sup>th</sup> percentile. More details are available in the abovementioned literature.

Table 5.5 – Fragility and loss function parameters for masonry infills walls (Cardone and Perrone, 2015).

Fragility Group	Damage States	Median IDR (%), PFA (g)	Dispersion, $\sigma_i$	Normalized repair cost ratios, $L_i$
Exterior masonry infills walls/ Interior partitions without opening	DS1	0.15%	0.25	0.19/0.16*
	DS2	0.40%	0.25	0.38/0.22
	DS3	1.0%	0.25	1.81/0.72
	DS4	1.75% (in-plane) 0.65g (out-of-plane)	0.25	1.83
Exterior masonry infills walls with windows	DS1	0.10%	0.25	0.19
	DS2	0.30%	0.25	0.33
	DS3	0.75%	0.25	1.23
	DS4	1.75% (in-plane) 0.65g (out-of-plane)	0.25	1.37
Exterior masonry infills walls with French windows/ Interior partitions with doors	DS1	0.075%	0.25	0.17/0.18*
	DS2	0.20%	0.25	0.31/0.33
	DS3	0.50%	0.25	1.25/1.34
	DS4	1.75% (in-plane) 0.65g (out-of-plane)	0.25	1.47

\* Values for interior partitions

Damage to acceleration-sensitive non-structural components is estimated using fragility functions and loss ratios based on the building-level relationships published by HAZUS (FEMA, 2015). The cost of acceleration-sensitive non-structural components is estimated as a percentage of the total construction cost of the building. It is suggested to assume a value of 20% of the total building cost (Martins et al., 2016).

### 5.5. Application to the case study building

The methodology for economic loss assessment described in the previous paragraph is applied to the case study building described in Chapter 3.

#### 5.5.1. Hazard Analysis and Engineering Demand Parameters

The seismic hazard curve at the site,  $\lambda_{Sa}$ , is defined by means of probabilistic seismic hazard analysis. The seismic hazard model for Portuguese territory used in this study is the model proposed in the SHARE research project, available at EFEHR (<http://www.efehr.org>), in combination with additional fault sources (Vilanova and Fonseca, 2007). Further information on the ground motion prediction equations considered can be found in (Silva, 2013).

In this work, the 5% damped pseudo-spectral acceleration,  $Sa(T_1)$  is used as the intensity measure.

Figure 5.4 shows the hazard curve for Lisbon corresponding to the average period  $T_1$  of the structure,

equal to 0.89 seconds. Soil type B as defined in Part 1 of Eurocode 8 (CEN, 2004) has been considered for the derivation of the hazard curve.

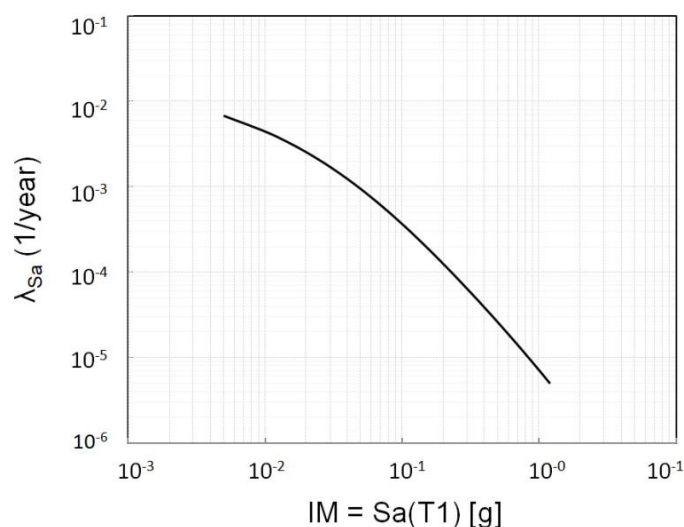


Figure 5.4 – Seismic hazard curves for Lisbon, for a return period  $T_1 = 0.89$  seconds.

For this study, five conditional mean spectra (CMS) are used for different probabilities of occurrence, i.e., 1%, 2%, 5%, 10% and 30% in 50 years (return period of 4975, 2475, 975, 475 and 140 years, respectively), corresponding to intensity levels of spectral acceleration,  $Sa(T_1)$ , ranging from 0.58g to 0.062g (see Annex A). For each IM level, 40 pairs of ground motion records are selected, each record consisting of two horizontal components compatible with the five CMS (one for each intensity level). The geometric means of the spectra of the two components are used to match the target spectral acceleration of the CMS at period  $T_1$ . Real ground motion records are selected using the SELEQ tool (Macedo and Castro, 2017), following the methodology proposed in (Araújo et al., 2016).

Figure 5.5 shows the engineering demand parameters (EDP) adopted in this study, namely the inter-storey drift ratio (IDR) and the peak floor acceleration (PFA), plotted for different levels of seismic intensity. In the figure,  $E[IDR|IM = Sa(T_1)]$  and  $E[PFA|IM = Sa(T_1)]$  represent, respectively, the expected (mean) IDRs and the expected PFAs for different seismic intensity levels.

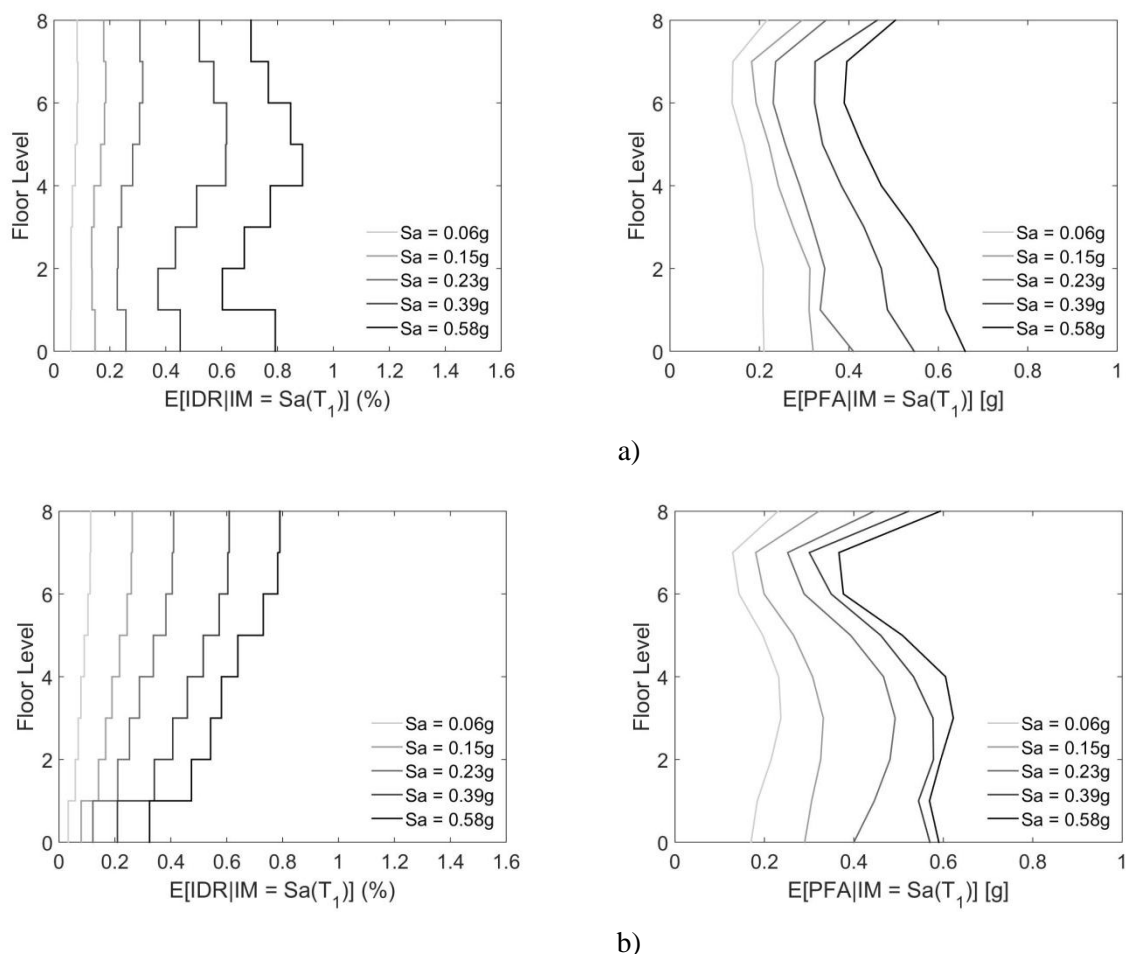


Figure 5.5 – Engineering demand Parameter (EDP) data as a function of the building levels for (a) the X and (b) Y direction. IDR, inter-storey drift ratio (left); PFA, peak floor acceleration (right).

To address the seismic assessment of the building, the following modelling parameters are identified as source of aleatory uncertainty: (i) the concrete compressive strength ( $f_c$ ), (ii) the steel yield reinforcement ( $f_y$ ), the reinforcing bars' embedment length ( $L_e$ ), the shear elastic modulus of the infill walls ( $G_w$ ) (see Section 3.4). The value adopted for the modelling parameters, together with their lower and upper limit values and coefficients of variation, are summarised in Table 3.5. The effect of the uncertainties is determined by associating to each ground motion a sample of the uncertainties taken from their distributions. The approach is acceptable if the number of time-histories is adequate to describe at least approximately the distribution of the random variables (Pinto and Franchin, 2014). In this case 40 models are generated and associated to each of 40 accelerograms for each IM level. This allows taking into account the uncertainties due to the structural response.

### 5.5.2. Damage analysis

#### *Fragility functions for RC columns*

In this study, the fragility functions and analytical expressions described in Section 5.2 are used to estimate the probability of reaching or exceeding different damage states in the non-ductile RC columns of the case study building. For DS1 and DS2 the values provided in (Aslani and Miranda, 2005) are used. For DS3 and DS4 the expressions (5.1) to (5.3) are used, which are a function of the inter-storey drift ratio in the component and the level of axial load (Aslani and Miranda, 2005). As an example, two types of columns are distinguished depending on the level of axial force and the amount of transverse reinforcement, namely an interior column (column 9) and an exterior one (column 2), which are identified in Figure 3.7. The corresponding fragility functions for the four damage states at three different storey levels of the building are shown in Figure 5.6. In the figure,  $P(DS \geq ds_j | IDR = idr)$  represents the probability of reaching or exceeding damage state  $i$  ( $ds_i$ ).

The fragility functions provide very useful information as they allow identifying the components that are more vulnerable in the building. It is worth noting that the IDR in the column corresponds to the chord rotation of each element. By comparing the level of damage at the different storeys, it can be observed that at the first storey (level 0-1) the damage is higher when compared to the upper storeys (levels 4-5 and 7-8) due to the higher level of axial load. It is also possible to observe that the damage is higher for the interior column (column 9).

#### *Fragility functions for RC walls*

The fragility functions of the RC wall of the case study building, defined according the procedure proposed in Section 5.3, is shown in Figure 5.7. In Figure 5.7a, the vertical axis,  $P(DS \geq ds_j | IDR = idr)$ , represents the probability of experiencing or exceeding a damage state  $i$  ( $ds_i$ ), given a certain IDR, while the vertical axis of Figure 5.7b represents the probability of being in each damage state,  $P(DS = ds_j | IDR = idr)$ .

The fragility curves show that the RC walls are much more vulnerable in comparison to the columns. For example, complete collapse is expected for a value of 1.5% IDR, while in the columns collapse is expected for IDR of about 3% for the exterior column and about 2% for the interior one, at the first storey.

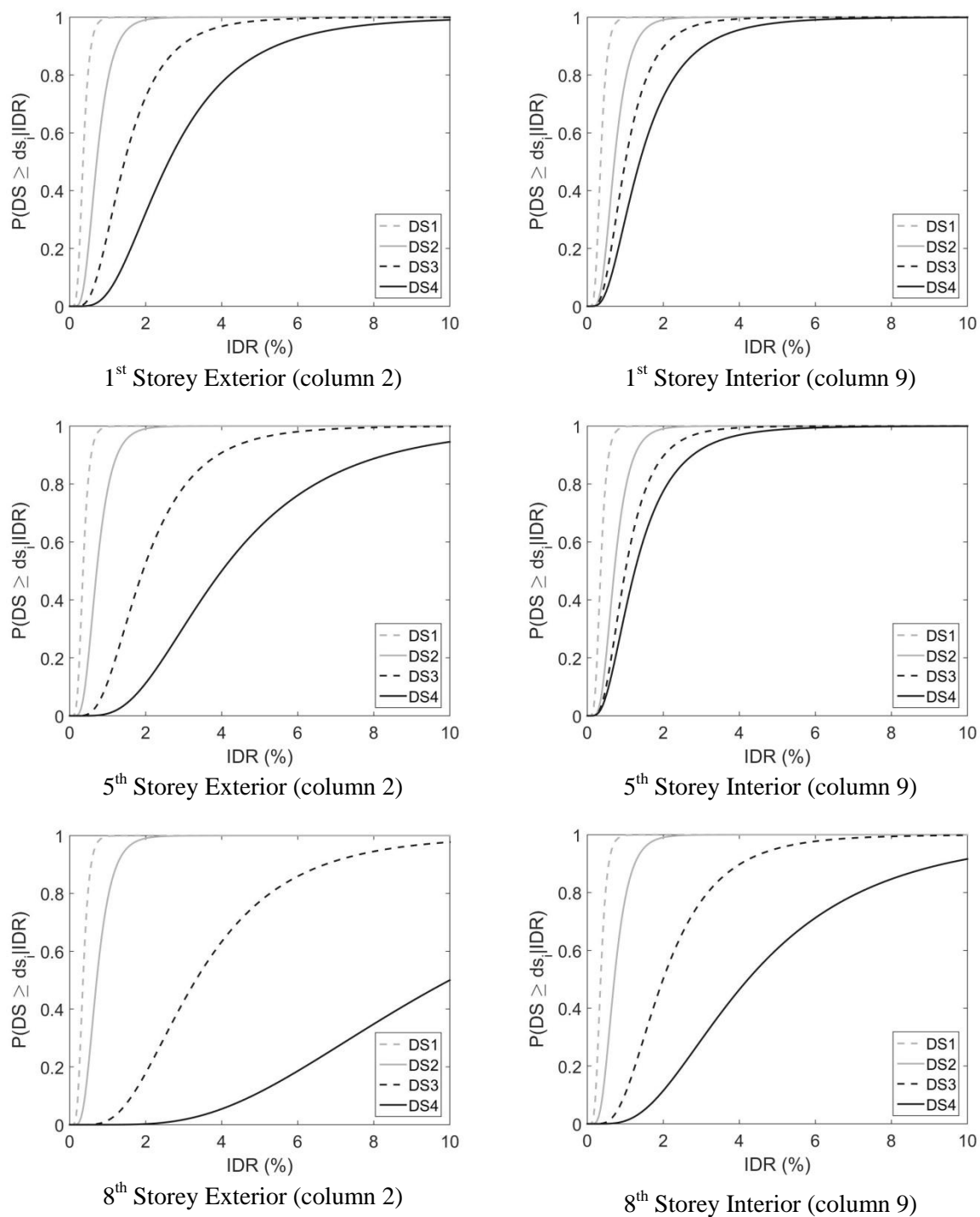


Figure 5.6 – Fragility functions corresponding to four damage states for RC columns 2 and 9 at three storey levels (1st, 5th and 8th storeys) of the case study building.

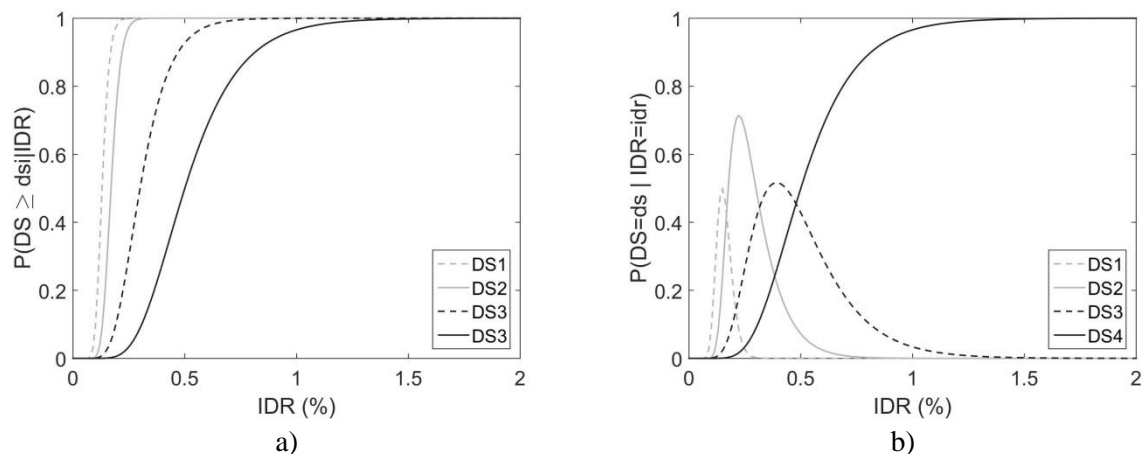


Figure 5.7 – Fragility functions of the RC wall: (a) probability of exceeding a damage state and (b) probability of being in each damage state.

### 5.5.3. Cost of structural and non-structural components

Table 5.6 lists the cost estimates of the case study building for the evaluation of its replacement cost. The replacement cost of the building is evaluated by multiplying the total floor area by an average construction cost per square meter. In the present study, the average construction value suggested by the Portuguese government for 2019 (615 €/m<sup>2</sup>) (Finanças, 2018) is adopted. In fact, reference values for construction costs are not available from official source in Portugal. As such it was used the price per m<sup>2</sup> as a proxy per cost. Furthermore, construction costs in Lisbon are increasing steeply in the last years and have a high variability depending on the quality of construction and location.

Table 5.6 – Cost estimates for the evaluation of replacement cost of the case study building.

Number of storeys	8
Footprint	10.1 x 37.1
Area (m <sup>2</sup> )	374.1
Cost per m <sup>2</sup> (€/m <sup>2</sup> )	615
Replacement cost (€)	1 840 572

The expected loss of structural components is normalized by the average cost of replacement of the component. In this study, the replacement cost of the structural elements is estimated as a fraction of the structure's replacement cost (see Table 5.6), considering the ratio between the volume of the element ( $V_i$ ) and the volume of the structure (Martins et al., 2016) – Equation (5.15).

$$Cost_i = C_{building} \frac{V_i}{\sum_{i=1}^{nElem} V_i} \quad (5.15)$$

The cost of acceleration-sensitive non-structural components has been estimated as defined in Section 5.2.4 and Section 5.4.2.

#### 5.5.4. Estimation of economic losses

In this section, the expected economic loss of the case study building as a function of the level of ground motion intensity is evaluated, starting from the evaluation of the structural and non-structural elements' repair losses conditioned on the level of ground motion intensity. The probability of collapse of the building is then evaluated and the collapse safety assessed. With all these results, and through convolution with the seismic hazard curve for the city of Lisbon, the EAL of the case study building is estimated.

##### *Loss estimation associated to structural and non-structural elements*

As reported in Section 5.2.4, the expected loss in a component conditioned on the EDP,  $E[Loss_i|EDP_i]$ , can be computed as a function of the cost of repairing the component when it is in different damage states and the probability of being in each damage state. Figure 5.8 and Figure 5.9 show the expected losses in columns and RC walls, respectively, as a function of the level of inter-storey drift ratio, IDR. Figure 5.8 presents the expected losses in columns located at three different stories of the case study building and for the case of an exterior and an interior column, represented, respectively, by column 2 and column 9.

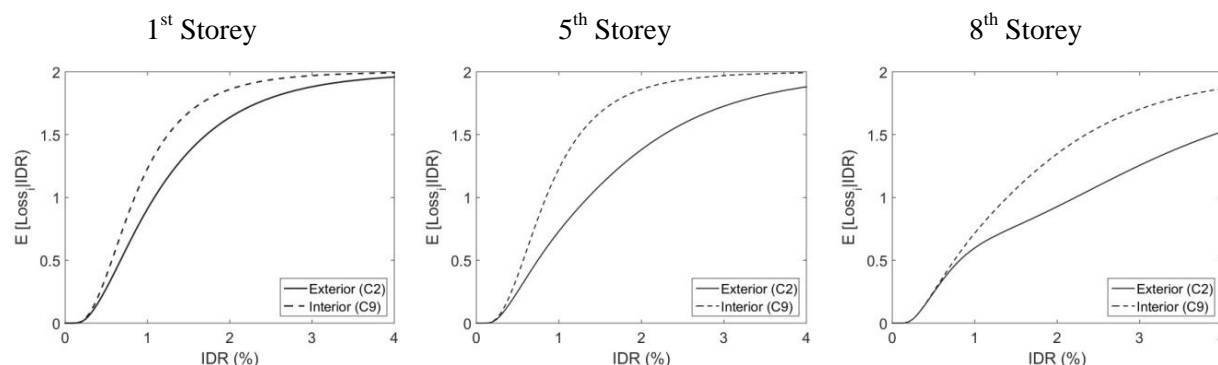


Figure 5.8 – Variation of the expected loss in an exterior and an interior column of the case study building as a function of the IDR, at levels 1<sup>st</sup>, 5<sup>th</sup> and 8<sup>th</sup>.

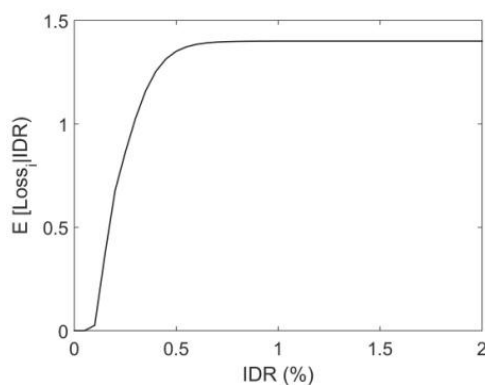


Figure 5.9 – Variation of the expected loss in RC walls of the case study building.

Useful information can be extracted from the figure. For example, at 2% IDR the expected loss in an exterior column at the 5<sup>th</sup> storey is approximately 1.3 times the cost of a new column, whereas the expected loss in an interior column in that same storey is approximately 1.8 times the cost of a new column. Therefore, it can be concluded that the average expected loss at the component level is higher for the interior columns located at the 5<sup>th</sup> storey than the exterior columns located at the 5<sup>th</sup> storey. As shown in Figure 5.9, and as expected, for similar levels of inter-storey drift ratio, RC walls are associated with higher losses in comparison to columns at all storeys.

After evaluating the expected loss in each component as a function of the level of deformation, Equation (5.5) can be used to obtain the component expected loss conditioned on the level of ground motion intensity, IM. Then, the repair loss is computed as the sum of the losses of both structural and non-structural components.

Figure 5.10 shows the contribution to the repair loss of each component category, i.e. structural, drift sensitive and acceleration-sensitive non-structural components, and the total repair loss, as a function of the intensity measure. The losses are normalized by the total building's replacement value.

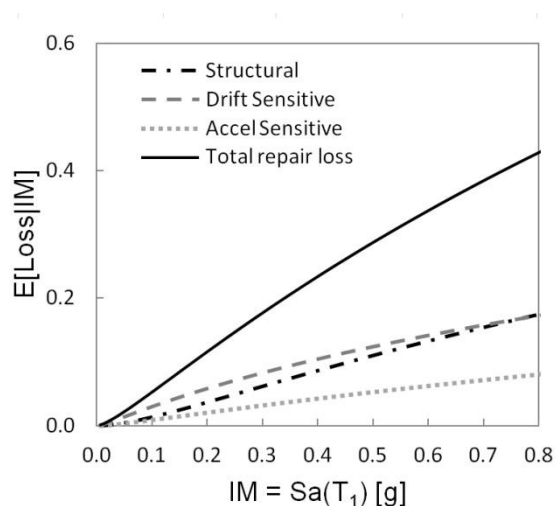


Figure 5.10 –Normalized losses due to repair in structural components and drift sensitive and acceleration non-structural components, for increasing levels of ground motion intensity.

### ***Expected economic losses***

If global collapse has occurred in the building, the expected loss of the building,  $E[Loss|C]$ , can be estimated on the basis of the replacement cost of the whole building. This value is larger than the cost of a new building since the costs of demolition and of debris removal should be added to the original cost. Moreover, the occurrence of a natural disaster often leads to higher repair costs for the same damage and hence to an increase of monetary losses (Olsen and Porter, 2011).

The expected loss given that the building has not collapsed but has to be demolished,  $E[Loss|NC \cap D]$ , includes, beside the replacement cost, the cost of demolishing the existing structure and the cost of removing debris from the site (Ramirez and Miranda, 2012).

### ***Residual inter-storey drifts***

The evaluation of economic losses is based on peak response quantities such as peak inter-storey drift ratios and peak floor accelerations. Nonetheless, some considerations are required. For example, it might be necessary to evaluate the influence of residual deformations by accounting for the possibility of having to demolish the building due to excessive residual inter-storey drifts (Ramirez and Miranda 2012). Previous studies, such as (Ramirez and Miranda, 2012), showed that residual inter-storey drifts have a lower impact on non-ductile buildings in comparison to modern building structures, in which neglecting losses from residual drifts can lead to a significant underestimation of economic losses. Non-ductile buildings, such as the case study building, are more vulnerable to other type of failure mechanism such as shear failure of non-ductile structural elements. Furthermore, the presence of a rigid lateral resisting system such as shear walls, make these buildings less likely to develop large lateral displacements. Nonetheless, the probability of demolishing the building due to residual inter-storey drift is evaluated and taken into account in the estimation of the total loss using Equation (5.4).

As suggested by (Ramirez and Miranda, 2012), in this study the probability of having to demolish the structure conditioned on the peak residual inter-storey drift is assumed to be lognormally distributed with a median of 0.015 and a logarithmic standard deviation of 0.3.

### ***Probability of collapse***

To estimate the total expected economic loss of the building as a function of the ground motion intensity,  $E[Loss_T|IM]$ , using Equation (5.4), it is required to estimate the probability of collapse as a function of the ground motion intensity,  $P(C|IM)$ .

In this study, it is assumed that the structure collapses if any vertical element reaches DS4. The probability of collapse  $P(C|IM)$  is assumed to be equal to the largest probability of any individual structural element to reach DS4:

$$P(C|IM) = \max [P(DS = DS4_i|IM)] \quad (5.16)$$

where  $P(DS=DS4_i | IM)$  is the probability of experiencing DS4 in the  $i$ th component conditioned on the ground motion intensity. It is important to note that, for the case study building, the first elements to reach collapse are the RC walls at the ground storey oriented in the X direction. These elements are characterised by the worst performance when compared to the columns, as indicated by the fragility curves presented in Figure 5.6 and Figure 5.7.

The probability of collapse is essential to evaluate the total economic losses but also the collapse safety, which is examined in this section. The collapse fragility for the case study building is shown in Figure 5.11. The structural collapse resistance is represented by the median collapse capacity expressed in terms of the ground-motion intensity measure,  $Sa(T_1)$ , and by the mean annual frequency (MAF) of collapse, which is obtained by integrating the collapse fragility over the entire hazard curve. The MAF amounts, for the case study building, to  $8 \times 10^{-4}$ , corresponding to a 4% probability of collapse in 50 years and a return period of 1225 years.

Recent studies adopted decision models for the verification of seismic collapse safety of buildings. For example, in (Dolšek et al., 2017) and (O'Reilly et al., 2018), acceptable levels of MAF of collapse of existing structures were identified within a range of  $10^{-5}$  to  $10^{-4}$ . Based on this criterion, the MAF of collapse of the case study building is not within the acceptable levels, thus the seismic performance of the building is deemed inadequate and a strengthening intervention is recommended.

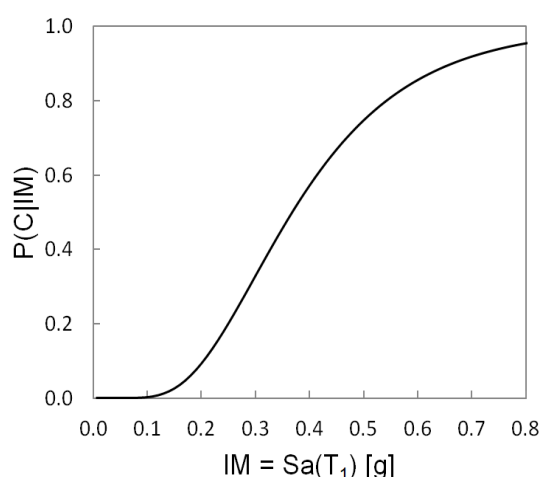


Figure 5.11 – Probability of collapse for the case study building.

### ***Total economic losses***

The total economic loss of the building at different levels of ground motion intensity is computed using Equation (5.4), as the sum of non-collapse losses due to repair, non-collapse losses due to demolition and collapse losses. Figure 5.12a shows the variation of the expected losses, defined as a fraction of the replacement value of the building, as a function of the ground motion seismic intensity. Figure 5.12a also shows the disaggregation of the total loss into the three components. As it is evident from the figure, repair losses increase up to  $Sa(T_1) = 0.28$  g. After that point, their contributions tend to decrease while collapse losses become more relevant. The contribution of losses resulting from having to demolish the building due to excessive residual drifts is, as expected, very low. According to the seismic zonation of the Portuguese territory (CEN, 2004), in Lisbon, the reference peak ground acceleration corresponds to 0.153 g ( $Sa(T_1) = 0.33$  g) for Type 1 seismic action. At this intensity level, the total expected losses are, approximately, 50% of the replacement cost of the structure. For the

same intensity level, the losses due to collapse are equal to 39% of the replacement cost of the structure, while the loss due to repair and to demolition are equal to 10% and 1%, respectively.

Figure 5.12b shows the MAF of exceeding a specific ground motion intensity level,  $\lambda_{Sa}$ , as a function of the total expected losses, for each IM. The area underneath the curve corresponds to the expected annual loss of the building. The value obtained is equal to 0.16 % of the replacement value of the case study building.

By integrating the repair loss over the seismic hazard curve, it is possible to obtain the contribution of repair costs to the EAL. The losses due to repair of the building in the non-collapse case contribute up to 60% of the total EAL. In fact, the repair losses, although being smaller than those due to stronger shaking, are associated to a higher probability of occurrence (Figure 5.12b).

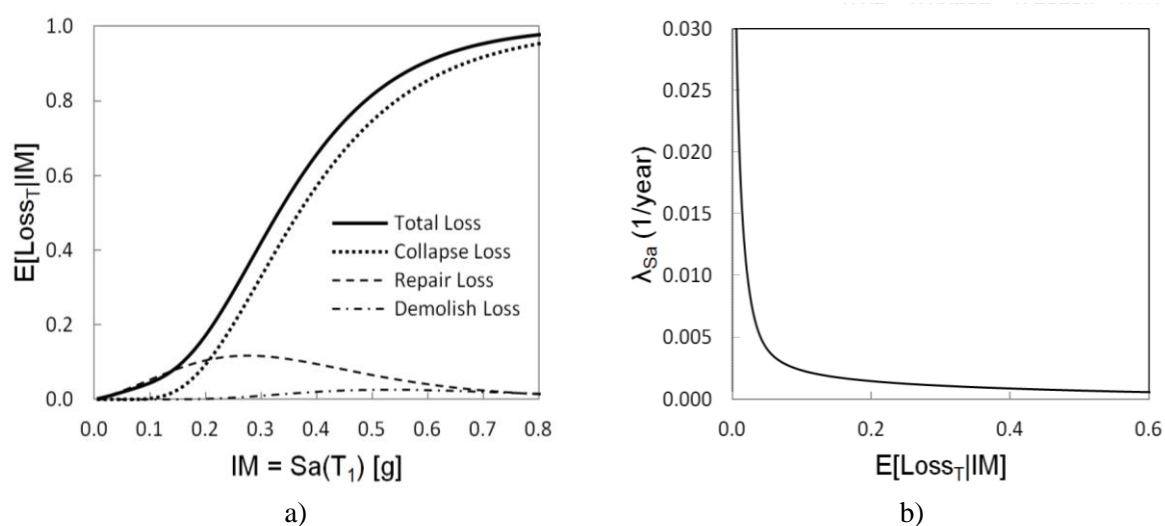


Figure 5.12 –Variations of the expected loss in the case study building as a function of the ground motion intensity, IM and (b) MAF of exceeding a specific ground motion intensity level,  $\lambda_{Sa}$ , as a function of the total expected losses, for each IM.

The results of this study in terms of EAL are in line with those obtained in similar studies, such as the work of (Martins et al., 2016), which reported values of EAL between 0.12% and 0.23% for two non-ductile residential buildings in Lisbon. Another interesting comparison can be made with loss assessment studies carried out for buildings located in Italy. In (Cardone and Perrone, 2017a) the EAL of a pre-70s residential 8 storeys RC frame building with masonry infills located in the city of L'Aquila were estimated around 0.75% of the replacement cost of the building. It should be noted that L'Aquila has a much higher seismic intensity than Lisbon. In (Romano et al., 2018) loss estimation of a three storey residential building was performed. The authors evaluated the EAL for the bare structure and for the structure including the contribution of masonry infills having obtained EAL values of 0.47% and 0.12%, respectively. The results reported for the uniform frame with infills are in line with the results obtained in this study.

## 5.6. Comparison with other studies – capacity and fragility curves

### 5.6.1. Capacity curves

In this section, the results in terms of capacity and fragility curves of the case study building are compared with previous studies performed on old RC buildings, aiming to show the importance of using an analytical methodology and a building specific loss assessment methodology, together with a detailed numerical model of the building for a reliable seismic performance evaluation.

As stated in the introduction to this chapter, previous studies have already addressed the estimation of fragility curves for old RC buildings in Portugal, such as the works of Carvalho et al. (2002) and Silva et al. (2015a). A comparison is herein made within the capacity curves of the RC wall-frame structure of this study and the works of Carvalho et al. (2002) and Silva et al. (2015a). The capacity curves (top displacement vs. base shear for the multi degree-of-freedom system) have been transformed into a capacity spectrum (spectral displacement vs. spectral acceleration for the equivalent single degree-of-freedom system) (Fajfar, 1999) and shown in Figure 5.13. The capacity curves of the case study building are shown for the X and Y directions and are identified as “Frame-wall” in Figure 5.13.

From the work of Carvalho et al. (2002), the results for the 6 floors and 10 floors buildings built before 1960 and between 1960 and 1983 (>1960) are depicted (Figure 5.13a). It is possible to notice: (i) comparable values of initial stiffness with the 10 floor buildings; (ii) significantly smaller ultimate displacement for the case study building (i.e., significantly lower ductility). From the work of Silva et al. (2015a), capacity curves for buildings with 8 floors, computed for pre-code and mid-code seismic zones C and A (according to the seismic design code of that period, Lisbon is in seismic zone A), are shown in Figure 5.13b. The frame-wall building of this study has a comparable initial stiffness to the Mid-Code - A typology but it exhibits much lower lateral load resistance.

It is evident that, in both works, the developed capacity curves (i.e. models) are not able to represent this building typology. In fact, the first work (Carvalho et al., 2002) is based on the FEMA methodology, which has been calibrated for buildings in the United States, with the employment of engineering judgment to modify the design parameters (e.g., strength coefficient, overstrength factor, elastic period and ductility factor) to the characteristics of the Portuguese constructions. In the second work (Silva et al., 2015a), and despite the employment of an analytical methodology and infilled frames, the presence of rigid elements such as the shear walls was not considered. These elements, designed to withstand low seismic forces (if any), are more vulnerable to brittle shear failure and tend to cause earlier collapse of the building.

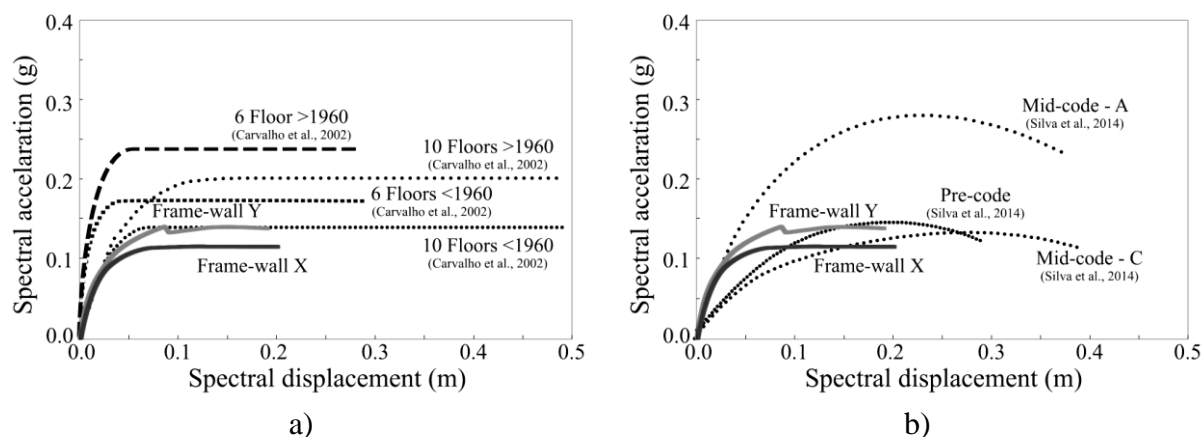


Figure 5.13 – Capacity curves for the case study buildings for the X and Y directions (identified as “Frame-wall”) and the results from (a) Carvalho et al. (2002) and (b) Silva et al. (2015)

### 5.6.2. Fragility curves

In this section, first the approach followed to derive fragility curves is briefly described and then a comparison with other studies is presented.

Different options exist for the definition of performance limit state criteria for the generation of fragility curves based on the level of damage of the structure. It is possible to employ local damage criteria, such as member deformation or concrete/steel strains (e.g., EC8-3 and ASCE 41-17), global ones, such as maximum global drift or maximum inter-storey drift or even multi-criteria (local and global).

Within the context of this study, the limit state criteria are defined considering the damage caused by the earthquake in the vertical structural elements (RC columns and walls). Some consideration for the definition of the damage states are based on the Turkish Earthquake Code (TEC, 2007) and the Guidelines referred in (Miyamoto et al., 2010). TEC 2007 is an advanced code which provides a clear characterization of the level of damage in the structure as a whole. According to the Guidelines (Miyamoto et al., 2010), if at least 75% of the total base shear force for any direction of loading can be carried by shear walls, the performance of the beams can be ignored. Four global Damage States (DS) are herein identified:

- Light Damage (DS1): reached if the vertical elements (columns and RC walls) have attained an IDR corresponding to the light cracking damage state for any direction of earthquake loading.
- Moderate Damage (DS2): reached if the vertical elements (columns and RC walls) carrying more than 20% of the storey shear have yielded (severe cracking).
- Extensive Damage (DS3): reached if the vertical elements (columns and RC walls) carrying more than 20% of the storey shear have attained shear failure.
- Collapse (DS4): reached if any column or RC wall has collapsed.

It is worth noting that, in this wall-frame system, a consistent percentage of the shear force demand is sustained by the RC walls. Figure 5.14 shows the shear ratio (total shear sustained by the columns, represented by dashed lines, or RC walls, solid lines, over the total shear force) at different IM levels. It is possible to conclude that up to 80% of the base shear force is sustained by the RC walls in the X direction (Figure 5.14a) and almost the whole shear force is resisted by the RC walls in the Y direction (Figure 5.14b). Therefore, the performance of the building is mainly controlled by the RC walls.

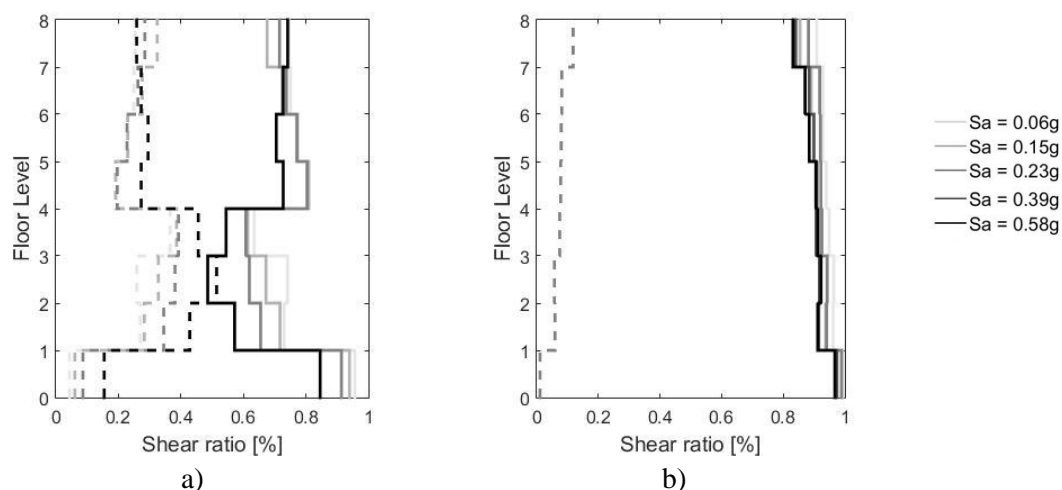


Figure 5.14 – Shear demand ratio in columns (dashed lines) and walls (continuous lines) at different IM levels in (a) the X direction and (b) Y direction

Having established a suitable set of damage levels, compatible fragility functions were developed for the case study structure. It is worth noting that the attainment of a certain damage state in each structural vertical element is based on the attainment of a certain IDR, as defined in Sections 5.2.3 and 5.3.

The probability of exceedance each global DS is calculated based on the MSA results (see Section 5.5.1), as the ratio of ground motion records that caused the exceedance of a given damage level at each intensity measure level to the total number of ground motion records (40 records). Each fragility function was assumed to follow a cumulative lognormal distribution, with logarithmic mean ( $\lambda$ ) and logarithmic standard deviation ( $\sigma$ ). Evaluation of the fragility function parameters is based on the maximum likelihood estimation method proposed by (Baker, 2011). Figure 5.15 shows the fragility curves obtained for the four damage states considered for the structure.

In Table 5.7, the parameter of fragility are compared with the ones obtained by Silva et al. (2015a) for buildings with 8 floors, computed mid-code seismic zones C and A. A comparison of the fragility curves is also shown in Figure 5.15. It is worth noting that in (Silva et al., 2015a) two different damage state criterion were used, i.e. maximum interstorey drift and maximum global drift (in Table 5.7 and Figure 5.15 the worst between the two was considered), and four limit state, i.e. slight

damage, moderate damage, extensive damage and collapse, herein identified as DS1, DS2, DS3 and DS4.

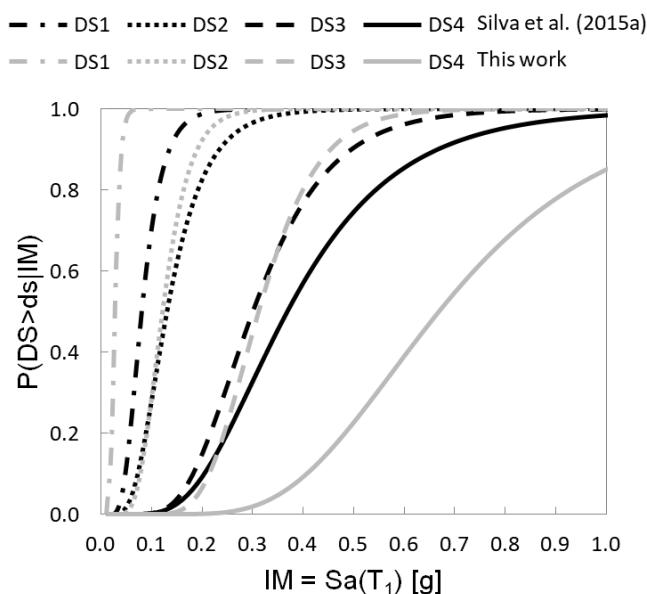


Figure 5.15 – Comparison of fragility functions between the RC wall-frame building typology in this study and the RC frame typology for Mid-Code soil type A analysed in (Silva et al., 2015a)

It is evident that the main difference lies in the definition of the collapse fragility curve (DS4). In fact, for the case study building, the collapse fragility is conditioned by the non-ductile behaviour of the RC walls, which suffer from the brittle shear failure, while the presence of shear walls was not considered in (Silva et al., 2015a).

Table 5.7 – Logarithmic mean ( $\lambda$ ) and logarithmic standard deviation ( $\sigma$ ) for the case study building and for the mid-code fragility functions for soil type A from (Silva et al., 2015a)

	This work		(Silva et al., 2015a) Mid-code A	
	$\lambda$	$\sigma$	$\lambda$	$\sigma$
DS1	-2.473	0.457	-3.613	0.314
DS2	-2.048	0.458	-2.110	0.350
DS3	-1.229	0.391	-1.167	0.294
DS4	-1.001	0.461	-0.404	0.375

## 5.7. Conclusions

This chapter focused on the probabilistic seismic performance assessment of old RC wall-frame buildings. A methodology based on nonlinear static analyses was proposed to derive fragility functions for these types of structural elements. In this context, a parametric study was conducted which resulted in a simplified formulation for deriving median inter-storey drift ratios for multiple

damage states. The proposed formulation can be used for performance-based assessment of existing RC frames with non-ductile RC walls.

The proposed methodology was employed in the probabilistic seismic performance loss assessment of an 8-storey RC wall-frame building located in Lisbon. The loss assessment adopted component-based fragility functions for the damage assessment of structural and drift-sensitive non-structural elements, while a simplified storey-based approach was used for acceleration-sensitive non-structural elements.

The value of expected annual losses obtained appear to be in line with those available in the literature for other non-ductile RC residential buildings. The results obtained clearly show that the contribution of non-structural and structural repair losses, associated to the non-collapse case, are the ones contributing most to the EAL. Moreover, the performance assessment indicates that the building is characterised by a relatively high probability of collapse for moderate seismic intensity levels, which results, through integration with the hazard curve, in high values of the mean annual frequency of collapse. This conclusion is justified with the non-ductile behaviour of the RC walls, which have a critical influence on the seismic behaviour of the building. This observation can be further confirmed by comparing the fragility functions derived for the RC walls with those adopted for the RC columns. The comparison reveals that the RC walls are much more vulnerable in comparison to the columns and reach complete collapse for inter-storey drift ratios much smaller than the columns. Therefore, retrofitting interventions should aim to improve the performance of the RC walls.

The results of this chapter highlight the importance of economic loss assessment results for guiding decisions about retrofitting strategies to improve the overall performance of non-ductile RC buildings, ideally in combination with the support of a cost-benefit analysis framework.

Capacity and fragility curves of the case study building were obtained and compared with previous studies performed on old RC buildings. The results showed that existing models are not capable of accounting for the non-ductile behaviour of the structure due to the presence of RC walls. Therefore, building specific loss assessment methodology, together with a detailed numerical model of the building are necessary for a reliable seismic performance evaluation.

## **6. FEASIBILITY OF RETROFITTING SOLUTIONS FOR OLD RC WALL-FRAME BUILDINGS**

### **6.1. Introduction**

The evaluation of the seismic structural behaviour is an important task in order to verify the actual need of structural retrofitting, whereas seismic rehabilitation interventions may involve significant costs. In this respect, earthquake loss estimation is an effective tool to provide owners and stakeholders with useful information to support financial and social decisions related to risk mitigation programs.

The definition of intervention methodologies depends on the deficiencies detected, at local and global levels, in the seismic structural evaluation: a less efficient evaluation may lead to inappropriate intervention solutions and/or high intervention costs.

The most adequate retrofitting strategy, or a combination of them, should be selected to improve the performance of the building (fib - bulletin 24, 2003) (Fardis, 2009). Guidelines such as the fib Bulletin on Seismic Assessment and Retrofit of Reinforced Concrete Buildings (fib - bulletin 24, 2003) and the ASCE 41-17 Seismic Evaluation and Retrofit of Existing Buildings (ASCE Standard, 2017) provide guidance on the cases where each measure is most effective. Each technique has its own advantages and drawbacks and is selected based, primarily, on technical criteria. The choice depends on: (i) the vulnerabilities identified in the seismic assessment, (ii) the locally available materials and technologies, (iii) cost considerations, (iv) the disruption of use it entails and the duration of the works, (v) architectural, functional and aesthetic considerations or restrictions, etc.

There are two main objectives in seismic retrofitting, i.e. to reduce demand or to increase capacity, and three main properties to examine: strength, stiffness and deformation capacity. In (Di Ludovico et al., 2017), a careful analysis and data collection of the reconstruction process after the L'Aquila earthquake was performed, with particular focus on the founding application made by private owners to the state. In that work, the types and costs of different repair and strengthening interventions designed by practitioners to attain the usability recovery of buildings were compared. It was shown that for RC building, FRP composite systems were the most commonly used for local strengthening intervention (58%), followed by RC jacketing of members (30%), while steel bracing was used only in the 7% of cases. Furthermore, in most buildings more than one strengthening technique was used to improve the seismic capacity of the structure; the use of steel bracing to increase the global stiffness and strength capacity of an existing building may imply the need of beam-column joint strengthening in order to sustain the localized actions provided by the inserted bracing systems (e.g., FRP or steel jacketing) (Di Ludovico et al., 2017). Analysis and comparison of the documentation of private

rehabilitation projects after L'Aquila was performed by (Dolce and Manfredi, 2015). From this analysis it appears that the use of composite material was consider more economic that the one of the steelwork, even though an attempt to contradict these result was made by experts in the steel structural sector (Mazzolani et al., 2018).

The work reported herein addresses the problem of strengthening one of the most vulnerable class of existing reinforced concrete buildings in Lisbon, namely RC wall-frame buildings, designed and built under old codes and practices. The seismic performance assessment was performed (Chapter 1) aiming to identify the expected deficiencies and failure modes of this building typology and to propose efficient retrofitting solutions. The vulnerability of this type of buildings was evident during the latest earthquake in Mexico (Galvis et al., 2017), where most of the collapsed buildings were old (pre-1985) non-ductile RC structures. In particular, RC walls designed to withstand low seismic forces (if any), are more vulnerable to brittle shear failure and tend to cause earlier collapse of the building. Shear failure in members can occur in old RC buildings designed without considering adequately the effect of horizontal actions, or in buildings with low concrete strength or without sufficient transverse reinforcement. This failure mode impairs the deformation capacity of the structure and, hence, has an important influence on the seismic performance of the buildings. Therefore, the effectiveness of different strengthening strategies to improve seismic response of the structure is investigated, at the same time seeking for a solution with a low economic and structural impact. To this objective, cost-benefit analysis provides an important tool for making decision about the best mitigation strategy, as recently showed by different authors (e.g., (Cardone et al., 2017), (Calvi, 2013), (Liel and Deierlein, 2013)).

In the present study, the effectiveness of two strengthening methodologies involving diagonal X steel braces and the application of Fibre Reinforced Polymers (FRPs) are evaluated for the case of the RC wall-frame building (Section 6.2). It is worth noting that the applicability of the retrofitting solution follows the main literature in the field, e.g. (Fardis, 2009), and regulation codes, e.g. (fib - bulletin 24, 2003) (fib - bulletin 35, 2006) (ASCE Standard, 2017) (CEN, 2010). The building performance, before and after strengthening, is evaluated using the vulnerability assessment methodology defined in Chapter 5. To evaluate the feasibility of each retrofitting solution, the initial cost of intervention will be compared with the benefits obtained through reduction in terms of expected annual loss reduction (Section 6.3).

## 6.2. Retrofitting strategies

### 6.2.1. Criteria for strengthening

The effectiveness of two retrofitting strategies are evaluated with the aim of improving the performance of the RC walls in the X direction, which are more vulnerable to brittle shear failure and tend to cause earlier collapse of the building. This is evident from Figure 6.1 where the shear demand of the RC walls, represented by means of bi-linearized curves obtained through nonlinear static analysis, is compared with the shear strength. On the left of Figure 6.1 it is represented the pushover curve of the first shear wall in the X direction versus the top displacement ductility (top displacement divided by the yield displacement), whereas on the right the correspondent for Y walls (See Figure 3.7).

The results of the seismic safety assessment in Chapter 1, Section 4.4, indicated that the most severe failure mode of the building corresponds to the shear failure (brittle failure mechanism) of the RC walls in both X and Y directions, while the columns have a reasonable flexural behaviour, developing a stable flexural response.

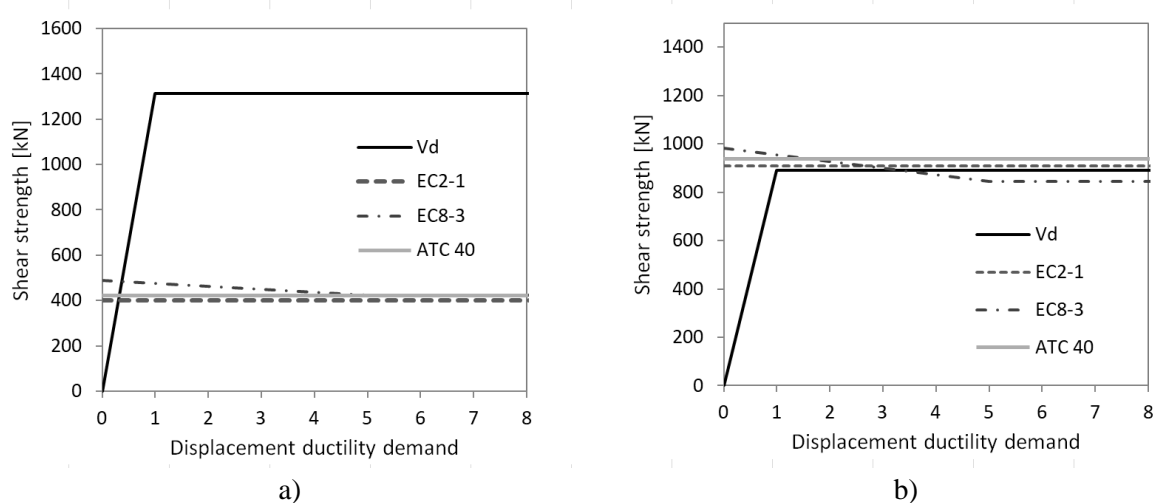


Figure 6.1 – Comparison of shear demand ( $V_d$ ) and shear strength as per different seismic codes, i.e. EC2-1, EC8-3 and ATC 40, for the RC walls in the X direction (a) and Y direction (b).

The shear resistance of RC walls and columns is calculated by means of shear resistance to web crushing,  $V_{Rd,max}$ , and shear resistance as controlled by the stirrups,  $V_{Rd,s}$ , and verified according to the minimum of the two values. In Figure 6.1, the shear strengths obtained with the expressions provided by EC8-3, EC2-1 and ATC-40 (Applied Technology Council, 1996) are compared, showing very similar results. In the same figure the shear demand,  $V_d$ , is also plotted, for the X and Y directions. It is evident that the shear failure of the wall in the X direction (Figure 6.1a) is reached for a very low value of the displacement ductility demand and for a value of PGA equal to 0.010 g, less than 10% of

the seismic action at the significant damage (SD) limit state (0.153 g). As stated before, this result is due to the very low amount of horizontal reinforcement (see Appendix A or Table 3.2).

### **6.2.2. Definition of retrofitting strategies**

The effectiveness of two retrofitting strategies are evaluated with the aim of improving the performance of the RC walls in the X direction, which, as previously shown, are more vulnerable to brittle shear failure and tend to cause earlier collapse of the building. As referred, this improvement of behaviour may be achieved by adopting one of the following approaches or strategies, or even combining them: (i) by reducing the seismic demands on members, (ii) by increasing the member capacities.

The deformation capacity and shear strength of individual members may be significantly upgraded through FRP-wrapping, without modifying at all their stiffness. This solution is investigated in Section 6.2.3. Reduction of seismic demand on the walls through retrofitting may be achieved by increasing the lateral stiffness. The lateral stiffness can be increased by adding a new lateral load resisting system to take almost all the full seismic action, e.g. steel bracing or new concrete walls. In this work, the effectiveness of applying steel braces at the ground storey level to reduce the shear demand on the RC walls is investigated (Section 6.2.4). This partial strengthening, as opposed to a global one, has the double aim to reduce the cost of intervention and allow the continued usage of the building during the retrofitting work.

### **6.2.3. Retrofitting using FRP**

Externally bonded Fibre Reinforced Polymers (FRPs) are used in seismic retrofitting to enhance or improve: (i) the flexural deformation capacity in plastic hinge regions, (ii) deficient lap splices, (iii) shear resistance. To improve the shear capacity of brittle components, the FRP overlay should be applied with the fibres mainly in the direction in which enhancement of shear strength is pursued. Unlike beams, columns and walls are subjected to a constant shear force within each storey. Hence, if shear strengthening is needed, it should be uniform throughout the height of the vertical element in a storey. Moreover, as the shear demand alternates between opposite values, the main direction of the FRP should be horizontal (Fardis, 2009).

The total shear capacity, as controlled by the stirrups and the FRP, is evaluated as the sum of the contribution from the existing concrete member and the contribution from the FRP (CEN, 2010) (CNR-DT 200, 2013). The contribution of FRP to the shear capacity for full wrapping with FRP or side bonded FRP strips may be calculated, respectively, with Equations (6.1) and (6.2), which correspond to Equations A.22 and A.23 of EC8-3, respectively:

$$V_{Rd,f} = 0.9 \cdot d \cdot f_{dd,e} \cdot 2 \cdot t_f \cdot (\cot\theta + \cot\beta) \cdot \frac{w_f}{s_f} \quad (6.1)$$

$$V_{Rd,f} = 0.9 \cdot d \cdot f_{dd,e} \cdot 2 \cdot t_f \cdot \frac{\sin\beta}{\sin\theta} \cdot \frac{w_f}{s_f} \quad (6.2)$$

where  $d$  is the effective cross sectional depth,  $\theta$  is the strut inclination angle and  $\beta$  is the angle between the strong fibre direction in the FRP strip (or sheet) and the axis of the member,  $t_f$  is the thickness,  $w_f$  is the width and  $s_f$  is the spacing of the strip (or sheet),  $f_{dd,e}$  is the design FRP effective debonding strength, which is different for fully wrapped or side bonded FRP (Equations A.24 and A.30 of EC8-3, respectively).

In this work, carbon FRP sheets are chosen. The following properties are assigned: elastic modulus of 240 GPa, thickness of 0.167 mm and ultimate strength ( $f_{ju}$ ) of 3800 MPa. Table 6.1 lists the value of the FRP shear contribution,  $V_{Rd,f}$ , for different number of layers,  $n_f$ . Considering the shear demand in the X direction (Figure 6.1), to enhance the shear resistance of the wall it would be necessary to fully wrap the wall with two layers of FRPs. Alternatively, where required by architectural or structural constraints (the RC walls are included in a stair core), a side-bonded jacket could be applied in more than two layers, for a maximum number of five layers, as suggested by (Fardis, 2009).

Table 6.1 – Shear contribution of FRPs.

	$n_f$	$f_{dd,e}$ (kN)	$V_{Rd,f}$ (kN)
Fully wrapped	1	789	986
	2	679	1697
Side bonded	1	517	746
	2	344	994
	5	207	1496

The numerical model of the building takes into account the flexural behaviour of the elements but not the interaction between flexure and shear. Therefore, the improved performance of the elements retrofitted with FRP is considered only in the post processing phase.

#### 6.2.4. Retrofitting with steel braces

The application of steel braces in selected bays of an existing RC building is effective for global strengthening, provided that a reliable, well detailed and technically sound connection between the steel elements and the existing concrete members is ensured (Varum et al., 2013) (Castro et al., 2017). Architectural constraints related to strengthening schemes can be addressed through alternative choices of bays to be braced. A strengthening solution could be achieved by using X, V or inverted V bracing. Alternative retrofitting methods of non-ductile RC frames include the use of eccentric steel

braces with vertical shear links as energy dissipation elements. Among these alternatives, diagonal X bracing is the most common technique, providing a considerable increase in terms of lateral strength and stiffness of the building (Kaushik et al., 2009). Nevertheless, the application of X bracing to an existing building can lead to possible side effects, particularly on columns attached to the bracing system (Rahimi and Maheri, 2018), such as increase of axial tensile force, which can lead to lap splice failure at the lower storeys of the frame. This is particularly true for taller buildings (Rahimi and Maheri, 2018).

A strengthening intervention using concentric X-diagonal steel braces is proposed herein in order to reduce the shear demand on the RC walls which suffer from brittle shear failure, as evidenced in Section 6.2.1. Figure 6.2 shows a possible layout of the bracing system. The diagonals are composed by hot-rolled, circular hollow section (CHS) steel profiles, directly connected to the beam-column nodes of the bay of the RC frame. This connection is considered to behave as a “nominally pinned joint” as defined in Part 1-8 of Eurocode 3 (CEN, 2011), i.e. it can transmit the internal axial forces without developing significant moments. As no specific rules for the design of hybrid RC-steel systems are provided in EC8-1, the provisions of the latter concerning steel frames with concentric braces were taken as reference and starting point for the design of the new steel braces. Regarding the lower and upper limits for the non-dimensional slenderness,  $\bar{\lambda}$ , of the braces, clause 6.7.3 (1) of EC8-1 states that  $1.3 \leq \bar{\lambda} \leq 2.0$ , for buildings with more than two storeys. The lower limit is defined to avoid overloading of the frame’s columns in the pre-buckling stage (i.e., when compressed and tensioned diagonals are active).

The braces’ cross-section (listed in Table 6.2) was selected with the objective to reduce the shear demand on the RC walls in the X direction, keeping these RC elements in the elastic region. For architectural reasons, no braces were applied in the Y direction. Moreover, and as discussed in Section 6.2.1, the building has an acceptable seismic performance in that direction.

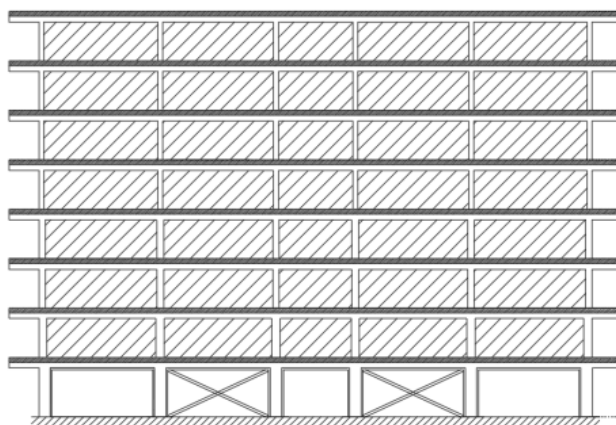


Figure 6.2 – Retrofitting scheme.

Table 6.2 –Section profile of steel braces.

Bay's dimension [m]	Brace type	$\bar{\lambda}$	$N_{cr}$ [kN]	$N_{pl,Rd}$ [kN]	$N_{b,Rd}$ [kN]
7x3.6	CHS 219.1x5.9	1.30	716.4	983.7	681.3

$N_{cr}$  – Euler's critical load;  $N_{pl,Rd}$  – yield resistance of the gross section;  $N_{b,Rd}$  – buckling load.

The modelling options for the steel braces are based on the conclusions of the studies conducted by (Uriz et al., 2008). An inelastic force-based beam-column element within the OpenSees computational framework is used for simulating the hysteretic behaviour of the steel braces. The element accounts for large displacements by embedding the basic system in a corotational framework. A force-based FE formulation with five integration sections is used to implement this model.

The connections between the steel braces and the RC frame are modelled as pinned regarding the out-of-plane rotation. In this approach, a zero-length element is defined in OpenSees. This element is defined by two coincident nodes that are connected by a linear elastic spring. The rigidity of the connection (i.e. the gusset plate) is modelled using rigid elastic elements as proposed by (Hsiao et al., 2012). Concerning the constitutive law defining the cyclic behaviour of the steel material, the Menegotto and Pinto (1973) model was employed, combined with the isotropic hardening rules proposed by (Filippou et al., 1983), with the following mechanical properties (mean values): (i) Modulus of elasticity (initial elastic stiffness):  $E_s = 210$  GPa; (ii) Yield stress (mean value):  $f_{ym} = 343.75$  MPa; (iii) Strain hardening parameter:  $\mu = 0.005$ ; (iv) Steel specific mass:  $\gamma_s = 7850$  kg/m<sup>3</sup>.

While the above-referred modelling aspects are consensual among authors, others like the number of FE's per individual brace and the brace's initial camber  $\Delta_0$  are not. It is however widely accepted that braces should be divided at least in two FE's, that are offset (initial camber) at mid-length of the brace, as to trigger flexural buckling. Based on the results of a parametric study (Uriz et al., 2008), in this work, the braces are modelled with four force-based elements, allowing the consideration of an initial geometrical imperfection of 0.1% of the brace length, and 5 integration points for each element.

### 6.2.5. Preliminary Results

Figure 6.3 shows the pushover curves, i.e. base shear versus top displacement at the centre of mass, for the X direction (the results in the two senses of loading are identical, as the structure is symmetric with respect to the Y axis). A modal load pattern is used in both direction because it provides more consistent results when compared with the results of non-linear time-history analysis, as shown in Chapter 1. The strengthening solution which involves the application of the steel braces is depicted in Figure 6.3a, while the strengthening solutions which involves the application of FRP in the RC walls is depicted in Figure 6.3b. The target displacement, obtained by applying the N2 method for the PGA prescribed in Lisbon for SD limit state, are depicted in Figure 6.3 as “dt SD”. They amount to 0.110 m

for the structure retrofitted with steel braces (Figure 6.3a) and to 0.118 m for the structure retrofitted with FRP (Figure 6.3b).

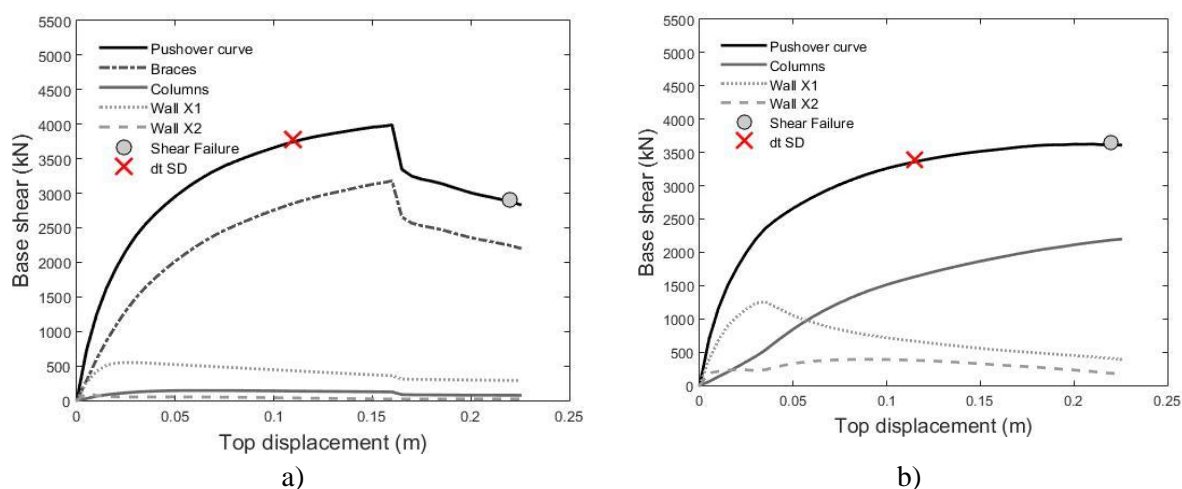


Figure 6.3 – Pushover curves in the X direction for the retrofitted building with (a) steel braces and (b) FRP. Target displacement and shear failure of the RC walls is indicated for the strengthened structure.

In the figures, the total base shear carried by the columns is depicted by the label “Columns”, while the base shear carried by the first RC wall in the X direction is labelled as “Wall X1” and the second as “Wall X2” (assuming a positive direction of the load - Figure 3.7) and corresponding to W1 and W4 in Figure 3.7.

It is clear that the use of steel bracing (Figure 6.3a) significantly reduces the potential for shear failures in the walls at the ground storey level. In fact, the shear demand is reduced as to keep the RC walls in the elastic region (see Figure 6.1). As stated before, the application of the FRP (Figure 6.3b) does not modify the stiffness of the structural elements but increases the shear strength of the walls, allowing them to reach their flexural capacity without developing a brittle mechanism.

By comparing the two pushover curves (black solid lines) it is evident that the application of the steel braces at the ground storey did not result in a significant increase of the lateral strength (Figure 6.3a). It is also worth noting that the fundamental periods of the structure before and after strengthening do not show any substantial difference. On the other hand, the absolute displacements at the lower stories are reduced. The distribution of the lateral displacements along the height of the structure as well as the inter-storey drifts are shown in Figure 6.4a and Figure 6.4b, respectively, where the results for the un-strengthened building are compared with the building retrofitted with braces and FRPs.

The shear demand to capacity ratio (D/C) in the RC walls of the two retrofitted schemes at the SD limit state are plotted in Figure 6.5. All shear D/C ratios fall below unity, indicating a positive effect of brace retrofitting in reducing the demand on the shear walls (Figure 6.5a). A similar result can be observed for the FRP retrofitting (Figure 6.5b), which increases the shear capacity of the walls leading

to D/C ratios below one. It is noted that the partial retrofitting at the ground storey results in a decrease in wall shear at the lower storey, but it does not have a negative influence on the upper storeys of the building, where the D/C ratio is unchanged, although shear walls may experience higher demand from the effects of higher modes of vibrations.

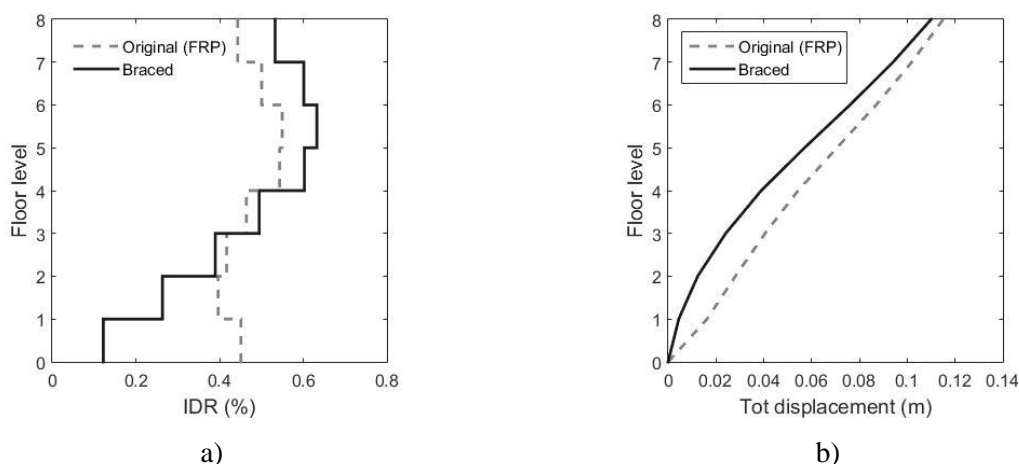


Figure 6.4 - Inter-storey drifts (IDR) (a) and lateral displacements profile (b) in the X direction.

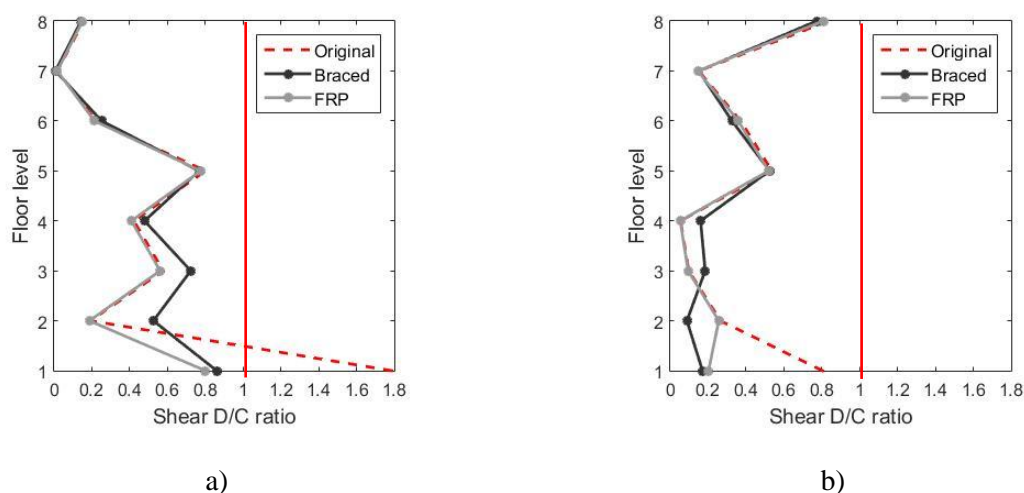


Figure 6.5 - Shear D/C ratio in (a) RC Wall1 and (b) RC Wall4 in the X direction.

### 6.3. Performance-based cost-benefit assessment

In this section, rehabilitation of the structure is addressed, considering the outcomes of the seismic and loss assessment conducted in Chapters 1 and 5. Three mitigation strategies are considered: (i) application of FRPs on the RC walls at the ground storey level only; (ii) retrofitting with steel braces at the open ground storey level; (iii) a combination of the two previous measures, i.e. steel braces at the open ground storey and FRP wrapping of RC walls along the building height.

The building specific loss assessment methodology described in Chapter 5 is applied, which involves the following steps: (i) hazard analysis; (ii) structural analysis; (iii) damage analysis; (iv) loss analysis. The cost of each intervention techniques is evaluated. Then, the feasibility of each retrofitting solution is evaluated by comparing the initial cost of intervention with the benefits obtained through reduction in terms of Expected Annual Loss (EAL) reduction.

### **6.3.1. Hazard analysis**

The hazard is provided in terms of mean annual frequency of the ground motion intensities. A site-specific hazard curve defines the probability of occurrence of an earthquake within a specific time-frame. The seismic hazard curve for Lisbon presented in Section 5.5.1 is used.

In this study, preference is given to the adoption of a Conditional Mean Spectrum (CMS) in detriment of using an Uniform Hazard Spectrum (UHS). In fact, a UHS is such that its ordinates, expressed in terms of spectral acceleration, have all the same marginal probability of exceedance in the fixed reference period  $V_R$  (e.g., 50 years) and are obtained from the seismic hazard curves, at different periods, for a certain probability of exceedance of interest (e.g. 1% in 50 years). It implies that large-amplitude spectral values will occur at all periods in a single ground motion (Baker, 2011). A CSM, instead, provides the expected (mean) response spectrum, conditioned on the occurrence of a target spectral acceleration ( $S_a$ ) at one period of interest and using the results of seismic hazard disaggregation.

### **6.3.2. Structural analysis**

For the structural analysis, Multiple Stripe Analyses (MSA) are performed. Five CMS are derived at different IM levels corresponding to return periods of 4975, 2475, 975, 475 and 140 years, respectively. At each IM level, 40 pairs of ground motion records were selected, each record consisting of two horizontal components compatible with the five CMS. The geometric means of the spectra of the two components are used to match the target spectral acceleration of the CMS at period  $T_1$ . As the period of the structure after strengthening, either with steel braces or FRPs, has not been significantly modified, the same pairs of ground motion derived for the original (not-strengthened) building are herein used.

The Engineering Demand Parameters (EDP), i.e. the Inter-storey Drift Ratio (IDR) and the Peak Floor Acceleration (PFA) are obtained from the structural analyses. Figure 6.6 and Figure 6.7 shows the median IDR for the building with FRPs and with steel braces, respectively. The retrofitting with FRPs prevents the premature brittle failure of the RC-walls but does not modify the elements' stiffness.

As for the building retrofitted with steel braces at the open ground storey, it is possible to notice that in the X direction, along which the steel braces are applied, the IDRs are reduced at the bottom

storeys but slightly higher in the upper storeys (Figure 6.7a): for this reason, a third intervention solution is considered, which involves, besides the application of steel braces at the ground storey, the FRP wrapping of the RC walls all along the height of the building. Since the application of the FRPs on the walls does not modify the stiffness of the structure, the IDRs does not change and correspond to those in Figure 6.7.

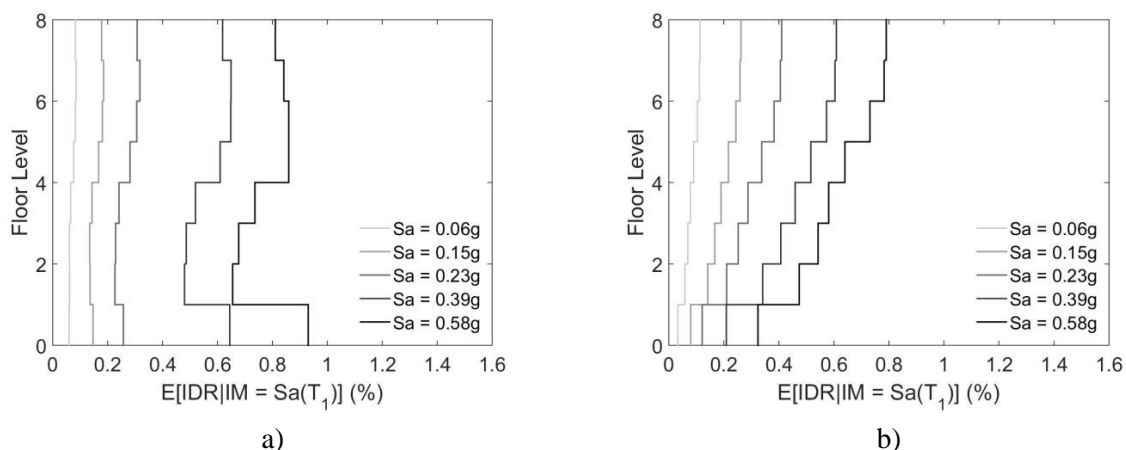


Figure 6.6 – IDR as a function of the building height for the (a) X and (b) Y direction for the building strengthened with FRPs.

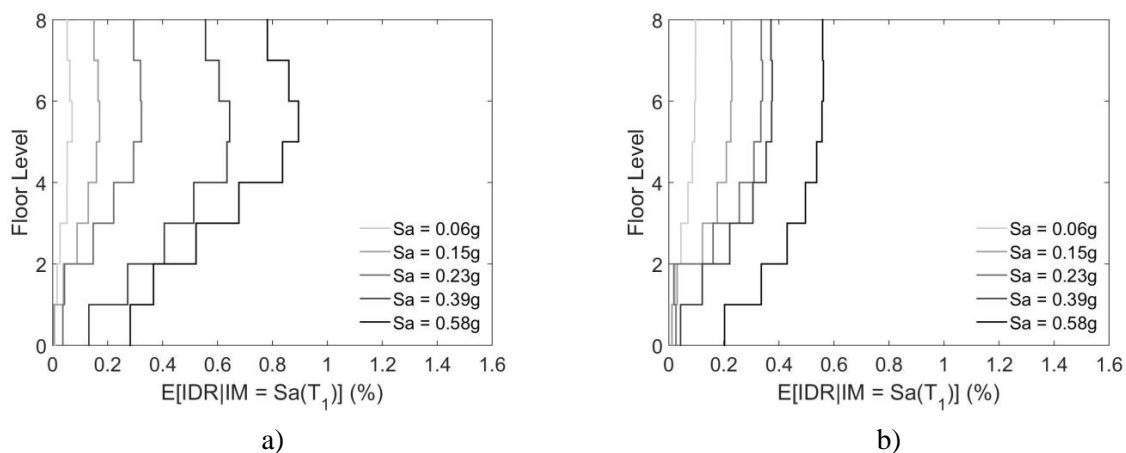


Figure 6.7 – IDR as a function of the building height for the (a) X and (b) Y direction for the building strengthened with steel braces.

### 6.3.3. Damage analysis

Post-rehabilitation fragility curves and loss functions are evaluated for structural and non-structural components. In this study, the aforementioned fragility functions and analytical expressions described in Chapter 5 - Section 5.2 and Section 5.3 - are used to estimate the probability of reaching or exceeding different damage states in the non-ductile RC columns and walls of the case study building. In Chapter 5, damage states are defined, based on the level of damage in the component and the repair actions needed to restore it to the undamaged state. Fragility functions at different damage states are combined with loss functions to obtain “the magnitude of consequences associated with the damage in

each component” (FEMA P-58). Structural and non-structural losses are evaluated for every level of ground motion intensity and then aggregated to obtain the total expected losses due to repair of structural and non-structural components.

Fragility functions of the RC walls retrofitted with FRP are derived with Equations (5.10) to (5.13) taking into account the confining action derived from the application of the FRP sheets (CNR-DT 200, 2013) (CEN, 2010).

#### 6.3.4. Loss analysis

As defined in Section 5.5.4, the probability of collapse as a function of the intensity measure,  $P(C/IM)$ , is assumed to be equal to the largest probability of any individual structural vertical element to reach DS4. Figure 6.8 shows the collapse fragility functions for each retrofitting solution and for the original building (which was shown in Figure 5.11). The figure shows that the retrofitting decreases the predicted collapse rates, though the extent of the improvement depends on the retrofit.

Table 6.3 summarizes the structural collapse resistance of the original and the retrofitted cases, i.e. the median collapse capacity and the Mean Annual Frequency (MAF) of collapse, which is obtained through the integration of the structure’s collapse capacity distribution with the seismic hazard curve (the interval of integration herein adopted is from 0.005 to 3.00g). Modelling earthquake recurrence by a Poisson distribution, the computed frequencies of collapse for the retrofitted cases range between  $3.2$  to  $5.9 \times 10^{-4}$  collapses per year. Therefore, compared to metrics obtained for the original building, the retrofitted structures show moderately better seismic performance in terms of reduced collapse and life-safety risk.

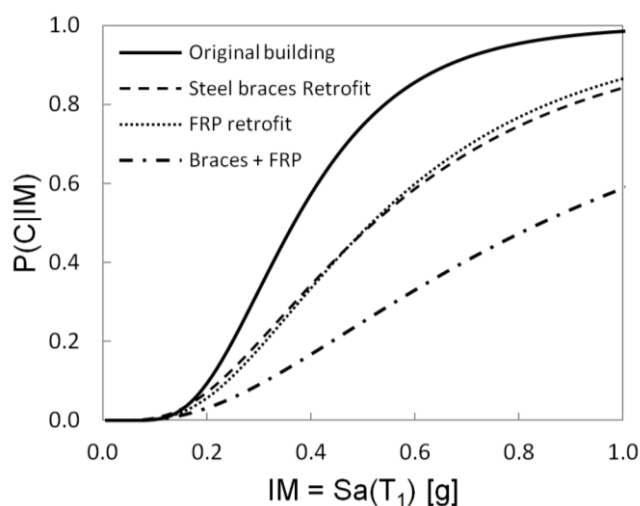


Figure 6.8 – Collapse fragility functions for the original structure and the structure retrofitted with steel braces, FRPs and a combination of the two.

Table 6.3 – Median collapse capacity and mean annual frequency of collapse of the original and retrofitted structure.

Retrofit description	Median collapse capacity $S_a(T_1)$ (g)	MAF of Collapse ( $10^{-4}$ )
Original	0.37	8.0
X-braces	0.52	5.9
FRP	0.52	5.5
Braces + FRPs	0.84	3.2

### 6.3.5. Cost-benefit analysis

Total economic losses are evaluated as the weighted sum of three components, i.e. losses resulting if the building collapses, losses associated with repairs, and losses resulting from having to demolish the building due to excessive residual drifts (see equation (5.4)). The vulnerability curves for the three retrofitting solutions are shown in Figure 6.9. Similar results are obtained for the two retrofitting strategies involving FRPs at the ground storey level (Figure 6.9a) and steel braces at the ground storey level (Figure 6.9b). As previously observed, the application of steel braces at the ground storey level leads to an increase in the IDR demand in the upper storeys of the building and the consequent increase of losses at those storeys.

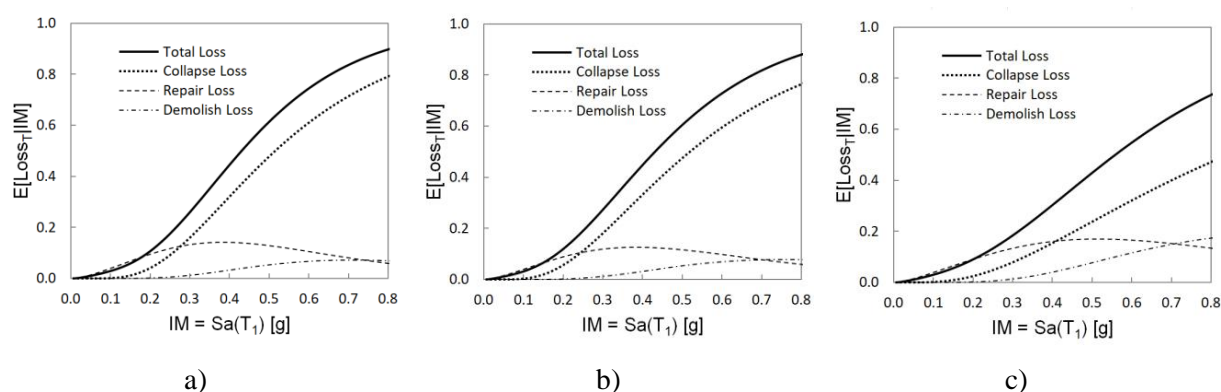


Figure 6.9 – Variations of the expected loss in the case study building retrofitted with FRP (a), steel braces (b) and the combination of FRP along all the height and steel braces (c).

Evaluation of the cost and benefit of each strengthening intervention is conducted herein in order to evaluate the actual convenience in choosing one of the examined strengthening strategies. In this work, an effort is made to consider cost-effective retrofitting solutions which should also allow continued usage of the building during the retrofitting work.

In the following paragraphs a description of the construction manufacturing costs required to carry out the seismic consolidation operation using the techniques examined is reported. The unit price of each work should include the cost of materials, labour, transportation and hire, which should be added to the costs of safety and the profit of the construction company (Mazzolani et al., 2018). In order to

consider reliable and realistic repair costs, the CYPE database (CYPE, 2014), which contains detailed and up-to-date construction costs for the Portuguese building stock, has been utilized. The prices absent in this database refer to the prices applied by the construction companies that work with these techniques.

Table 6.4 shows a summary of the unit costs of retrofitting with FRP sheets, including scaffolding, partial demolition and reconstruction of partition walls and finishing works. The estimated total cost of this intervention is €15 829, considering full wrapping of the T-shaped RC walls at the ground storey with FRP horizontal sheets. Based on the indications provided by the manufacturers, the steel braces installation has an average unit price of €5.00/kg (varying from €3/kg to €9/kg), which includes material costs, production costs and on-site assembly costs (Table 6.5). Considering that four X-braces must be installed, two on each side of the structure (Figure 6.2), and that the mass of the CHS 219.1x5.9 is 31.00 kg/m, the total mass of the steel for these devices is 1984 kg. The total cost for retrofitting through the installation of steel braces is estimated at 15 277 Euro.

While direct losses include all the costs incurred by the stakeholders to repair the building, there are a series of indirect losses which are related to the costs occurring during the building reparation, e.g. interruption of activities, inhabitant relocation but also losses associated to injuries and occupant fatalities (Cardone et al., 2017). As stated by (Liel and Deierlein, 2013) the cost of retrofitting that gives a positive return should be no more than about 10 to 30% of the building replacement value when benefits derived from reduction of fatality risks are not considered.

Table 6.4 – Cost of retrofitting with FRP.

<b>Description</b>	<b>Unit</b>	<b>Unit cost [€/unit]</b>
Scaffolding	m <sup>2</sup>	17.62
Demolition of interior partition wall	m <sup>2</sup>	4.51
FRP laminates	m <sup>2</sup>	97.88
FRP sheets	m <sup>2</sup>	106.53
Reconstruction of interior partition wall	m <sup>2</sup>	26.82
Plastering	m <sup>2</sup>	4.29

Table 6.5 – Cost of retrofitting with steel braces.

<b>Description</b>	<b>Unit</b>	<b>Unit cost [€/unit]</b>
Scaffolding	m <sup>2</sup>	17.62
Steel Bracings	kg	5.00

For the sake of simplicity, in this study the indirect losses are assessed considering only the costs of relocating the inhabitants for the downtime required to repair the building (Calvi, 2013). It is assumed

that each person occupies a building area of 25 m<sup>2</sup> and that the cost of relocating in another structure is €30 per day. Considering a building cost of €615/m<sup>2</sup> (see Table 5.6), it results that the area occupied by each person costs €15 375. Consequently, the indirect losses due to downtime, expressed in terms of building replacement cost, is equivalent to 0.20% of the building replacement cost per day (€30/day/€15 075). The downtime cost is evaluated by multiplying this cost for the total estimated downtime and added to the retrofitting costs. It is worth saying that the retrofitting strategies were chosen to allow low downtime of the building during the retrofitting works. For the case of retrofitting with braces no downtime is considered, as it only involves few frames of the open ground storey of the building.

The total costs of intervention are shown in Table 6.6 as a percentage of the replacement value of the building.

Through convolution of the vulnerability curves with the seismic hazard curve for the city of Lisbon, the expected annual loss (EAL) of the case study building is estimated. EAL represents the estimated losses, in terms of an average annual amount, associated with repairing earthquake damage, considering the frequency and severity of possible future earthquakes represented by the seismic hazard at the site of interest. The EAL for the retrofitted cases are reported in Table 6.6 and range between 0.096 to 0.116% of the total replacement value of the building.

Benefits of seismic mitigation are evaluated in terms of improved performance of the building (reduced risk of damage). If associated with reduced economic losses, benefits can be evaluated as the difference in Near Present Value (NPV) of expected annual losses for the retrofitted (NPV<sub>R</sub>) and the original (NPV<sub>O</sub>) buildings (Calvi, 2013) (Liel and Deierlein, 2013). The NPV of benefits, which represents the expected present value of benefits over the building's remaining lifespan (*t*), is given by Equation (6.3). The *r* factor represents the social discount rate and has been assumed equal to 1%, equal to the inflation rate in Portugal in 2018 ([www.pordata.pt](http://www.pordata.pt)). A building lifespan of 50 years (*T*) is assumed. Benefit-cost ratios are evaluated with Expression (6.4) (Calvi, 2013). A break-even analysis has been conducted to compare the different retrofit strategies considered in this study. The break-even time represents the number of years required to fully amortize the cost of retrofitting with the benefits derived from the reduction of expected losses and is calculated by imposing the ratio in equation (6.4) to be equal to one.

$$NPV = EAL \sum_{t=1}^T (1 + r)^{-t} \quad (6.3)$$

$$\frac{Benefit}{Cost} = \frac{NPV_O - NPV_R}{Cost_{retrofit}} \quad (6.4)$$

The results of this study are shown in Table 6.6. The expected annual losses and benefits are expressed as a percentage of the replacement value of the building, which amounts to €1 840 572. Benefit-cost ratios higher than one shows a positive effect of these retrofitting strategies. Within the three solutions, retrofitting with steel braces can be considered the most cost effective solution, as it shows higher benefit-cost ratios and also shorter break event time.

It is evident that a thoughtful design intervention reduces the costs while increasing the effectiveness of the retrofit. It is worth noting that the benefit of retrofitting has been partially underestimated, since only indirect loss related to inhabitants' relocation was considered, but not those related to damage to building contents or injuries and fatalities.

The outcome of this study greatly depends on the hazard properties of the building site. Future research shall include the examination of additional case study buildings in order to confirm the outcomes of the cost-benefit analyses carried out in this study.

Table 6.6 – Benefit-cost ratios for the original building and for each one of the strengthening strategies.

	EAL (%)	Benefit (%)	Cost of retrofit (%)	Benefit-Cost Ratio	Break-even (years)
Original	0.164	-	-	-	-
X-braces	0.116	1.46	0.83	1.76	21
FRP	0.108	1.68	1.27	1.29	33
X-braces + FRP	0.096	2.05	2.03	1.01	50

#### 6.4. Conclusions

The work reported herein addresses the problem of strengthening one of the most vulnerable class of existing reinforced concrete buildings in Lisbon, namely RC wall-frame buildings with an open ground storey (pilotis), designed and built under old codes and engineering practices. The feasibility of partial strengthening of such buildings was examined, with the ultimate aim to develop an efficient retrofitting plan for this typology.

Three local retrofitting methods were used, namely partial strengthening at the open ground storey with steel braces, FRP-wrapping of single elements (individual RC walls) at the ground storey only and a combination of the two, involving steel braces at the open ground storeys and FRP wrapping of the walls along the building height. It is worth noting that FRP composite materials have received increasing attention in the past few decades as a potential material for retrofitting of existing RC structures.

The purpose of this study was to design two seismic local interventions, applied to a group of members that suffer from structural deficiencies in order to achieve the desired seismic performance.

By means of nonlinear static analyses, the seismic performance of the existing and retrofitted buildings was evaluated. By comparing the pushover curves, it becomes evident that the retrofitting solutions lead to comparable results in terms of maximum strength and stiffness and allow mitigating the initial vulnerabilities. Fulfilment of the safety requirements defined by EC8-3 was assessed comparing, for each structural element, the seismic demand with the corresponding capacity at the SD limit state. It was shown that all the shear demand to capacity ratios in the RC walls of the retrofitted schemes fall below unity, indicating a positive effect resulting from the retrofitting.

A building specific loss assessment methodology and a cost-benefit analysis were then performed, which indicated that local methods of intervention, as opposed to a complete strengthening to comply with current standards for new buildings, are perhaps the only retrofitting option that might be acceptable by the owners of such buildings, for two important reasons: (i) low cost of intervention and (ii) low downtime of the building during the retrofitting work.

Compared to metrics obtained for the original building, the retrofitted structures exhibit moderately better seismic performance in terms of reduced collapse and life-safety risks and economic risks.

Future research shall include examination of additional case study buildings in order to confirm the outcomes of the cost-benefit analyses carried out in this study.



## 7. FINAL REMARKS AND FUTURE WORK

### 7.1. Final remarks

This thesis focused on the vulnerability and economic loss assessment of reinforced concrete frame-wall buildings that are typically found in Lisbon and in other European cities which were designed before the introduction of modern seismic codes. The research addressed different aspects, namely:

- (i) the definition of modelling approaches and discussion on modelling issues which concern the specific typology;
- (ii) the characterization of the building structural behaviour with focus on torsional effects;
- (iii) the derivation of member fragility and loss functions;
- (iv) the selection of retrofiting techniques to reduce seismic vulnerability.

A robust numerical model is fundamental for the assessment of seismic performance, especially for old RC buildings. Limited investigation has been carried out so far to assess the contribution of Strain Penetration (SP) effects at the anchorage region of RC walls. The outcomes of this thesis show that SP effects introduces a non-negligible flexibility at the base of the walls which becomes more relevant as the anchorage conditions deteriorate, namely with the consideration of smooth rebars and reduced anchorage lengths. A simplified methodology has been used to take this phenomenon into account in a beam element formulation that consists of reducing the Young's Modulus and the maximum steel strength of the rebars. It was observed that, for ribbed rebars with appropriate embedment length, the reduction in the Young's Modulus should be in the order of 20% to 30%, whilst in the presence of smooth rebars this value should increase to values of the order of 50%, regardless of the embedment length. In what concerns the rebars' strength, this value is naturally dependent on the embedment length, and may need to be reduced to values of the order of 80% of its expected value. A set of general expressions to estimate this parameter for different anchorage lengths were proposed.

It is known that torsional effects may affect the seismic response, especially of old RC buildings. In this study, the applicability of the N2 method in its original formulation and the Extended N2 method were analysed through a comparison with the more reliable nonlinear time-history analysis. Moreover, the influence of torsion on the response parameters, namely chord rotation and shear strength was examined. The studies conducted allowed to conclude that the Extended N2 method provides a conservative estimate of the structural response in comparison with nonlinear time-history analysis. However, its application is essential for predicting the torsional response of a torsionally flexible building, for which the original N2 method does not provide accurate estimates. A proposal was made to evaluate the shear demand by taking into account the nonlinear behaviour of the structure. The torsional behaviour worsens the seismic response of the structure, leading to brittle

failure of the RC walls for values of PGA significantly smaller than those obtained for the torsionally balanced structure.

Despite the focus on a case study building, a general procedure was defined for the vulnerability assessment of old RC buildings. The procedure considers the contribution of uncertainties to the building's capacity and the uncertainties in the seismic demand. The uncertainties in terms of capacity were considered by applying a Monte Carlo simulation for the generation of different structural models for each realization of the random variables, while the uncertainties in seismic demand were obtained by considering a set of 40 records compatible with seismic action type 1 defined in Eurocode 8 for Lisbon and by considering the appropriate soil type.

The procedure adopted for the loss analysis makes use of component-based fragility and loss functions to assess damage in structural and non-structural elements. An analytical procedure was proposed to estimate the fragility parameters of non-ductile reinforced concrete walls with smooth reinforcing bars and light transversal reinforcement, taking into account strength penetration effects. A few of repair techniques were discussed, based on the extent of damage in the various components, for which repair costs associated to the Portuguese reality were considered. Economic losses were estimated based on the contribution of three components: (i) losses associated to damage on structural and non-structural components, (ii) losses resulting if the building collapses and (iii) losses resulting from having to demolish the building due to excessive residual drifts. The final fragility and vulnerability curves were defined by adopting the minimum value between the results obtained in the X and Y directions for each building class.

The value of expected annual losses (EAL) obtained in this study, which is around 0.16 % of the replacement value of the building, is in line with those reported in similar studies performed on old RC structures in Europe. It was found that losses due to repair of the building in the non-collapse case contribute up to 60% to the total value of EAL. The repair losses, although being smaller than those due to stronger shaking, are associated to a higher probability of occurrence. Nevertheless, the performance assessment indicated that the building is characterised by a relatively high probability of collapse for moderate seismic intensity levels, which results, through integration with the hazard curve, in high values of the mean annual frequency of collapse. This conclusion is justified with the non-ductile behaviour of the RC walls, which have a critical influence on the seismic behaviour of the building and can be further confirmed by comparing the fragility functions derived for the RC walls with those adopted for the RC columns.

One of the aims of this work was to review the present criteria and effective tools to reduce seismic risk by improving the structural response, i.e. by increasing constructions resilience. Resilience to earthquake disasters should be a goal of any community living in a seismically active area. At the same time, it is a difficult task because of the inherent uncertainty of future earthquake activity and

the pressure to reduce costs, especially for conventional buildings. In any post-disaster situation, decisions affecting rebuilding activities are made in the context of the local culture/environment and the perceptions and biases of the key actors and stakeholders. Earthquake resilience will only happen if it is required or the public demands it. Therefore, it will only occur if it is quantified and found to be cost-effective in the long run and to the benefit of society. The results of this thesis highlight the importance of economic loss assessment results for guiding decisions about retrofitting strategies to improve the overall performance of non-ductile RC buildings, ideally in combination with the support of a cost-benefit analysis framework. The engineer should be able to communicate seismic risk in a way that is easily understood by stakeholders such as owners, bankers, and insurers. The evaluation of the expected annual loss is an effective way of communicating the seismic vulnerability of built structure and infrastructure to owners and insurers and it provides quantitative information to assist stakeholders in making risk management decisions. This parameter may refer to direct losses only or include indirect losses, and can be used for several purposes, including the evaluation of insurance premium. Furthermore, this value could be used to evaluate the increased value of a building because of a retrofitting intervention. As in the case of Italy, the EAL can also be used by governments to introduce regulations that allow some taxation deduction in some proportion to the EAL reduction.

The feasibility of partial strengthening of the building was examined, with the ultimate aim to develop an efficient retrofitting plan for this building typology. Three local methods of retrofitting were used, the first involving the partial strengthening at the open ground storey with steel braces, the second the FRP-wrapping of single elements (individual RC walls) and the third as a combination of FRP wrapping and steel braces. To evaluate the feasibility of each retrofitting solution, the initial cost of intervention was compared with the benefits obtained through the reduction in terms of expected annual loss. It is shown that local methods of intervention, as opposed to a complete strengthening to comply with current standards for new buildings, are perhaps the only retrofitting option that might be acceptable by the owners of such buildings, for two important reasons: (i) low cost of intervention and (ii) low downtime of the building during the retrofitting work.

In summary, the findings presented in this thesis provide a better understanding of the seismic performance and damage assessment of wall-frame reinforced concrete structures and provide some guidance for retrofitting these structures.

## **7.2. Future developments**

According to the work herein developed and presented, the contributions of this thesis are envisioned to be further extended in the following aspects:

- Further exploration of parameters to represent the uncertainty in the structural modelling and the consideration of more building sites with different hazard levels;

- Derivation of fragility and loss ratios for non-structural elements, such as masonry infills and partition walls, specific for the Portuguese reality;
- Consideration of possible alternative strategies for the reduction of earthquake damage to non-structural elements, e.g.: (i) strengthening of infills and partitions through different techniques and materials, and (ii) application of seismic isolation devices;
- Examination of additional case study buildings, e.g. low- to high-rise old RC frame buildings, in order to produce fragility/vulnerability functions and generate a number of risk metrics (e.g. annual frequency of collapse and expected annual loss).

## REFERENCES

- Almeida, J. P., Tarquini, D. and Beyer, K. (2016) 'Modelling Approaches for Inelastic Behaviour of RC Walls: Multi-level Assessment and Dependability of Results', *Archives of Computational Methods in Engineering*, 23(1), pp. 69–100. doi: 10.1007/s11831-014-9131-y.
- Anagnostopoulos, S. A., Kyrkos, M. T. and Stathopoulos, K. G. (2015) 'Earthquake induced torsion in buildings: Critical review and state of the art', *Earthquake and Structures*, 8(2), pp. 305–377. doi: 10.12989/eas.2015.8.2.305.
- Applied Technology Council (1996) 'Seismic evaluation and retrofit of concrete buildings (Volume 1)', *Atc-40*, 1, p. 346. doi: 10.1193/1.1586093.
- Araújo, M., Macedo, L., Marques, M. and Castro, J. M. (2016) 'Code-based record selection methods for seismic performance assessment of buildings', *Earthquake Engineering & Structural Dynamics*, 45(1), pp. 129–148. doi: 10.1002/eqe.2620.
- Araújo, M. and Castro, J. M. (2016) 'On the quantification of local deformation demands and adequacy of linear analysis procedures for the seismic assessment of existing steel buildings to EC8-3', *Bulletin of Earthquake Engineering*, 14(6), pp. 1613–1642. doi: 10.1007/s10518-016-9897-4.
- ASCE Standard (2017) *ASCE/SEI 41-17. Seismic Evaluation and Retrofit of Existing Buildings, Seismic Evaluation and Retrofit of Existing Buildings*. Reston, VA: American Society of Civil Engineers. doi: 10.1061/9780784414859.
- Aslani, H. and Miranda, E. (2005) *Probabilistic earthquake loss estimation and loss disaggregation in buildings. Report No. 157*. Stanford, CA: The John A. Blume Earthquake Engineering Center.
- ATC (2018) *Applied Technology Council, FEMA P-58 Next-generation Seismic Performance Assessment for Buildings, Vol. 1- Methodology, Federal Emergency Management Agency, Washington, DC*. Available at: [https://www.fema.gov/media-library-data/1396495019848-0c9252aac91dd1854dc378feb9e69216/FEMAP-58\\_Volume1\\_508.pdf](https://www.fema.gov/media-library-data/1396495019848-0c9252aac91dd1854dc378feb9e69216/FEMAP-58_Volume1_508.pdf).
- Baker, J. W. (2011) 'Conditional Mean Spectrum: Tool for Ground-Motion Selection', *Journal of Structural Engineering*, 137(3), pp. 322–331. doi: 10.1061/(ASCE)ST.1943-541X.0000215.
- Beyer, K., Dazio, A. and Priestley, M. J. N. (2008) 'Inelastic wide-column models for U-shaped reinforced concrete walls', *Journal of Earthquake Engineering*, 12(SUPPL. 1), pp. 1–33. doi: 10.1080/13632460801922571.
- Beyer, K., Dazio, A. and Priestley, M. J. N. (2011) 'Shear Deformations of Slender Reinforced Concrete Walls under Seismic Loading', *ACI Structural Journal*, 108(2). doi: 10.14359/51664252.

- Bhatt, C. and Bento, R. (2011) ‘Assessing the seismic response of existing RC buildings using the extended N2 method’, *Bulletin of Earthquake Engineering*, 9(4), pp. 1183–1201. doi: 10.1007/s10518-011-9252-8.
- Biskinis, D. E., Roupakias, G. K. and Fardis, M. N. (2005) ‘Degradation of Shear Strength of Reinforced Concrete Members with Inelastic Cyclic Displacements’, 2019(101), pp. 1–15.
- Bommer, J., Spence, R., Erdik, M., Tabuchi, S., Aydinoglu, N., Booth, E., Del Re, D. and Peterken, O. (2002) ‘Development of an earthquake loss model for Turkish catastrophe insurance’, *Journal of Seismology*, 6(3), pp. 431–446. doi: 10.1023/A:1020095711419.
- Bommer, J. J. and Pinho, R. (2006) ‘Adapting earthquake actions in Eurocode 8 for performance-based seismic design’, *Earthquake Engineering and Structural Dynamics*, 35(1), pp. 39–55. doi: 10.1002/eqe.530.
- Bosco, M., Ghersi, A. and Marino, E. M. (2012) ‘Corrective eccentricities for assessment by the nonlinear static method of 3D structures subjected to bidirectional ground motions’, *Earthquake Engineering & Structural Dynamics*, 41(13), pp. 1751–1773. doi: 10.1002/eqe.2155.
- Calabrese, A., Almeida, J. P. and Pinho, R. (2010) *Numerical issues in distributed inelasticity modeling of RC frame elements for seismic analysis*, *Journal of Earthquake Engineering*. doi: 10.1080/13632461003651869.
- Calvi, G., Pinho, R., Magenes, G., Bommer, J., Restrepo, L. and Crowley, H. (2006) ‘Development of Seismic Vulnerability Assessment Methodologies over the Past 30 Years, ISET Journal of Earthquake Technology, Paper No. 472, 43(3), 75-104.’, *ISET Journal of Earthquake Technology*, 43(472), pp. 75–104.
- Calvi, G. M. (2013) ‘Choices and criteria for seismic strengthening’, *Journal of Earthquake Engineering*, 17(6), pp. 769–802. doi: 10.1080/13632469.2013.781556.
- Calvi, G. M. and Pinho, R. (2004) *LESSLOSS: a European integrated project on risk mitigation for earthquakes and landslides. Research Report Rose 2004/02*. Pavia: IUSS Press.
- Cardone, D. (2016) ‘Fragility curves and loss functions for RC structural components with smooth rebars’, *Earthquake and Structures*, 10(5), pp. 1181–1212. doi: 10.12989/eas.2016.10.5.1181.
- Cardone, D., Gesualdi, G. and Perrone, G. (2017) ‘Cost-Benefit Analysis of Alternative Retrofit Strategies for RC Frame Buildings’, *Journal of Earthquake Engineering*, 23(2), pp. 208–241. doi: 10.1080/13632469.2017.1323041.
- Cardone, D. and Perrone, G. (2015) ‘Developing fragility curves and loss functions for masonry infill walls’, *Earthquake and Structures*, 9(1), pp. 257–279. doi: 10.12989/eas.2015.9.1.257.

- Cardone, D. and Perrone, G. (2017a) ‘Damage and Loss Assessment of Pre-70 RC Frame Buildings with FEMA P-58’, *Journal of Earthquake Engineering*. Taylor & Francis, 21(1), pp. 23–61. doi: 10.1080/13632469.2016.1149893.
- Cardone, D. and Perrone, G. (2017b) ‘Damage and Loss Assessment of Pre-70 RC Frame Buildings with FEMA P-58’, *Journal of Earthquake Engineering*. Taylor & Francis, 21(1), pp. 23–61. doi: 10.1080/13632469.2016.1149893.
- Cardone, D., Rossino, M. and Gesualdi, G. (2018) ‘Estimating fragility curves of pre-70 RC frame buildings considering different performance limit states’, *Soil Dynamics and Earthquake Engineering*. Elsevier Ltd, (December 2014), pp. 0–1. doi: 10.1016/j.soildyn.2017.11.015.
- Caruso, C., Bento, R., Sousa, R. and Correia, A. A. (2019) ‘Modelling strain penetration effects in RC walls with smooth steel bars’, *Magazine of Concrete Research*, 71(17), pp. 894–906. doi: 10.1680/jmacr.18.00052.
- Caruso, C. and Bento, R. (2019) *Steel smooth bars – Mechanical properties and monotonic tensile tests, Report CERIS DTC n° 3/2019*.
- Carvalho, E. C., Coelho, E., Campos-Costa, A., Sousa, M. L. and Candeias, P. (2002) ‘Vulnerability evaluation of residential buildings in Portugal’, *In Proceedings of the 12th European Conference on Earthquake Engineering*, 696.
- Casanova, A., Jason, L. and Davenne, L. (2012) ‘Bond slip model for the simulation of reinforced concrete structures’, *Engineering Structures*. Elsevier Ltd, 39, pp. 66–78. doi: 10.1016/j.engstruct.2012.02.007.
- Castro, J. M., Araújo, M., D’Aniello, M. and Landolfo, R. (2017) ‘Strengthening of RC Buildings with Steel Elements’, pp. 139–162. doi: 10.1007/978-981-10-5858-5\_6.
- Celarec, D., Ricci, P. and Dolšek, M. (2012) ‘The sensitivity of seismic response parameters to the uncertain modelling variables of masonry-infilled reinforced concrete frames’, *Engineering Structures*, 35, pp. 165–177. doi: 10.1016/j.engstruct.2011.11.007.
- Celarec, D., Vamvatsikos, D. and Dolšek, M. (2011) ‘Simplified estimation of seismic risk for reinforced concrete buildings with consideration of corrosion over time’, *Bulletin of Earthquake Engineering*, 9(4), pp. 1137–1155. doi: 10.1007/s10518-010-9241-3.
- CEN (2001a) *Eurocode 2: Design of concrete structures - Part 1: General rules and rules for buildings, EN 1992-1*. Edited by E. C. for S. (CEN). Brussels.
- CEN (2001b) *Metallic materials - Tensile testing - Part 1: Method of test at ambient temperature, EN 10002-1*. Edited by E. C. for S. (CEN). Brussels.

CEN (2004) *Eurocode 8: Design of structures for earthquake resistance. Part 1: General rules, seismic actions and rules for buildings Eurocode, EN 1998-1*. Edited by European Committee for Standardization (CEN). Brussels.

CEN (2010) *Eurocode 8: Design of structures for earthquake resistance. Part 3: Assessment and retrofitting of buildings Eurocode, EN 1998-3*. Edited by E. C. for S. (CEN). Brussels.

CEN (2011) *Eurocode 3: Design of steel structures - Part 1-8: Design of joints*,.

Chopra, A. K. and Goel, R. K. (2002) 'A modal pushover analysis procedure for estimating seismic demands for buildings', *Earthquake Engineering and Structural Dynamics*, 31(3), pp. 561–582. doi: 10.1002/eqe.144.

Chopra, A. K. and McKenna, F. (2016) 'Modeling viscous damping in nonlinear response history analysis of buildings for earthquake excitation', *Earthquake Engineering & Structural Dynamics*, 45(2), pp. 193–211. doi: 10.1002/eqe.2622.

Choudhury, T. and Kaushik, H. B. (2018) 'Component Level Fragility Estimation for Vertically Irregular Reinforced Concrete Frames', *Journal of Earthquake Engineering*. Taylor & Francis, 2469, pp. 1–25. doi: 10.1080/13632469.2018.1453413.

CNR-DT 200 (2013) *Istruzioni per la Progettazione, l'Esecuzione ed il Controllo di Interventi di Consolidamento Statico mediante l'utilizzo di Compositi Fibrorinforzati*.

Cornell, C. A., Jalayer, F., Hamburger, R. O. and Foutch, D. A. (2002) 'Probabilistic Basis for 2000 SAC Federal Emergency Management Agency Steel Moment Frame Guidelines', *Journal of Structural Engineering*, 128, pp. 526–533. doi: 10.1061/(ASCE)0733-9445(2002)128:4(526).

Crowley, H., Rodrigues, D., Silva, V., Despotaki, V., Castro, J. M., Akkar, S., Hancilar, U. and Pitilakis, K. (2018) 'Towards a Uniform Earthquake Risk Model for Europe', in *Proceedings of the 16th European Conference on Earthquake Engineering*, pp. 1–10.

CYPE (2014) *Price generator*. Available from: <http://www.geradordeprecos.info/> (accessed in May 2014).

Dazio, A., Beyer, K. and Bachmann, H. (2009) 'Quasi-static cyclic tests and plastic hinge analysis of RC structural walls', *Engineering Structures*. Elsevier Ltd, 31(7), pp. 1556–1571. doi: 10.1016/j.engstruct.2009.02.018.

Deierlein, G. G., Krawinkler, H. and Cornell, C. A. (2003) 'A framework for performance-based earthquake engineering', *Pacific Conference on Earthquake Engineering*. doi: 10.1061/9780784412121.173.

Dolce, M. and Manfredi, G. (2015) 'Libro bianco sulla ricostruzione privata fuori dai centri storici nei

comuni colpiti dal sisma dell'Abruzzo del 6 Aprile 2009', in ReLuis (ed.), p. 224.

Dolšek, M. and Fajfar, P. (2008) 'The effect of masonry infills on the seismic response of a four storey reinforced concrete frame-a probabilistic assessment', *Engineering Structures*, 30(11), pp. 3186–3192. doi: 10.1016/j.engstruct.2008.04.031.

Dolšek, M., Lazar Sinković, N. and Žižmond, J. (2017) 'IM-based and EDP-based decision models for the verification of the seismic collapse safety of buildings', *Earthquake Engineering and Structural Dynamics*, 46(15), pp. 2665–2682. doi: 10.1002/eqe.2923.

Earthquake Commission (EQC) (2019) 'EQCover Insurers Guide', (July).

Fajfar, P. (1999) 'Capacity spectrum method based on inelastic demand spectra', *Earthquake Engineering & Structural Dynamics*, 28(9), pp. 979–993. doi: 10.1002/(SICI)1096-9845(199909)28:9<979::AID-EQE850>3.0.CO;2-1.

Fajfar, P. (2000) 'A Nonlinear Analysis Method for Performance-Based Seismic Design', *Earthquake Engineering and Structural Dynamics*, 16(3), pp. 573–592. doi: 10.1193/1.1586128.

Fajfar, P., Marusic, D. and Perus, I. (2005) 'Torsional effects in the pushover-based seismic analysis of buildings', *Journal of Earthquake Engineering*, 9(6), pp. 831–854. doi: 10.1080/13632460509350568.

Fardis, M. N. (2009) *Seismic Design, Assessment and Retrofitting of Concrete Buildings*. Dordrecht: Springer Netherlands (Geotechnical, Geological, and Earthquake Engineering). doi: 10.1007/978-1-4020-9842-0.

Favvata, M. J., Naoum, M. C. and Karayannis, C. G. (2013) 'Limit states of RC structures with first floor irregularities', *Structural Engineering and Mechanics*, 47(6), pp. 791–818. doi: 10.12989/sem.2013.47.6.791.

FEMA (2000) *HAZUS ® 99 Estimated Annualized Earthquake Losses for the United States*.

FEMA (2015) *Technical and User's Manual of Advanced Engineering Building Module (AEBM) "HAZUS MH 2.1"*, Federal Emergency Management Agency. Edited by F. E. M. Agency. Federal Emergency Management Agency.

FEMA 356 (2000) 'FEMA 356 - Prestandard and commentary for the seismic rehabilitation of buildings, FEDERAL EMERGENCY MANAGEMENT AGENCY', *Report FEMA-356, Washington, DC*.

Fernandes, C., Varum, H. and Costa, a (2007) 'Concrete-steel bond characterization of RC structural elements built with smooth plain reinforcement bars', *2nd Symposium 'Connections between Steel and Concrete'*, (September), pp. 1–10.

Ferreira, D. (2016) *Seismic Assessment of an Old Reinforced Concrete Building in the City of Lisbon. Thesis to obtain the Master's degree in Civil Engineering.*, University of Lisbon, Portugal.

fib (2013) *fib Model Code for Concrete Structures 2010, fib Bulletin 70*. Weinheim, Germany: Wiley-VCH Verlag GmbH & Co. KGaA. doi: 10.1002/9783433604090.

fib - bulletin 24 (2003) *Seismic assessment and retrofit of reinforced concrete buildings*. Available at: <http://www.theeuropeanlibrary.org/tel4/record/2000053204861>.

fib - bulletin 35 (2006) 'Retrofitting of concrete structure by externally bonded FRPs, (with emphasis on seismic applications)'

Filippou, F. C., Popov, E. P. and Bertero, V. V. (1983) 'Modeling of R/C Joints under Cyclic Excitations', *Journal of Structural Engineering*, 109(11), pp. 2666–2684. doi: 10.1061/(ASCE)0733-9445(1983)109:11(2666).

Finanças (2018) 'Portaria n.º 330-A/2018', *Diário da República 1.ª série—N. 245 de 20 de dezembro*.

Furtado, A., Rodrigues, H., Arêde, A. and Varum, H. (2016) 'Simplified macro-model for infill masonry walls considering the out-of-plane behaviour', *Earthquake Engineering & Structural Dynamics*, 45(4), pp. 507–524. doi: 10.1002/eqe.2663.

Galvis, F., Miranda, E., Heresi, P., Dávalos, H. and Silos, J. R. (2017) 'Preliminary Statistics of Collapsed Buildings in Mexico City in Puebla-Morelos Earthquake', p. 17. Available at: [http://www.learningfromearthquakes.org/2017-09-19-puebla-mexico/images/2017\\_09\\_19\\_Puebla\\_Mexico/pdfs/Preliminary\\_Report\\_Mexico2017\\_v7.pdf](http://www.learningfromearthquakes.org/2017-09-19-puebla-mexico/images/2017_09_19_Puebla_Mexico/pdfs/Preliminary_Report_Mexico2017_v7.pdf).

Goda, K., Kiyota, T., Pokhrel, R. M., Chiaro, G., Katagiri, T., Sharma, K. and Wilkinson, S. (2015) 'The 2015 Gorkha Nepal Earthquake: Insights from Earthquake Damage Survey', *Frontiers in Built Environment*, 1(June). doi: 10.3389/fbuil.2015.00008.

Goda, K., Wenzel, F. and Daniell, J. (2014) 'Insurance and Reinsurance Models for Earthquake', in Beer, M. et al. (eds) *Encyclopedia of Earthquake Engineering*. Berlin, Heidelberg: Springer Berlin Heidelberg, pp. 1–24. doi: 10.1007/978-3-642-36197-5\_261-1.

Goodnight, J. C., Kowalsky, M. J., Nau, J. M. and Goodnight, J. C. (2015) 'Prepared By : January 2015 Prepared For ', 4000(January).

Greifenhagen, C. and Lestuzzi, P. (2005) 'Static cyclic tests on lightly reinforced concrete shear walls', *Engineering Structures*, 27(11), pp. 1703–1712. doi: 10.1016/j.engstruct.2005.06.008.

Haddad, J., Cattari, S. and Lagomarsino, S. (2017) 'Preliminary and Sensitivity Analysis To Set the Investigation Plan for the Seismic Assessment of Existing Buildings', pp. 12–15.

- Hsiao, P. C., Lehman, D. E. and Roeder, C. W. (2012) 'Improved analytical model for special concentrically braced frames', *Journal of Constructional Steel Research*. Elsevier Ltd, 73, pp. 80–94. doi: 10.1016/j.jcsr.2012.01.010.
- James, R., Kit, D., Report, E., Kit, H. S., Kit, A. S., Vervaeck, A., Report, E. Q., Kit, F. W., Kit, B. K. and Sai, J. A. (2015) 'CEDIM Forensic Disaster Analysis - Nepal Earthquake - Report No . 3 CEDIM Forensic Disaster Analysis Group , CATDAT and Earthquake-Report . com Nepal Earthquakes – Report # 3', (3).
- Jarimba, A. (2016) 'Vulnerabilidade Sísmica dos Edifícios porticados de Betão Armado da cidade de Lisboa- décadas de 1960-80', *Master thesis*.
- Jendele, L. and Cervenka, J. (2006) 'Finite element modelling of reinforcement with bond', *Computers and Structures*, 84(28), pp. 1780–1791. doi: 10.1016/j.compstruc.2006.04.010.
- Júlio, E. S., Branco, F. and Silva, V. D. (2003) 'Structural rehabilitation of columns with reinforced concrete jacketing', *Progress in Structural Engineering and Materials*, 5(1), pp. 29–37. doi: 10.1002/pse.140.
- Kam, W., Pampanin, S. and Elwood, K. (2011) 'Seismic performance of reinforced concrete buildings in the 22 February Christchurch (Lyttelton) earthquake', *Bull New Zeal Soc Earthq Eng*, 44, pp. 239–78. Available at: <http://hdl.handle.net/10092/9006>.
- Kaushik, H. B., Rai, D. C. and Jain, S. K. (2009) 'Effectiveness of Some Strengthening Options for Masonry-Infilled RC Frames with Open First Story', *Journal of Structural Engineering*, 135(8), pp. 925–937. doi: 10.1061/(asce)0733-9445(2009)135:8(925).
- Kohrangi, M., Bazzurro, P. and Vamvatsikos, D. (2016) 'Vector and Scalar IMs in Structural Response Estimation, Part II: Building Demand Assessment', *Earthquake Spectra*, 32(3), pp. 1525–1543. doi: 10.1193/053115EQS081M.
- Kreslin, M. and Fajfar, P. (2012) 'The extended N2 method considering higher mode effects in both plan and elevation', *Bulletin of Earthquake Engineering*, 10(2), pp. 695–715. doi: 10.1007/s10518-011-9319-6.
- Liel, A. B., Haselton, C. B., Deierlein, G. G. and Baker, J. W. (2009) 'Incorporating modeling uncertainties in the assessment of seismic collapse risk of buildings', *Structural Safety*, 31(2), pp. 197–211. doi: 10.1016/j.strusafe.2008.06.002.
- Liel, A. B. and Deierlein, G. G. (2013) 'Cost-benefit evaluation of seismic risk mitigation alternatives for older concrete frame buildings', *Earthquake Spectra*, 29(4), pp. 1391–1411. doi: 10.1193/030911EQS040M.

Lowes, L. N. and Moehle, J. P. (1999) 'Finite Element Modeling of Reinforced Concrete Beam-Column Bridge Connections', *Department of Civil and Environmental Engineering*, p. 419.

Di Ludovico, M., Prota, A., Moroni, C., Manfredi, G. and Dolce, M. (2017) *Reconstruction process of damaged residential buildings outside historical centres after the L'Aquila earthquake: part II—“heavy damage” reconstruction*, *Bulletin of Earthquake Engineering*. Springer Netherlands. doi: 10.1007/s10518-016-9979-3.

Macedo, L. and Castro, J. M. (2017) 'SeEQ: An advanced ground motion record selection and scaling framework', *Advances in Engineering Software*. Elsevier Ltd, 114, pp. 32–47. doi: 10.1016/j.advengsoft.2017.05.005.

Mander, J. B., Priestley, M. J. N. and Park, R. (1988) 'Theoretical Stress-Strain Model for Confined Concrete', *Journal of Structural Engineering*, 114(8), pp. 1804–1826. doi: 10.1061/(ASCE)0733-9445(1988)114:8(1804).

Martins, L., Silva, V., Marques, M., Crowley, H. and Delgado, R. (2016) 'Development and assessment of damage-to-loss models for moment-frame reinforced concrete buildings', *Earthquake Engineering & Structural Dynamics*, 45(5), pp. 797–817. doi: 10.1002/eqe.2687.

Mazzolani, F. M., Formisano, A. and Vaiano, G. (2018) 'Seismic upgrading of reinforced concrete buildings: BRB and FRP', *Costruzioni metalliche, Jan-Feb*, pp. 25–50.

McKenna, F., Fenves, G. L. and Scott, H. M. (2000) 'Open system for earthquake engineering simulation (OpenSEES)', *Pacific Earthquake Engineering Research Center, University of California, California*.

Melo, J., Fernandes, C., Varum, H., Rodrigues, H., Costa, A. and Arêde, A. (2011) 'Numerical modelling of the cyclic behaviour of RC elements built with plain reinforcing bars', *Engineering Structures*, 33(2), pp. 273–286. doi: 10.1016/j.engstruct.2010.11.005.

Mendes, L. A. M. and Castro, L. M. S. S. (2013) 'A new RC bond model suitable for three-dimensional cyclic analyses', *Computers and Structures*, 120, pp. 47–64. doi: 10.1016/j.compstruc.2013.01.007.

Menegotto, M. and Pinto, P. E. (1973) 'Method of analysis for cyclically loaded R.C. plane frames including changes in geometry and non-elastic behaviour of elements under combined normal force and bending', in *Proceedings of IABSE Symposium on Resistance and Ultimate Deformability of Structures Acted on by Well Defined Repeated Loads*. Zurich, Switzerland, pp. 15–22.

Miyamoto, H. K., Gilani, A. S. J., Erdurmus, S. B. and Akdogan, M. E. (2010) 'Development of Guidelines and Effective Retrofit Strategies for Public Schools and Hospitals in Istanbul, Turkey', pp.

268–280. doi: 10.1061/41084(364)26.

Monti, G., Filippou, F. C. and Spacone, E. (1997) ‘Finite Element for Anchored Bars under Cyclic Load Reversals’, *Journal of Structural Engineering*, 123(5), pp. 614–623. doi: 10.1061/(ASCE)0733-9445(1997)123:5(614).

Mouroux, P. and Le Brun, B. (2006) ‘Presentation of RISK-UE project’, *Bulletin of Earthquake Engineering*, 4(4), pp. 323–339. doi: 10.1007/s10518-006-9020-3.

Neuenhofer, A. and Filippou, F. C. (1997) ‘Evaluation of Nonlinear Frame Finite-Element Models’, *Journal of Structural Engineering*, 123(7), pp. 958–966. doi: 10.1061/(ASCE)0733-9445(1997)123:7(958).

O’Reilly, G. J., Perrone, D., Fox, M., Monteiro, R. and Filiatrault, A. (2018) ‘Seismic assessment and loss estimation of existing school buildings in Italy’, *Engineering Structures*. Elsevier, 168(April), pp. 142–162. doi: 10.1016/j.engstruct.2018.04.056.

Oesterle, R. G., Fiorato, A. E., Johal, L. S., Carpenter, J. E. and Russell, H. G. (1976) *Earthquake Resistant Structural Walls. Tests of Isolated Walls*.

Olsen, A. H. and Porter, K. A. (2011) ‘What We Know about Demand Surge: Brief Summary’, *Natural Hazards Review*, 12(2), pp. 62–71. doi: 10.1061/(asce)nh.1527-6996.0000028.

Paulay, T. and Priestley, M. J. N. (1992) *Seismic Design of Reinforced Concrete and Masonry Buildings*, ISBN: 978-0-471-54915-4, Wiley. doi: 10.1002/9780470172841.fmatter.

Peter Fajfar, M. E. (2000) ‘A Nonlinear Analysis Method for Performance Based Seismic Design’, *Earthquake Spectra*, 16(3), pp. 573–592. doi: 10.1193/1.1586128.

Pinho, R. (2012) ‘GEM: a participatory framework for open, state-of-the-art models and tools for earthquake risk assessment’, in *Proceedings of the 15th World Conference on Earthquake Engineering*. Lisboa.

Pinto, P. E. and Franchin, P. (2014) ‘Existing Buildings: The New Italian Provisions for Probabilistic Seismic Assessment’, in Ansal, A. (ed.) *Perspectives on European Earthquake Engineering and Seismology, Geotechnical, Geological and Earthquake Engineering*, 34. Springer, pp. 97–130. doi: 10.1007/978-3-319-07118-3.

Popovics, S. (1973) ‘A numerical approach to the complete stress-strain curve of concrete’, *Cement and Concrete Research*, 3(5), pp. 583–599. doi: 10.1016/0008-8846(73)90096-3.

Porter, K. A. (2003) ‘An Overview of PEER’s Performance-Based Earthquake Engineering Methodology’, *9th International Conference on Applications of Statistics and Probability in Civil Engineering*, 273(1995), pp. 973–980.

Priestley, M., Calvi, G. M. and Kowalsky, M. (2007) *Direct Displacement-Based Seismic Design of Structures*. Edited by I. IUSS Press, Pavia. IUSS Press, Pavia, Italy.

Priestley, M. J. N., Seible, F. and Calvi, G. M. (1996) ‘Seismic Design and Retrofit of Bridges.pdf’, p. 705. doi: 10.1002/9780470172858.

Rahimi, A. and Maheri, M. R. (2018) ‘The effects of retrofitting RC frames by X-bracing on the seismic performance of columns’, *Engineering Structures*, 173(March), pp. 813–830. doi: 10.1016/j.engstruct.2018.07.003.

Ramirez, C. M. and Miranda, E. (2009) *Building-specific loss estimation methods & tools for simplified performance-based. Report No. 171, Blume Center Report*. Edited by T. J. A. B. E. E. Center. Stanford, CA.

Ramirez, C. M. and Miranda, E. (2012) ‘Significance of residual drifts in building earthquake loss estimation’, *Earthquake Engineering & Structural Dynamics*, 41(11), pp. 1477–1493. doi: 10.1002/eqe.2217.

REBA (1967) *Regulamento de Estruturas de Betão Armado, Decreto Lei no 47/723 de 20 de Maio do Ministério das Obras Públicas, Diário da República*. Lisbon, Portugal.

Reyes, J. C. and Chopra, A. K. (2011) ‘Three-dimensional modal pushover analysis of buildings subjected to two components of ground motion, including its evaluation for tall buildings’, *Earthquake Engineering & Structural Dynamics*, 40(7), pp. 789–806. doi: 10.1002/eqe.1060.

Romano, F., Faggella, M., Gigliotti, R., Zucconi, M. and Ferracuti, B. (2018) ‘Comparative seismic loss analysis of an existing non-ductile RC building based on element fragility functions proposals’, *Engineering Structures*. Elsevier, 177(August), pp. 707–723. doi: 10.1016/j.engstruct.2018.08.005.

Romão, X., Delgado, R. and Costa, A. (2009) ‘Practical aspects of demand and capacity evaluation of RC members in the context of EC8-3’, *Earthquake Engineering & Structural Dynamics*, (March), p. n/a-n/a. doi: 10.1002/eqe.953.

RSA (1983) *Regulamento de Segurança e Acções para Estruturas de Edifícios e Pontes, Decreto-Lei nº235/83, de 31 de Maio, Diário da República*. Lisbon, Portugal: (in portuguese).

RSCCS (1958) *Regulamento de Segurança das Construções Contra os Sismos, Decreto-Lei n. 41658, Diário da República*. Lisbon, Portugal.

RSEP (1961) ‘Regulamento de Solicitações em Edifícios e Pontes (RSEP), , Decreto nº44041, de 18 de Novembro’, *Diário do Governo*, p. 44041.

Salem, H. M. and Maekawa, K. (2004) ‘Pre- and Postyield Finite Element Method Simulation of Bond of Ribbed Reinforcing Bars’, *Journal of Structural Engineering*, 130(4), pp. 671–680. doi:

10.1061/(ASCE)0733-9445(2004)130:4(671).

SEAOC (1995) ‘Vision 2000 - A Framework for Performance Based Earthquake Engineering’, *Structural Engineers Association of California*. doi: 10.1016/j.cplett.2012.10.038.

Sezen, H. and Moehle, J. P. (2004) ‘Strength and deformation capacity of reinforced concrete columns with limited ductility’, in *Test*. Vancouver, B.C., Canada: 13th World Conference on Earthquake Engineering.

Silva, V. (2013) *Development of Open Models and Tools for Seismic Risk Assessment: Application to Portugal(PhD thesis)*. University of Aveiro, Portugal. Available at: <http://www.efehr.org/en/home/>.

Silva, V., Crowley, H., Pagani, M., Monelli, D. and Pinho, R. (2014) ‘Development of the OpenQuake engine, the Global Earthquake Model’s open-source software for seismic risk assessment’, *Natural Hazards*, 72(3), pp. 1409–1427. doi: 10.1007/s11069-013-0618-x.

Silva, V., Crowley, H., Varum, H., Pinho, R. and Sousa, L. (2015a) ‘Investigation of the characteristics of Portuguese regular moment-frame RC buildings and development of a vulnerability model’, *Bulletin of Earthquake Engineering*, 13(5), pp. 1455–1490. doi: 10.1007/s10518-014-9669-y.

Silva, V., Crowley, H., Varum, H. and Pinho, R. (2015b) ‘Seismic risk assessment for mainland Portugal’, *Bulletin of Earthquake Engineering*, 13(2), pp. 429–457. doi: 10.1007/s10518-014-9630-0.

Sousa, R. (2015) ‘Development and Verification of Innovative Modelling Approaches for the Analysis of Framed Structures Subjected to Earthquake Action’, pp. 126–179.

Sousa, R., Campos-Costa, A., Costa, A. and Candelas, P. (2019) ‘Fiabilidade estrutural de edifícios existentes de betão armado sem dimensionamento sismorresistente’, in *11º Congresso Nacional de Sismologia e Engenharia Sísmica*. Lisbon, Portugal.

TEC (2007) ‘Specifications for Structures to be Built in Disaster Areas’. Available at: <http://www.koeri.boun.edu.tr/deprenmmuh/eski/DBYBHY2007-English-Chapters1,2.pdf>.

Uriz, P., Filippou, F. C. and Mahin, S. A. (2008) ‘Model for Cyclic Inelastic Buckling of Steel Braces’, *Journal of Structural Engineering*, 134(4), pp. 619–628. doi: 10.1061/(asce)0733-9445(2008)134:4(619).

Varum, H. (2003) *Seismic assessment, strengthening and repair of existing buildings (avaliação, reparação e reforço sísmico de edifícios existentes)*.

Varum, H., Teixeira-Dias, F., Marques, P., Pinto, A. V. and Bhatti, A. Q. (2013) ‘Performance evaluation of retrofitting strategies for non-seismically designed RC buildings using steel braces’, *Bulletin of Earthquake Engineering*, 11(4), pp. 1129–1156. doi: 10.1007/s10518-012-9421-4.

- Del Vecchio, C., Del Zoppo, M., Di Ludovico, M., Verderame, G. M. and Prota, A. (2017) ‘Comparison of available shear strength models for non-conforming reinforced concrete columns’, *Engineering Structures*. Elsevier Ltd, 148(October), pp. 312–327. doi: 10.1016/j.engstruct.2017.06.045.
- Verderame, G. M., Ricci, P., Esposito, M. and Sansiviero, F. C. (2011) ‘Le caratteristiche meccaniche degli acciai impiegati nelle strutture in c.a. realizzate dal 1950 al 1980’, in *Proceedings of the XXVI National AICAP Conference “Le prospettive di sviluppo delle opere in calcestruzzo strutturale nel terzo millennio”*. Padova, Italy.
- Verderame, G. M., Fabbrocino, G. and Manfredi, G. (2008a) ‘Seismic response of r.c. columns with smooth reinforcement. Part I: Monotonic tests’, *Engineering Structures*, 30(9), pp. 2277–2288. doi: 10.1016/j.engstruct.2008.01.025.
- Verderame, G. M., Fabbrocino, G. and Manfredi, G. (2008b) ‘Seismic response of r.c. columns with smooth reinforcement. Part II: Cyclic tests’, *Engineering Structures*, 30(9), pp. 2289–2300. doi: 10.1016/j.engstruct.2008.01.024.
- Vilanova, S. P. and Fonseca, J. F. B. D. (2007) ‘Probabilistic Seismic-Hazard Assessment for Portugal’, *Bulletin of the Seismological Society of America*, 97(5), pp. 1702–1717. doi: 10.1785/0120050198.
- Wei, H.-H., Shohet, I. M., Skibniewski, M. J., Shapira, S., Levy, R., Levi, T., Salamon, A. and Zohar, M. (2015) ‘Assessment of Casualty and Economic Losses from Earthquakes Using Semi-empirical Model’, *Procedia Engineering*, 123, pp. 599–605. doi: 10.1016/j.proeng.2015.10.113.
- Zanini, M. A., Hofer, L. and Pellegrino, C. (2015) ‘Le polizze assicurative come strumento finanziario per il trasferimento del rischio sismico: stato dell’arte’, *XVI Convegno - ANIDIS 2015, L’Aquila*, (October).
- Zhao, J. and Sritharan, S. (2007) ‘Modeling of Strain Penetration Effects in Fiber-Based Analysis of Reinforced Concrete StructuresConcrete Structures’, *ACI Structural Journal*, 104(2), pp. 860–866. doi: 10.14359/18525.

## ANNEX A

Appendix A presents the information about RC elements (columns, RC walls and beams). Table A.1 describes the characteristics of the RC walls, Table A.2 the characteristics of the columns and Table A.3 the characteristics of the beams. In the tables, “ $A_s$ ” represents the longitudinal reinforcement area and “ $A_c$ ” the cross-section area. The RC walls and columns number refer to Figure 3.7, the beams number refer to Figure A.1.

Table A.1 – Geometric characteristics and reinforcement of the RC walls.

Wall Number	Level	Length (m)	Width (m)	Long. Reinforcement	$A_s$ (cm <sup>2</sup> )	$A_c$ (m <sup>2</sup> )
W <sub>1y</sub> – W <sub>2</sub> – W <sub>3</sub> – W <sub>4y</sub>	L 0 - 1	0.25	4.00	(19Φ3/8"x 2) + ((2Φ7/8"+ 4Φ3/4") x 2)	65.42	1.000
	L 1 - 2	0.25	4.00	(19Φ5/16"x 2) + ((2Φ5/8"+ 6Φ3/8") x 2)	35.48	1.000
	L 2 - 3	0.25	4.00	(19Φ5/16"x 2) + (2Φ5/8" x 2)	26.96	1.000
	L 3 - 4	0.25	4.00	(19Φ5/16"x 2) + (2Φ5/8" x 2)	26.96	1.000
	L 4 - 5	0.25	4.00	(19Φ5/16"x 2) + (2Φ5/8" x 2)	26.96	1.000
	L 5 - 6	0.25	4.00	(19Φ5/16"x 2) + (2Φ5/8" x 2)	26.96	1.000
	L 6 - 7	0.25	4.00	(19Φ5/16"x 2) + (2Φ5/8" x 2)	26.96	1.000
	L 7 - 8	0.25	4.00	(19Φ5/16"x 2) + (2Φ5/8" x 2)	26.96	1.000
W <sub>1x</sub> - W <sub>4x</sub>	L 0 - 1	0.15	3.00	(13Φ1/4"x 2)	8.32	0.450
	L 1 - 2	0.15	3.00	(13Φ1/4"x 2)	8.32	0.450
	L 2 - 3	0.15	3.00	(13Φ1/4"x 2)	8.32	0.450
	L 3 - 4	0.15	3.00	(13Φ1/4"x 2)	8.32	0.450
	L 4 - 5	0.15	3.00	(13Φ1/4"x 2)	8.32	0.450
	L 5 - 6	0.15	3.00	(13Φ1/4"x 2)	8.32	0.450
	L 6 - 7	0.15	3.00	(13Φ1/4"x 2)	8.32	0.450
	L 7 - 8	0.15	3.00	(13Φ1/4"x 2)	8.32	0.450

Horizontal reinforcement ties are characterised by Φ 1/4" spaced every 25 cm, for the walls in the X direction (W<sub>1x</sub> and W<sub>4x</sub>), and by Φ 5/16" spaced every 25 cm for the walls in the Y direction (W<sub>1y</sub> – W<sub>2</sub> – W<sub>3</sub> – W<sub>4y</sub>).

Table A.2 – Geometric characteristics and reinforcement of the columns.

Column Number	Level	Length (m)	Width (m)	Long. Reinforcement	A <sub>s</sub> (cm <sup>2</sup> )	A <sub>c</sub> (m <sup>2</sup> )
C1 - C8	L 0 - 1	0.70	0.30	2Φ7/8"+ 2Φ7/8"	15.50	0.210
	L 1 - 2	0.50	0.25	3Φ5/8"+ 3Φ5/8"	11.90	0.125
	L 2 - 3	0.40	0.25	2Φ5/8"+ 2Φ5/8"	7.94	0.100
	L 3 - 4	0.40	0.25	2Φ5/8"+ 2Φ5/8"	7.94	0.100
	L 4 - 5	0.30	0.25	2Φ5/8"+ 2Φ5/8"	7.94	0.075
	L 5 - 6	0.30	0.25	2Φ5/8"+ 2Φ5/8"	7.94	0.075
	L 6 - 7	0.30	0.25	2Φ5/8"+ 2Φ5/8"	7.94	0.075
	L 7 - 8	0.30	0.25	2Φ5/8"+ 2Φ5/8"	7.94	0.075
C2 - C5	L 0 - 1	0.70	0.30	2Φ7/8"+ 2Φ7/8"	15.50	0.210
	L 1 - 2	0.50	0.25	3Φ5/8"+ 3Φ5/8"	11.90	0.125
	L 2 - 3	0.50	0.25	3Φ5/8"+ 3Φ5/8"	11.90	0.125
	L 3 - 4	0.50	0.25	3Φ5/8"+ 3Φ5/8"	11.90	0.125
	L 4 - 5	0.40	0.25	2Φ5/8"+ 2Φ5/8"	7.94	0.100
	L 5 - 6	0.40	0.25	2Φ5/8"+ 2Φ5/8"	7.94	0.100
	L 6 - 7	0.40	0.25	2Φ5/8"+ 2Φ5/8"	7.94	0.100
	L 7 - 8	0.40	0.25	2Φ5/8"+ 2Φ5/8"	7.94	0.100
C3 - C4	L 0 - 1	0.70	0.30	2Φ7/8"+ 2Φ7/8"	15.50	0.210
	L 1 - 2	0.50	0.25	3Φ5/8"+ 3Φ5/8"	11.90	0.125
	L 2 - 3	0.40	0.25	2Φ5/8"+ 2Φ5/8"	7.94	0.100
	L 3 - 4	0.40	0.25	2Φ5/8"+ 2Φ5/8"	7.94	0.100
	L 4 - 5	0.30	0.25	2Φ5/8"+ 2Φ5/8"	7.94	0.075
	L 5 - 6	0.30	0.25	2Φ5/8"+ 2Φ5/8"	7.94	0.075
	L 6 - 7	0.30	0.25	2Φ5/8"+ 2Φ5/8"	7.94	0.075
	L 7 - 8	0.30	0.25	2Φ5/8"+ 2Φ5/8"	7.94	0.075
C7 - C12	L 0 - 1	0.70	0.30	5Φ1"+ 5Φ1"	50.70	0.210
	L 1 - 2	0.60	0.25	5Φ1"+ 5Φ1"	50.70	0.150
	L 2 - 3	0.50	0.25	3Φ1"+ 3Φ1"	30.40	0.125
	L 3 - 4	0.40	0.25	3Φ5/8"+ 3Φ5/8"	11.90	0.100
	L 4 - 5	0.30	0.25	2Φ5/8"+ 2Φ5/8"	7.94	0.075
	L 5 - 6	0.30	0.25	2Φ5/8"+ 2Φ5/8"	7.94	0.075
	L 6 - 7	0.30	0.25	2Φ5/8"+ 2Φ5/8"	7.94	0.075
	L 7 - 8	0.30	0.25	2Φ5/8"+ 2Φ5/8"	7.94	0.075
C8 - C11	L 0 - 1	0.70	0.30	5Φ11/8"+ 5Φ11/8"	64.20	0.210
	L 1 - 2	0.60	0.25	5Φ11/8"+ 5Φ11/8"	64.20	0.150
	L 2 - 3	0.60	0.25	3Φ11/8"+ 3Φ11/8"	38.50	0.150
	L 3 - 4	0.50	0.25	3Φ1"+ 3Φ1"	30.40	0.125
	L 4 - 5	0.40	0.25	3Φ5/8"+ 3Φ5/8"	11.90	0.100
	L 5 - 6	0.40	0.25	3Φ5/8"+ 3Φ5/8"	11.90	0.100

	L 6 - 7	0.40	0.25	3Φ5/8"+ 3Φ5/8"	11.90	0.100
	L 7 - 8	0.40	0.25	2Φ5/8"+ 2Φ5/8"	7.94	0.100
C9 - C10	L 0 - 1	0.70	0.30	5Φ1"+ 5Φ1"	50.70	0.210
	L 1 - 2	0.60	0.25	5Φ1"+ 5Φ1"	50.70	0.150
	L 2 - 3	0.50	0.25	3Φ1"+ 3Φ1"	30.40	0.125
	L 3 - 4	0.40	0.25	3Φ1"+ 3Φ1"	30.40	0.100
	L 4 - 5	0.30	0.25	4Φ5/8"+ 4Φ5/8"	15.90	0.075
	L 5 - 6	0.30	0.25	4Φ5/8"+ 4Φ5/8"	15.90	0.075
	L 6 - 7	0.30	0.25	4Φ5/8"+ 4Φ5/8"	15.90	0.075
	L 7 - 8	0.30	0.25	2Φ5/8"+ 2Φ5/8"	7.94	0.075
C13-14-15-16	L 0 - 1	0.20	0.20	4Φ1/2"	5.07	0.040
	L 1 - 2	0.20	0.20	4Φ1/2"	5.07	0.040
	L 2 - 3	0.20	0.20	4Φ1/2"	5.07	0.040
	L 3 - 4	0.20	0.20	4Φ1/2"	5.07	0.040
	L 4 - 5	0.20	0.20	4Φ1/2"	5.07	0.040
	L 5 - 6	0.20	0.20	4Φ1/2"	5.07	0.040
	L 6 - 7	0.20	0.20	4Φ1/2"	5.07	0.040
	L 7 - 8	0.20	0.20	4Φ1/2"	5.07	0.040
C17 - C22	L 0 - 1	0.70	0.30	2Φ7/8"+ 2Φ7/8"	15.50	0.210
	L 1 - 2	0.50	0.25	3Φ3/4"+ 3Φ3/4"	17.20	0.125
	L 2 - 3	0.40	0.25	2Φ5/8"+ 2Φ5/8"	7.94	0.100
	L 3 - 4	0.40	0.25	2Φ5/8"+ 2Φ5/8"	7.94	0.100
	L 4 - 5	0.30	0.25	2Φ5/8"+ 2Φ5/8"	7.94	0.075
	L 5 - 6	0.30	0.25	2Φ5/8"+ 2Φ5/8"	7.94	0.075
	L 6 - 7	0.30	0.25	2Φ5/8"+ 2Φ5/8"	7.94	0.075
	L 7 - 8	0.30	0.25	2Φ5/8"+ 2Φ5/8"	7.94	0.075
C18 - C21	L 0 - 1	0.70	0.30	2Φ7/8"+ 2Φ7/8"	15.50	0.210
	L 1 - 2	0.50	0.25	(3Φ5/8"+ 2Φ7/8") x 2	27.40	0.125
	L 2 - 3	0.50	0.25	3Φ5/8"+ 3Φ5/8"	11.90	0.125
	L 3 - 4	0.50	0.25	3Φ5/8"+ 3Φ5/8"	11.90	0.125
	L 4 - 5	0.40	0.25	2Φ5/8"+ 2Φ5/8"	7.94	0.100
	L 5 - 6	0.40	0.25	2Φ5/8"+ 2Φ5/8"	7.94	0.100
	L 6 - 7	0.40	0.25	2Φ5/8"+ 2Φ5/8"	7.94	0.100
	L 7 - 8	0.40	0.25	2Φ5/8"+ 2Φ5/8"	7.94	0.100
C19 - C20	L 0 - 1	0.70	0.30	2Φ7/8"+ 2Φ7/8"	15.50	0.210
	L 1 - 2	0.50	0.25	3Φ5/8"+ 3Φ5/8"	11.90	0.125
	L 2 - 3	0.40	0.25	2Φ5/8"+ 2Φ5/8"	7.94	0.100
	L 3 - 4	0.40	0.25	2Φ5/8"+ 2Φ5/8"	7.94	0.100
	L 4 - 5	0.30	0.25	2Φ5/8"+ 2Φ5/8"	7.94	0.075
	L 5 - 6	0.30	0.25	2Φ5/8"+ 2Φ5/8"	7.94	0.075

	L 6 - 7	0.30	0.25	2Φ5/8"+ 2Φ5/8"	7.94	0.075
	L 7 - 8	0.30	0.25	2Φ5/8"+ 2Φ5/8"	7.94	0.075

Horizontal reinforcement ties are characterised by Φ 1/4" spaced every 20 cm.

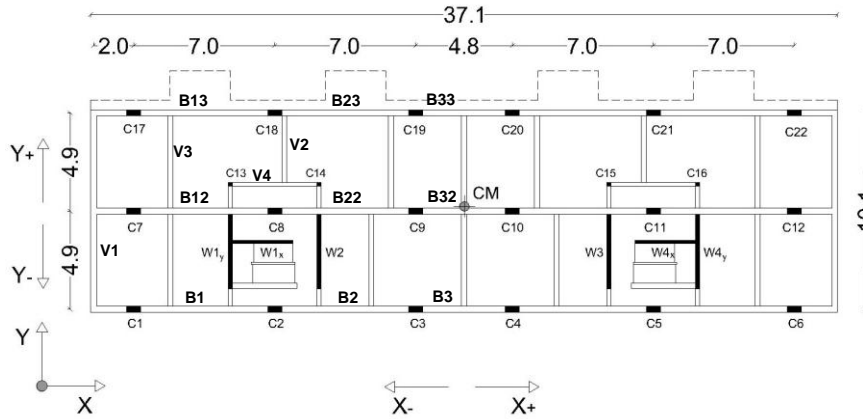


Figure A.1 – Case study building: structural plan layout

Table A.3 – Geometric characteristics and reinforcement of the beams.

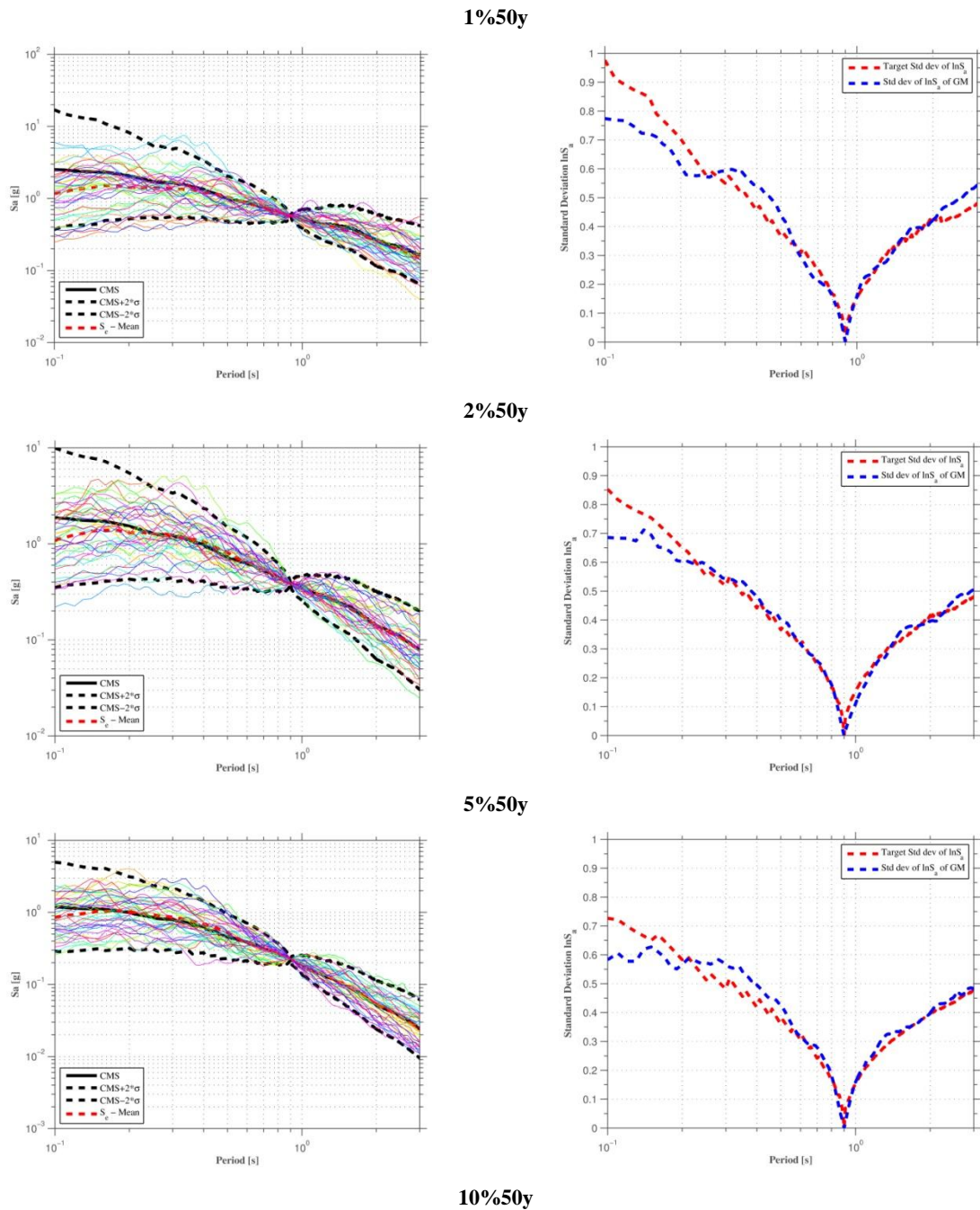
Beam number	Level	Width (m)	Height (m)	Length (m)	Upper Left Reinforc.	As left (cm <sup>2</sup> )	Upper Right Reinforc.	As right (cm <sup>2</sup> )	Midspan Reinforcement	As inf. (cm <sup>2</sup> )
B1	L 1	0.30	0.65	9.00	4Φ3/4"	11.50	3Φ7/8"+ 2Φ3/4"	17.33	2Φ3/4"+ 1Φ5/8"	7.72
	L 2-7	0.25	0.65	9.00	4Φ3/4"	11.50	4Φ3/4"	11.50	2Φ3/4"	5.73
	L 8	0.25	0.65	9.00	2Φ5/8"	3.97	3Φ5/8"+ 2Φ3/4"	11.69	3Φ5/8"	5.96
B2	L 1	0.30	0.65	7.00	3Φ7/8"+ 2Φ3/4"	17.33	4Φ3/4"+ 1Φ5/8"	13.49	2Φ3/4"	5.73
	L 2-7	0.25	0.65	7.00	4Φ3/4"	11.50	4Φ3/4"	11.50	2Φ3/4"	5.73
	L 8	0.25	0.65	7.00	3Φ5/8"+2Φ3/4"	11.69	4Φ5/8"	7.94	3Φ5/8"	5.96
B3	L 1	0.30	0.65	2.40	4Φ3/4"+1Φ5/8"	13.49	4Φ3/4"+ 1Φ5/8"	13.49	2Φ3/4"	5.73
	L 2-7	0.25	0.65	2.40	4Φ3/4"	11.50	4Φ3/4"	11.50	2Φ3/4"	5.73
	L 8	0.25	0.65	2.40	4Φ5/8"	7.94	4Φ5/8"	7.94	2Φ5/8"	3.97
B12	L 1	0.30	0.65	9.00	3Φ1"+ 3Φ11/8"	34.50	3Φ1"+ 3Φ11/8"	34.50	3Φ1"	15.20
	L 2-7	0.25	0.65	9.00	3Φ1"+ 3Φ7/8"	26.80	3Φ1"+ 3Φ7/8"	26.80	3Φ1"	15.20
	L 8	0.25	0.65	9.00	2Φ7/8"+2Φ3/4"	13.47	6Φ1"	30.40	4Φ7/8"	15.50
B22	L 1	0.30	0.65	7.00	3Φ1"+ 3Φ11/8"	34.50	3Φ1"+ 3Φ11/8"	34.50	3Φ1"	15.20
	L 2-7	0.25	0.65	7.00	3Φ1"+ 3Φ7/8"	26.80	5Φ1"	25.30	3Φ1"	15.20
	L 8	0.25	0.65	7.00	6Φ1"	30.40	2Φ7/8"+ 2Φ1"	17.84	4Φ7/8"	15.50

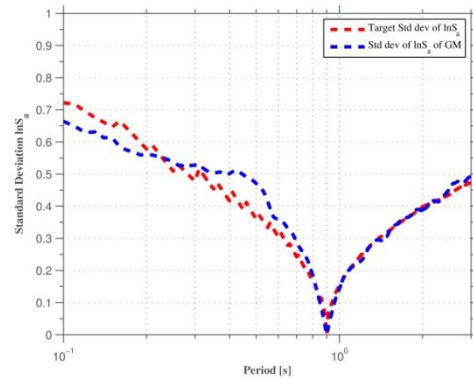
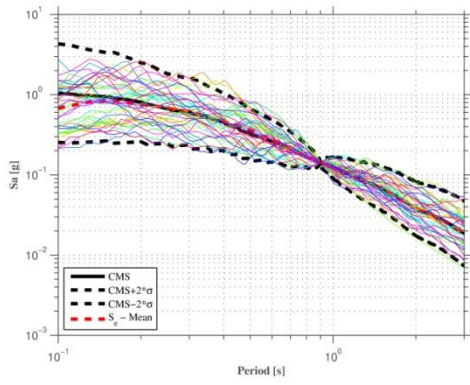
B32	L 1	0.30	0.65	2.40	3Φ1"+ 3Φ11/8"	34.50	3Φ1"+ 3Φ11/8"	34.50	3Φ1"	15.20
	L 2-7	0.25	0.65	2.40	5Φ1"	25.30	5Φ1"	25.30	2Φ1"	10.10
	L 8	0.25	0.65	2.40	2Φ7/8"+ 2Φ1"	17.84	2Φ7/8"+ 2Φ1"	17.84	2Φ7/8"	7.74
B13	L 1	0.30	0.65	9.00	5Φ3/4"	14.30	3Φ3/4"+ 3Φ1"	23.79	5Φ3/4"	14.30
	L 2-7	0.25	0.65	9.00	5Φ3/4"	14.30	3Φ3/4"+ 2Φ1"	18.69	5Φ3/4"	14.30
	L 8	0.25	0.65	9.00	3Φ5/8"	5.96	3Φ5/8"+ 2Φ3/4"	11.69	3Φ5/8"	5.96
B23	L 1	0.30	0.65	7.00	3Φ3/4"+ 3Φ1"	23.79	2Φ3/4"+ 2Φ1"	15.83	5Φ3/4"	14.30
	L 2-7	0.25	0.65	7.00	3Φ3/4"+ 2Φ1"	18.69	5Φ3/4"	14.30	5Φ3/4"	14.30
	L 8	0.25	0.65	7.00	3Φ5/8"+2Φ 3/4"	11.69	4Φ5/8"	7.94	3Φ5/8"	5.96
B33	L 1	0.30	0.65	2.40	2Φ3/4"+ 2Φ1"	15.83	2Φ3/4"+ 2Φ1"	15.83	2Φ3/4"	5.73
	L 2-7	0.25	0.65	2.40	5Φ3/4"	14.30	5Φ3/4"	14.30	2Φ3/4"	5.73
	L 8	0.25	0.65	2.40	4Φ5/8"	7.94	4Φ5/8"	7.94	3Φ5/8"	5.96
V1-L	L 1-8	0.25	0.35	7.31	2Φ5/16"+1 Φ1/2"	2.26	2Φ5/8"+ 1Φ1/2"+ 2Φ5/16"	6.23	3Φ1/2"	3.80
V1-R	L 1-8	0.25	0.35	7.31	2Φ5/8"+1Φ 1/2"+ 2Φ5/16"	6.23	2Φ5/16"+ 1Φ1/2"	2.26	3Φ1/2"	3.80
V2	L 1-8	0.25	0.25	3.43	2Φ5/16"+ 1Φ1/2"	2.26	2Φ5/16"+ 1Φ1/2"	2.26	3Φ1/2"	3.80
V3	L 1-8	0.25	0.30	19.50	2Φ5/16"+ 1Φ3/4"	3.86	2Φ5/16"+ 1Φ3/4"	3.86	2Φ3/8"+ 1Φ3/4"	4.29
V4	L 1-8	0.25	0.50	8.00	2Φ5/16"+ 2Φ3/4"	6.72	2Φ5/16"+ 2Φ3/4"	6.72	4Φ3/4"	11.50



## ANNEX B

In appendix B the five conditional mean spectrum used for the loss assessment analyses of Chapter 5 and 6 are presented, for probabilities of occurrence of 1%, 2%, 5%, 10% and 30% in 50 years. In Figure B.1 are represented on the left the response spectra for all the records in the set along with the target conditional spectrum (mean and mean + 2 std deviations), on the right comparison between the standard deviation of the set and the target standard.





30%/50y

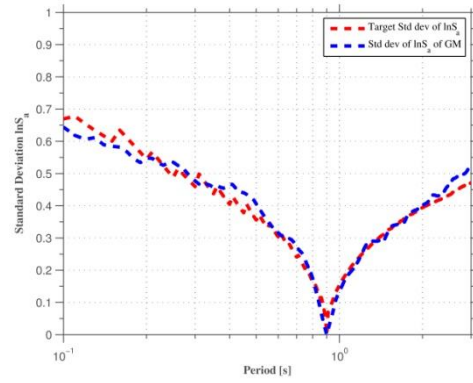
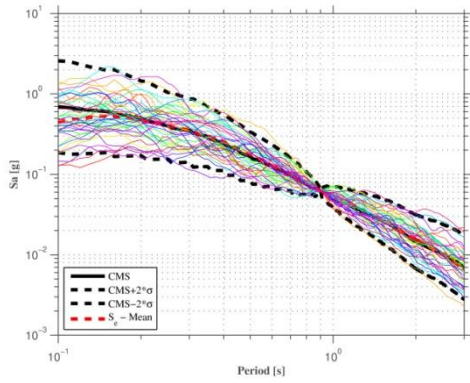


Figure B.1 – Response spectra for all the records in the set along with the target conditional spectrum (left), comparison between the standard deviation of the set and the target standard (right), for probabilities of occurrence of 1%, 2%, 5%, 10% and 30% in 50 years.



## ANNEX C

Tables C.1 to C.4 summary the estimated cost of the repair activities at each damage state. Table C.1 to C.3 summary the estimated cost (€) for repairing DS1 to DS3 for a column with dimensions 0.3x0.7m. Table C.4 summarises the estimated linear cost (€/m) of concrete jacketing the RC walls in Y-direction (0.25x3m), considering the cross-section dimensions. This linear cost must be multiplied by the height of the wall.

Table C.1 – Estimated cost of repairing light damage (DS1) for a column (0.3x0.7m).

Repair Actions	Unit	Unit cost [€/unit)	Quantity [Unit]	Cost [€]
Cleaning cracks' interior	m	3.64	1.50	5.46
Patching spalled concrete with mortar mix	m <sup>2</sup>	12.10	6.00	72.60
			Tot	78.06

Table C.2 – Estimated cost of repairing moderate damage (DS2) for a column (0.3x0.7m).

Repair Actions	Unit	Unit cost [€/unit)	Quantity [Unit]	Cost [€]
Cleaning cracks' interior	m	3.64	3.00	10.92
Epoxy crack injection	m	88.50	3.00	265.49
Patching spalled concrete with mortar mix	m <sup>2</sup>	12.10	6.00	72.60
			Tot	349.01

Table C.3 – Estimated cost of repairing severe damage (DS3) for a column (0.3x0.7m).

Repair Actions	Unit	Unit cost [€/unit]	Quantity [Unit]	Cost [€]
Cleaning cracks' interior	m	3.64	6.00	21.84
Replacement of buckled or fractured bars	m <sup>3</sup>	162.36	0.32	51.14*
Injection of cracks with epoxy	m	88.50	6.00	530.98
Replacement of concrete that is loose, or has spalled, or has been removed to replace bars	m <sup>2</sup>	82.86	6.00	497.14
			Tot	1101.10

\*Obtained considering a cost of 1.353 €/kg and 120 kg/m<sup>3</sup>.

Table C.4 – Linear cost of concrete jacketing (DS3) of RC walls.

Repair Actions	Unit	Unit cost [€/unit]	Quantity [Unit]	Cost [€/m]
Surface roughening	m <sup>2</sup>	40.52	6.30	255.3
Bonding agent (epoxy)	kg	13.35	2.70	36.0
Concrete	m <sup>3</sup>	111.63	1.04	115.5
Reinforcing steel bar	kg	0.74	113.40	83.9
Formwork	m <sup>2</sup>	10.50	7.50	78.8
Specialised worker	h	18.05	2.00	36.1
Regular worker	h	17.64	1.00	17.6
			Tot	623.3